



Universiteit  
Leiden  
The Netherlands

## Preparing for CADASIL therapy

Gravesteijn, G.

### Citation

Gravesteijn, G. (2020, October 28). *Preparing for CADASIL therapy*. Retrieved from <https://hdl.handle.net/1887/137984>

Version: Publisher's Version

License: [Licence agreement concerning inclusion of doctoral thesis in the Institutional Repository of the University of Leiden](#)

Downloaded from: <https://hdl.handle.net/1887/137984>

**Note:** To cite this publication please use the final published version (if applicable).

Cover Page



Universiteit Leiden



The handle <http://hdl.handle.net/1887/137984> holds various files of this Leiden University dissertation.

**Author:** Gravesteijn, G.

**Title:** Preparing for CADASIL therapy

**Issue Date:** 2020-10-28

# Preparing for CADASIL therapy

Gido Gravesteijn

ISBN: 978-94-6332-670-4

© 2020 Gido Gravesteyn

Cover design and lay-out: Gido Gravesteyn

Printing: GVO drukkers & vormgevers

The research described in this thesis was financially supported by the Netherlands Brain Foundation. Printing of this thesis was financially supported by Alzheimer Nederlands.

All rights reserved. No part of this thesis may be reproduced, stored in a retrieval system, or transmitted in any form or by any means, without the prior permission of the author.

# Preparing for CADASIL therapy

Proefschrift

ter verkrijging van  
de graad van Doctor aan de Universiteit Leiden,  
op gezag van Rector Magnificus prof. mr. C.J.J.M. Stolker,  
volgens besluit van het College voor Promoties  
te verdedigen op woensdag 28 oktober 2020  
klokke 15.00 uur

door

Gido Gravesteyn  
geboren te Zaanstad  
in 1989

Promotor: Prof. dr. A. Aartsma-Rus

Co-promotores: Dr. S.A.J. Lesnik Oberstein  
Dr. J.W. Rutten

Leden promotiecommissie: Prof. dr. O.C. Meijer  
Prof. dr. M. Duering<sup>1</sup>  
Dr. H. Karlström<sup>2</sup>

<sup>1</sup> Institute for Stroke and Dementia Research,  
Klinikum der Universität München, Germany

<sup>2</sup> Division of Neurogeriatrics,  
Karolinska Institutet, Sweden.

# CONTENT

Chapter 1	Introduction	7
Chapter 2	Progression and classification of granular osmiophilic material (GOM) deposits in functionally characterized human <i>NOTCH3</i> transgenic mice	29
Chapter 3	Naturally occurring <i>NOTCH3</i> exon skipping attenuates <i>NOTCH3</i> protein aggregation and disease severity in CADASIL patients	57
Chapter 4	Long-term disease progression in CADASIL: an 18-year follow-up study	79
Chapter 5	Serum Neurofilament Light-chain correlates with CADASIL disease severity and survival	99
Chapter 6	Discussion and future perspectives	117
Appendices	Nederlandse samenvatting	131
	List of abbreviations	141
	List of co-author affiliations	143
	List of publications	145
	Portfolio	146
	Curriculum Vitae	149
	Dankwoord	150



# Chapter 1

## General introduction



CADASIL (cerebral autosomal dominant arteriopathy with subcortical infarcts and leukoencephalopathy) is the most prevalent hereditary small vessel disease.<sup>1,2</sup> CADASIL patients typically develop recurrent strokes from mid-adult age onwards, leading to progressive cognitive impairment and ultimately vascular dementia.<sup>1</sup> In 1996, archetypal cysteine altering missense mutations in *NOTCH3* (*NOTCH3*<sup>95</sup>) were discovered to cause CADASIL.<sup>2</sup> Since then, numerous CADASIL patients and families have been identified world-wide, leading to an estimated minimum prevalence of 2 - 5 CADASIL patients per 100,000 persons.<sup>3-6</sup> In The Netherlands, there are currently more than 275 diagnosed CADASIL families. To date, there is no therapy that can delay or prevent CADASIL.

The first chapter provides a background for the studies that are described in this thesis, which are all aimed at advancing pre-clinical CADASIL therapy development towards future clinical trials. CADASIL clinical signs and symptoms, neuroimaging features, molecular genetics and pathophysiology are described. In addition, the recent advances in therapy development and requirements for clinical trial readiness are discussed.

### **CADASIL clinical symptoms and neuroimaging features**

CADASIL is characterized by recurrent (transient) ischemic events and cognitive decline. CADASIL patients typically suffer from their first ischemic stroke between 45-60 years of age, but age at first stroke can vary from the third decade and to the eighth decade.<sup>7-12</sup> Ischemic events typically present as a classical lacunar syndrome with motor or sensory deficits.<sup>13</sup> Almost all patients with a classical CADASIL disease course ultimately develop gait disturbances, urine incontinence and vascular dementia.<sup>7</sup>

The first sign of cognitive decline is often impaired executive function, which can be present before the first stroke.<sup>14-18</sup> This is followed by slowed processing speed,<sup>15,17</sup> and later on by a decline in verbal fluency and visuospatial abilities.<sup>15-17,19</sup> Although recognition, semantic and episodic memory also deteriorate late in the disease course, they are well preserved compared to other domains.<sup>15-17</sup> Ultimately, the global cognitive impairment progresses towards vascular dementia with full care-dependency.

One-third to three-quarters of CADASIL patients develop migraine, often in the third decade, before the first ischemic event.<sup>7,8,10,11,20</sup> Migraine is accompanied by aura in ~80% of patients.<sup>7,8,10,11,20</sup> Women with CADASIL are more prone to develop migraine, and have a younger age at onset.<sup>11,20</sup> One-third of patients suffer from at least one atypical aura in their life, with motor deficits, confusion and decreased consciousness, which may be difficult to differentiate from transient ischemic attacks (TIAs).<sup>10,20</sup> In some cases, a migrainous encephalopathy may occur.<sup>10,20</sup>

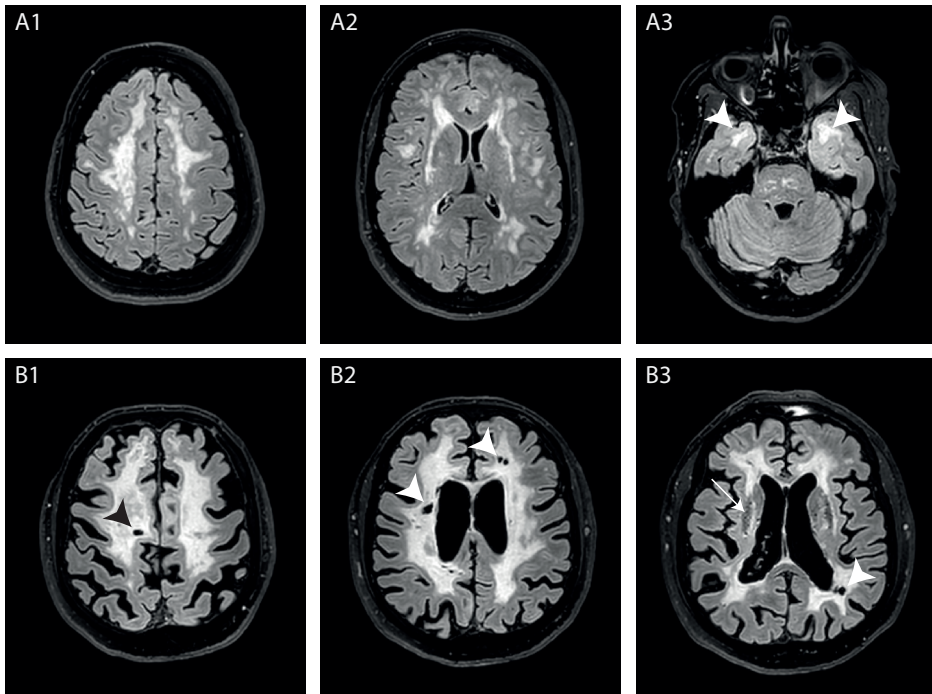


**Figure 1.1: Characteristic neuroimaging features in CADASIL**

(A) FLAIR images of a CADASIL patient without disability showing WMH in the semi-oval centre (A1), in the external capsules and periventricular areas (A2), and in the anterior temporal lobes (A3) (arrowheads). (B) FLAIR images of a CADASIL patient with disability showing multiple lacunes (arrowheads) and confluent WMH affecting almost all the supratentorial white matter. Multiple enlarged perivascular spaces are present in the basal ganglia (Virchow-Robin spaces, arrow), which are collectively also called *état criblé* or *status cribrosum*.

One-third of the patients suffer from mood disorders, most often a depressive episode.<sup>7,10</sup> Apathy occurs in 40% of the patients and is independent of depression. Other psychiatric disturbances are reported, including anxiety, psychotic disorders and adaptation disorders.<sup>7,10</sup>

The most prominent signs on MRI include white matter hyperintensities on T2-weighted and FLAIR images, and lacunes (Figure 1.1).<sup>12,21–27</sup> From the age of 20 onwards, focal subcortical WMHs can be present in the anterior temporal lobes and periventricular areas, and later also in the external capsules and semi-oval center.<sup>12,27</sup> Although anterior temporal lobe WMHs are frequently observed, they are not always present.<sup>12,27–29</sup> Over time, subcortical WMH lesion load increases and WMH may become confluent in almost all the white matter.<sup>22,30</sup> From a mean age of 40–50 years onwards, lacunes can be observed. Neuroradiological signs may also include brain atrophy, enlarged perivascular spaces,<sup>24,31</sup> and microbleeds on susceptibility-weighted imaging, the frequency of which seems to partially depend on the ethnicity of the population studied.<sup>28,32,33</sup> In the Asian population, for example, microbleeds are more frequent and there is a higher risk of intracerebral haemorrhage.<sup>12,28,34,35</sup>

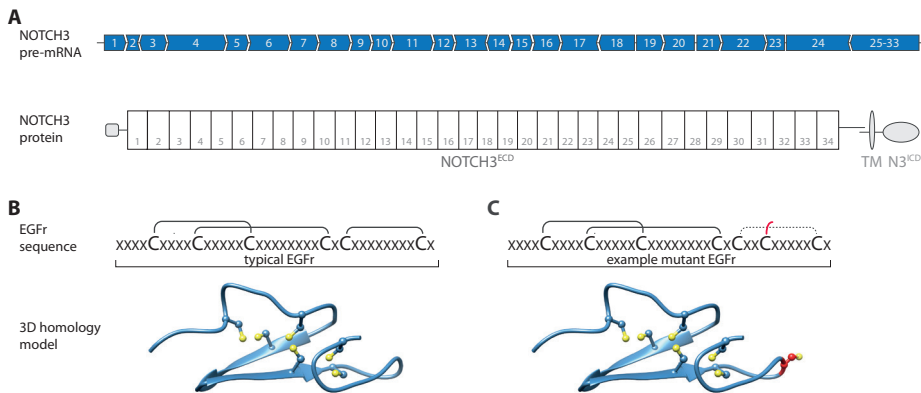


**Figure 1.2: Schematic representation of *NOTCH3* exons, *NOTCH3* protein and EGFr domains**

(A) *NOTCH3* is one of the four *NOTCH* homologues in humans and encodes for a transmembrane receptor protein.<sup>40,54</sup> The *NOTCH3* gene consists of 33 exons. Exon 2-24 encode for 34 similar epidermal growth factor-like repeat (EGFr) domains, located within the ectodomain of the *NOTCH3* protein (*NOTCH3*<sup>ECD</sup>).<sup>40,54</sup> One exon can encode one or more, complete or partial, EGFr domains. (B) A schematic figure and 3D homology modelling of a wildtype EGFr domain showing the disulphide pairing of the six cysteine residues. Each wildtype EGFr domain contains six cysteine residues that form three disulphide bridges (C<sup>1</sup>-C<sup>3</sup>, C<sup>2</sup>-C<sup>4</sup>, and C<sup>5</sup>-C<sup>6</sup>), thereby maintaining the structural integrity of the protein.<sup>47</sup> The number of amino acids between C<sup>4</sup>-C<sup>5</sup> and C<sup>5</sup>-C<sup>6</sup> is highly conserved and is always 1 amino acid or 8 amino acids, respectively. The number of amino acids is variable between the other cysteine residues (typically 4-6 amino acids between C<sup>1</sup>-C<sup>2</sup>; 4-5 amino acids between C<sup>2</sup>-C<sup>3</sup>; and 6-9 amino acids between C<sup>3</sup>-C<sup>4</sup>). (C) A schematic figure and 3D homology modelling of a mutant EGFr domain, in which the number of cysteine residues is altered to an uneven number, leading to incorrect protein folding and increased multimerization.

## CADASIL genetics

CADASIL is caused by highly stereotypical mutations in the *NOTCH3* gene.<sup>36,37</sup> In adults, the transmembrane receptor *NOTCH3* is mainly expressed in pericytes and vascular smooth muscle cells (VSMCs), which are collectively called mural cells.<sup>38-40</sup> *NOTCH3* expression is required for VSMC maturation, arterial identity, and blood vessel integrity.<sup>39,41-44</sup> The extracellular domain of *NOTCH3* (*NOTCH3*<sup>ECD</sup>) includes 34 epidermal growth factor-like repeat (EGFr) domains, with each EGFr domain having a fixed number of 6 cysteine residues (Figure 1.2). In CADASIL, mutations alter the canonical number of six cysteines in an EGFr domain to an uneven number of cysteines (*NOTCH3*<sup>Cys</sup>), usually five or seven.<sup>1,36,45,46</sup> This results in an unpaired cysteine residue, which leads to incorrect EGFr folding, abnormal protein folding and increased *NOTCH3*<sup>ECD</sup> multimerization.<sup>47-50</sup> Almost all *NOTCH3*<sup>Cys</sup> mutations are missense mutations, the majority of which are located in exon 4. However, mutations can occur in exons that encode for any of the 34 EGFr domains (i.e. exon 2-24).<sup>37,46</sup> *NOTCH3*<sup>Cys</sup> mutations located in EGFr domains 7-34 have recently been found to be associated with a milder CADASIL phenotype and increased survival compared to

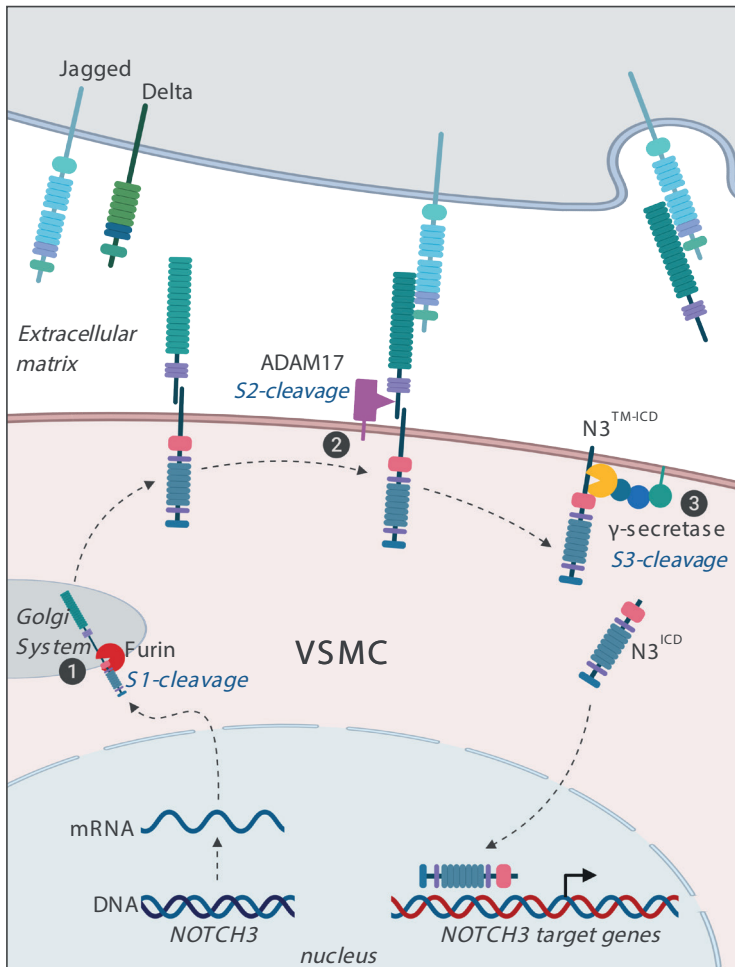


**Figure 1.3: NOTCH3 processing and signalling**

(1) The 280 kDa NOTCH3 precursor protein is cleaved in the Golgi system by Furin (S1 cleavage), resulting in a non-covalently bound heterodimeric protein, which is subsequently transported to the cell surface.<sup>40,54</sup> (2) Upon binding of a ligand (Jagged 1 or 2, Delta 1, 3 or 4) to EGFR domain 10-11, a mechanical traction force is applied to the NOTCH3<sup>ECD</sup>, exposing the extracellular NRR near the cell membrane, that consists of LNR domains (light purple) and the heterodimerization domain. Next, the C-terminal part of the heterodimerization domain is cleaved by ADAM17 (S2-cleavage).<sup>55</sup> (3) Then, γ-secretase cleaves off the NOTCH3<sup>ICD</sup>, which is comprised of a RAM domain (red) and several ANK (blue), two nuclear localisation signals, a transactivation domain (not shown) and a PEST domain (blue) involved in degradation regulation.<sup>40,54,56</sup> In the nucleus, the NOTCH3<sup>ICD</sup> interacts with the RBPJ protein and co-activator Mastermind-like (MAML) to activate downstream gene transcription.<sup>40,54,56</sup> ADAM17: a disintegrin and metalloproteinase domain-containing protein 17 (also known as TACE); ANK: ankyrin repeat; LNR: Lin12-Notch repeats; MAML: Mastermind-like; NOTCH3<sup>ECD</sup>: NOTCH3 ectodomain; NOTCH3<sup>ICD</sup>: NOTCH3 intracellular domain; NRR: negative regulatory region; PEST: proline, glutamate, serine and threonine (PEST)-rich; RAM: RBPJ-associated module; RBPJ: recombining binding protein suppressor of hairless.

*NOTCH3*<sup>cys</sup> mutations in EGFr domains 1-6, which are largely encoded by exon 4.<sup>51</sup> Some patients have small *NOTCH3* in-frame deletions, insertions or splice site mutations, which also result in an uneven number of cysteines in the given mutant EGFr domain.<sup>46</sup> *NOTCH3* signalling is considered to be intact for almost all *NOTCH3*<sup>cys</sup> mutations.<sup>50,52,53</sup> Only when the mutation is located in the ligand binding domain of the *NOTCH3* protein (i.e. EGFr domains 10 and 11), *NOTCH3* signalling is found to be reduced (*NOTCH3* signalling is described in Figure 1.3).<sup>50,52,53</sup>

### CADASIL pathophysiology

*NOTCH3*<sup>cys</sup> mutations lead to *NOTCH3*<sup>ECD</sup> multimerization and aggregation in the blood vessel walls, in the vicinity of vascular smooth muscle cells and pericytes (Figure 1.4).<sup>47,49,57-59</sup> The *NOTCH3*<sup>ECD</sup> aggregates are observed in the vessel walls of the small cerebral arteries, but also of the small arteries throughout the body.<sup>60</sup> Immunohistochemical *NOTCH3*<sup>ECD</sup> staining of skin biopsies shows *NOTCH3*<sup>ECD</sup> aggregates in skin arteries in almost all CADASIL patients, from at least early adulthood onwards.<sup>60,61</sup> Ultrastructurally, deposits of granular osmiophilic material (GOM) can be found near mural cells in the basement membrane of the small (brain) arteries and capillaries.<sup>62-67</sup> GOM deposits are considered to be pathognomonic for CADASIL.<sup>64,66</sup>

*NOTCH3*<sup>ECD</sup> aggregates and GOM deposits sequester functionally important extracellular matrix proteins, such as TIMP3, vitronectin, HTRA1, endostatin and LTBP-1, thereby contributing to the disease pathology.<sup>68-70</sup> One potential mechanism contributing to disease pathogenesis involves the sequestration of HTRA1 in *NOTCH3*<sup>ECD</sup> aggregates, resulting in an HTRA1 loss-of-function profile in the extracellular matrix with subsequent accumulation and dysfunction of HTRA1's substrates.<sup>68,70,71</sup> In addition, the abundance of TIMP3 in the cerebrovasculature is reported to have an effect via the ADAM17/HB-EGF/(ErbB1/ErbB4) pathway on vascular smooth muscle cell hyperpolarisation, pressure-induced myogenic tone and impaired cerebral blood flow autoregulation.<sup>72,73</sup>

Histologically, CADASIL is characterized by arterial wall thickening, especially of the small to medium-sized arteries (Figure 1.4). These vessels show thickened fibrotic walls with intense collagenous staining, marked vascular smooth muscle cell degeneration and a smooth muscle actin (SMA) positive intima, but not a substantially narrowed lumen.<sup>62,74-78</sup> These pathological changes are associated with impaired regulation of cerebral blood flow, altered VSMC morphology, white matter hyperintensities, blood-brain-barrier leakage and ultimately ischemic events and vascular cognitive impairment.<sup>62,74-79</sup>

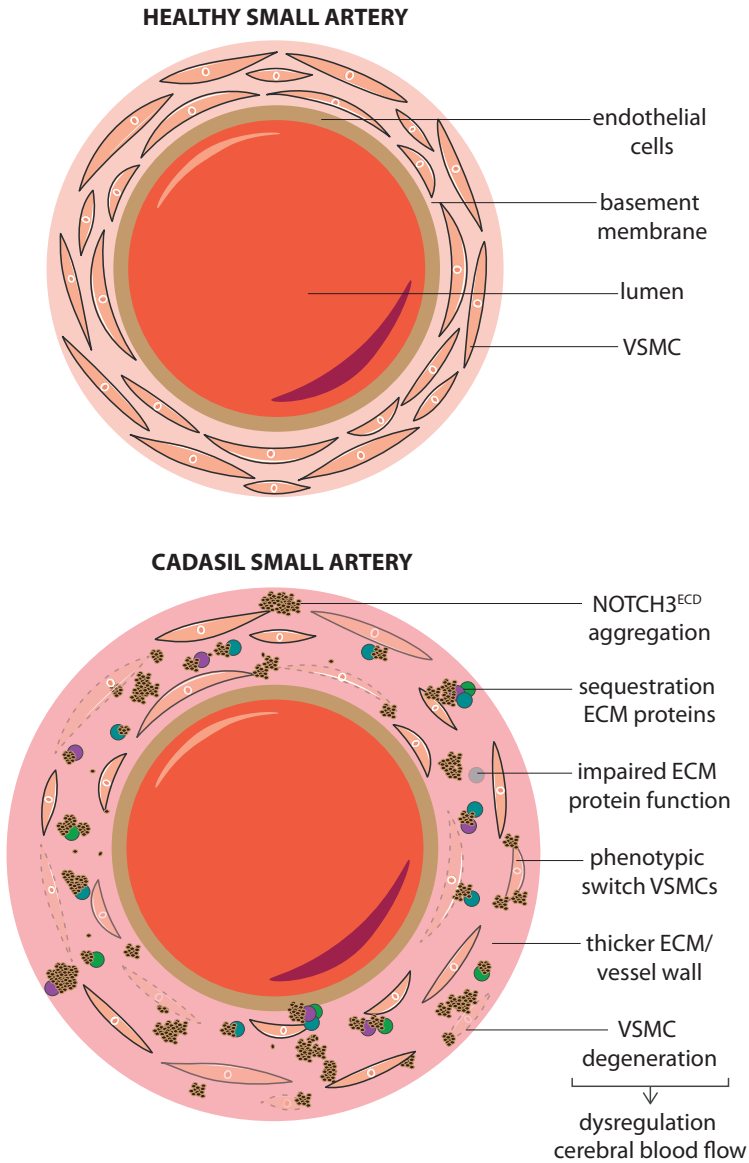


**Figure 1.4: Hallmarks of CADASIL vessel wall pathology**

NOTCH3 proteins with a cysteine altering mutation lead to extracellular aggregates of the NOTCH3<sup>ECD</sup>, which sequester other extracellular matrix proteins, leading to extracellular matrix dysregulation, vessel wall thickening, blood-brain-barrier leakage, changes in VSMC phenotype and VSMC degeneration.<sup>62,71,82,74-81</sup>

## Characterization of a CADASIL mouse model

Various CADASIL mouse models with a *NOTCH3*<sup>95</sup> mutation recapitulate the NOTCH3<sup>ECD</sup> aggregates and GOM deposits found in CADASIL patients.<sup>63,70,83–89</sup> The humanized transgenic *NOTCH3*<sup>Arg182Cys</sup> mouse model, that was developed in the Leiden University Medical Center, overexpresses the full length human *NOTCH3* gene with a typical CADASIL mutation from a genomic construct at expression levels of 100%, 150%, 200% and 350% relative to endogenous mouse *Notch3* expression. In brains of these mice, the amount of NOTCH3<sup>ECD</sup> aggregates correlates with age and with the expression level of mutant *NOTCH3*, and NOTCH3<sup>ECD</sup> aggregates can be observed as early as age 6 weeks in the mouse strain with 350% human *NOTCH3*<sup>Arg182Cys</sup> expression. In this strain, GOM deposits were observed from the age of 6 months. Although the presence of GOM deposits in patients and animal models has been extensively reported, there have been no studies describing progression of GOM deposits from their incipience onwards.

Histological white matter abnormalities, cerebrovascular reactivity, myogenic tone, and blood brain barrier leakage have been studied in CADASIL mouse models, but had not yet been fully characterized in the Leiden mouse model.<sup>63,70,83–89</sup>

[Chapter 2](#) describes the longitudinal characterization of GOM deposits in the Leiden humanized transgenic *NOTCH3*<sup>Arg182Cys</sup> mouse model, and provides a five-tier classification system for GOM deposits in mice. Analysis of patient material showed that this classification system is translatable to GOM in patient tissue.<sup>90</sup> [Chapter 2](#) also describes the characterization of the Leiden humanized transgenic *NOTCH3*<sup>Arg182Cys</sup> mouse model in terms of histology, neuroimaging, cerebrovascular reactivity and cognition.<sup>90</sup>

## Therapy development in CADASIL

NOTCH3<sup>ECD</sup> aggregation is considered to have a pivotal role in CADASIL pathogenesis. Therefore, the focus of current therapeutic interventions is on counteracting NOTCH3<sup>ECD</sup> aggregation (Figure 1.5).<sup>91,92</sup> Other therapeutic strategies aim at increasing NOTCH3 signalling and reducing endothelial and mural cell degeneration.<sup>43,93</sup>

The Leiden CADASIL research group developed a therapeutic approach aimed to prevent and halt the formation of mutant NOTCH3<sup>ECD</sup> using an approach called ‘NOTCH3 cysteine correction’, aimed at correcting the number of cysteine residues in the mutant protein’s EGFR domains. This is accomplished by removing the respective mutant EGFR domain from the NOTCH3 protein.<sup>94</sup> NOTCH3 cysteine correction can be achieved using a splice modulating therapy called exon skipping (Figure 1.5B<sub>1</sub>). In exon skipping, short strands of modified RNA (antisense oligonucleotides, ASOs) bind to the *NOTCH3* pre-mRNA, thereby hiding an exon

from the splicing machinery, effectively excluding the mutant exon from the mature mRNA. This results in a NOTCH3 protein lacking the mutant EGFR domain. This modified protein is predicted to maintain canonical NOTCH protein structure, with correct disulphide bridge formation. *In vitro* proof-of-concept has been obtained for NOTCH3 cysteine correction by exon skipping, showing that the shorter NOTCH3 protein that is formed after NOTCH3 exon skipping retains signalling function.<sup>94</sup> However, whether NOTCH3 cysteine correction also reduces NOTCH3<sup>ECD</sup> aggregation could not be assessed *in vitro*.

The principle of NOTCH3 cysteine correction can also be applied at the DNA level using gene editing (Figure 1.5B). CRISPR/Cas9 has recently evolved rapidly into a useful tool for gene editing in *in vitro* model systems. In addition, CRISPR/Cas9 holds the promise of treating incurable genetic disease.<sup>95</sup> Chapter 3 describes the first in-human evidence that NOTCH3 cysteine correction is associated with reduced NOTCH3<sup>ECD</sup> aggregation, by analysis of a family with naturally occurring NOTCH3 exon skipping.<sup>96</sup> Chapter 3 also describes *in vitro* proof-of-concept of NOTCH3 cysteine correction using CRISPR/Cas9-mediated genomic deletion of exons eligible for cysteine correction.<sup>96</sup>

Two alternative therapeutic approaches that are being developed by other laboratories are antibody-based. One approach aims to counteract NOTCH3<sup>ECD</sup> aggregation using passive immunization (Figure 1.5C).<sup>92</sup> Passive immunization with a monoclonal antibody targeting NOTCH3<sup>ECD</sup> in a CADASIL mouse model showed a protective effect on vasodilative cerebral blood flow response and pressure-induced myogenic tone, suggesting that immunization rescues the ADAM17/HB-EGF/(ErbB1/ErbB4) pathway. However, chronic passive immunization did not halt the formation of NOTCH3<sup>ECD</sup> aggregates, GOM deposits or myelin debris in mouse brain.<sup>92</sup>

Another antibody-based approach targets the negative regulatory region of the NOTCH3 protein, which thereby increases NOTCH3 signalling, but does not counteract NOTCH3<sup>ECD</sup> aggregation (Figure 1.5D).<sup>43</sup> This approach might be beneficial for the patients with a loss-of-function NOTCH3<sup>95</sup> mutation in the ligand binding domain. Whether patients with a NOTCH3<sup>95</sup> mutation outside the ligand binding domain would benefit from this approach remains uncertain, since it remains a matter of debate whether NOTCH3 signalling is reduced in CADASIL, and if it is, whether this contributes to the disease pathomechanism.<sup>51,70,97</sup>

Finally, another approach aims to diminish CADASIL-associated degeneration of endothelial cells and vascular smooth muscle cells by administration of two hematopoietic growth factors suggested to be neuroprotective, i.e. stem cell factor and granulocyte colony-stimulating factor.<sup>93</sup> Administration of these factors in a CADASIL mouse model resulted in

attenuated mural cell degeneration, increased vascular density, signs of reduced capillary endothelial cells damage, and retained cognition in a CADASIL mouse model.<sup>93,98</sup> However, it remains largely unclear whether the observed therapeutic effects are due to a specific effect of the treatment on CADASIL signs, or due to an aspecific effect not related to CADASIL.

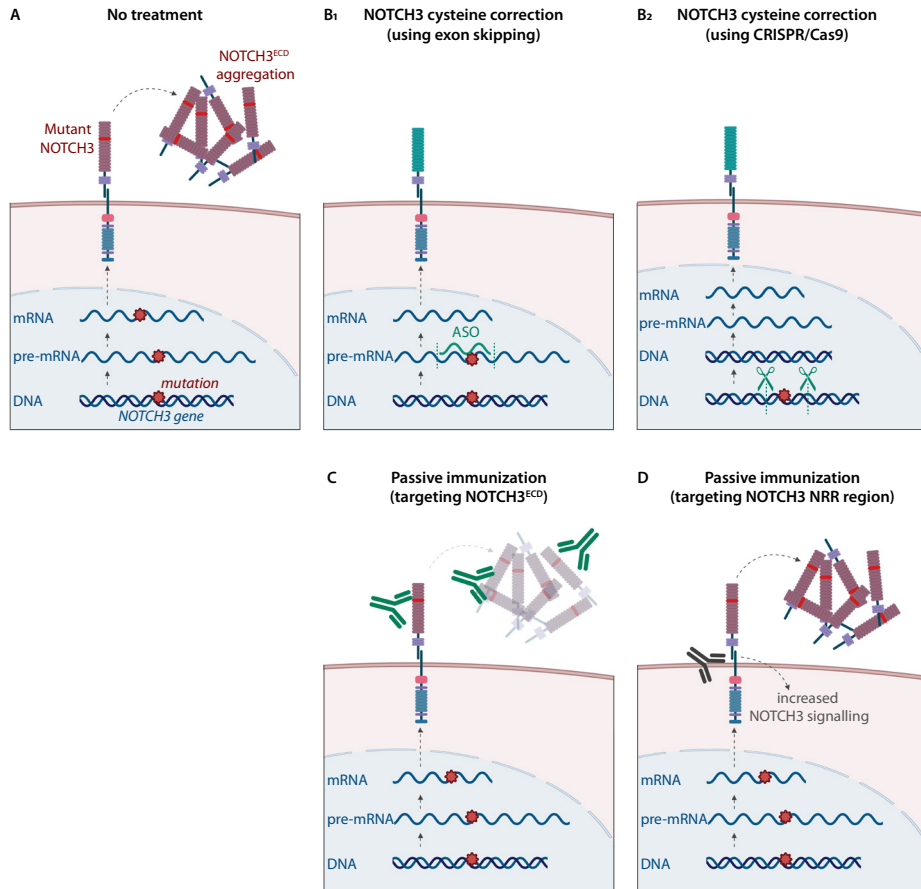


**Figure 1.5: Therapeutic approaches which are currently being developed**

(A) *NOTCH3* gene mutations are translated into mutant NOTCH3<sup>ECD</sup> proteins, leading to NOTCH3<sup>ECD</sup> aggregation. (B) NOTCH3 cysteine correction aims to prevent the formation of mutant NOTCH3<sup>ECD</sup>. Mutant exons are excluded from the mature mRNA using short antisense oligonucleotide strands (ASOs) (B<sub>1</sub>),<sup>94</sup> or are removed from the *NOTCH3* gene using CRISPR/Cas9 (B<sub>2</sub>).<sup>96</sup> (C) Chronic passive immunization with antibodies targeting NOTCH3<sup>ECD</sup> are aimed at counteracting the toxic effect of NOTCH3<sup>ECD</sup> and NOTCH3<sup>ECD</sup> aggregation.<sup>92</sup> (D) Antibodies targeting the negative regulatory region (NRR) of the extracellular NOTCH3 protein are aimed at restoring NOTCH3 signalling in the case of mutations affecting the ligand binding domain.<sup>43</sup>

## CADASIL natural history

Before a therapeutic approach for CADASIL can be tested in clinical trials, information needs to be available on the natural history of CADASIL and the variability in disease progression. This information is required to select a relatively homogeneous patient (sub)group that is most likely to benefit from a potential therapy, and to identify disease measures that can be used as read-out for disease severity and therapeutic benefit.

Previously, follow-up studies of 2, 3 and 7 years were performed in CADASIL patients and controls, showing that lacunes and the level of brain atrophy – and not the extent of WMH – are associated with clinical deterioration, and that lacunes and brain atrophy could potentially be used as surrogate endpoints.<sup>9,99–104</sup> Moreover, signs of advanced CADASIL disease, such as gait disturbances, disability and dementia, are associated with signs of advanced disease on brain MRI and mortality.<sup>19,101,102,105</sup> These follow-up studies analysed disease progression on a group level, rather than studying interindividual differences. Taking this heterogeneity at the individual level into account is important, as there is a large variability in disease severity and progression between families and even between patients within families.

Chapter 4 describes an 18-year follow-up study in CADASIL patients, showing that disease course can remain remarkably stable over 18 years in some patients, and that disease progression is highly variable between patients: some patient had stroke and multiple lacunes before the age of 50 years, while others remained free of stroke and lacunes until well within their sixties.

## Measuring CADASIL disease severity

For future clinical trials, a robust and sensitive read-out to assess disease severity and therapeutic benefit is required in order to get approval from regulators (such as the Food and Drug Administration [FDA, USA] and the European Medicines Agency [EMA]). These regulators will judge whether a therapy is safe to use, has a sufficient efficacy and leads to clinical benefit as experienced by the patients, based on data from clinical trials (on many aspects, including toxicity, pharmacokinetics, pharmacodynamics, dose finding, adverse effects, efficacy and effectiveness). This read-out is required to be able to measure a therapeutic effect in a short time frame, since clinical trials often do not span more than 2 years. In CADASIL, hard endpoints for clinical studies are for example incident stroke, disability, dementia, or survival. A major disadvantage of these hard endpoints is that, due to disease variability, they require large cohorts and a long follow-up in order to observe sufficient events (e.g. number of patients experiencing a stroke) to sufficiently power an interventional study.<sup>106</sup>

Other read-outs, such as biomarkers, could be used as surrogate endpoints, provided that these surrogate endpoints predict future clinical benefit. Biomarkers are defined as ‘objectively measured and evaluated as an indicator of normal biological processes, pathogenic processes or pharmacological responses to a therapeutic intervention’.<sup>107</sup> Several types of biomarkers exist, including diagnostic biomarkers, prognostic biomarkers, monitoring biomarkers and pharmacodynamic biomarkers (Figure 1.6). Especially monitoring and pharmacodynamic biomarkers are imperative to monitor target engagement and to measure efficacy of the therapeutic compound in future clinical trials.

### *Clinical measures*

Measures for functional independence, such as the modified Rankin scale (mRS), and measures for cognitive function, such as the Cambridge Cognitive Examination (CAMCOG), have been reported to change over 2-, 3- or 7-year time span in CADASIL patients.<sup>19,102,106</sup> Furthermore, cognitive tests of specific domains, such as the Trail Making Tests for executive function, have been shown to be associated with an increase in MRI disease markers.<sup>101,109</sup> The disadvantage of clinical measures as monitoring markers, is that large sample sizes would be needed. In that respect, the use of neuroimaging measures would be more advantageous.<sup>106,110</sup>

### *Neuroimaging and cerebrohemodynamic biomarkers*

Promising neuroimaging measures that could be used as monitoring biomarkers are lacune count or lacune volume and brain parenchymal fraction (BPF, brain volume relative to intracranial volume), as they reflect neuronal damage and are strongly associated with clinical deterioration and cognitive impairment in symptomatic CADASIL patients.<sup>9,99–104</sup>

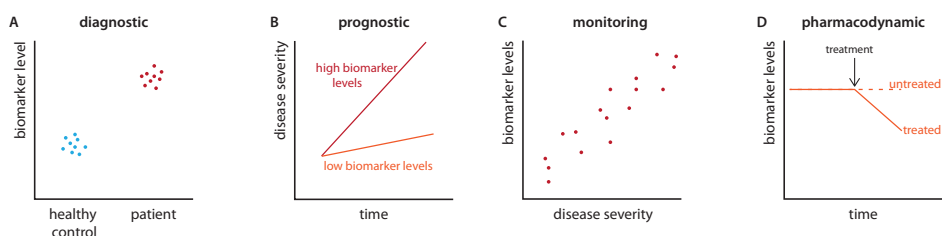


**Figure 1.6: Types of biomarkers**

(A) A diagnostic biomarker can detect or confirm the presence of a disease or a disease subtype. (B) Prognostic biomarkers are used to predict the likelihood of a clinical event, disease recurrence or progression in patients who have a certain disease. (C) A monitoring biomarker is determined serially to assess the status of a disease over time. (D) A pharmacodynamic biomarker is a type of monitoring biomarker that is able to show a biological response after exposure to a (therapeutic) product or agent.<sup>108</sup> Pharmacodynamic biomarkers do not necessarily have to be associated with anticipated future clinical benefit. The term therapeutic biomarkers is sometimes used to indicate a monitoring biomarker that shows a response after therapy that is anticipated to give clinical benefit.

WMH volume does not correlate with disease severity or disease progression, and therefore does not fulfill the criteria for surrogate marker.<sup>101–104</sup> Diffusion Tensor Imaging (DTI), which measures the microstructural integrity of the brain, has been shown to change over time in normal appearing white matter of CADASIL patients, correlating with cognitive function.<sup>111–114</sup> Most, but not all, studies have reported a reduction in resting cerebral blood flow (CBF) and cerebrovascular reactivity (CVR) in CADASIL patients<sup>115–117</sup> and CADASIL mouse models.<sup>86,118,119</sup>

The disadvantage of MRI-based markers is that MRI is relatively expensive, time consuming and often non-uniform across different sites.

#### *Fluid biomarkers*

A monitoring biomarker in blood could be a good alternative to MRI markers, as blood is easily accessible, blood withdrawal is minimally invasive, can be repeated at multiple time-points, is relatively cheap and can be uniformly analysed at one study site. A blood biomarker that reflects neuronal damage is Neurofilament Light-chain (NfL).<sup>120</sup> Serum NfL levels reflect active small vessel disease and could therefore also be promising as a biomarker for symptomatic CADASIL patients.<sup>121,122</sup> Other potential blood biomarkers for CADASIL that were identified in pre-clinical studies are levels of Notch3, Endostatin, Htra1 and Igf-bp1, as blood levels of these proteins were different between a CADASIL mouse model and wildtype mice.<sup>43,123</sup> These proteins, together with TGF- $\beta$ -associated proteins, have also been found to be highly abundant in blood vessel walls of CADASIL patients.<sup>68,71</sup> Biomarkers in other fluids, such as the cerebrospinal fluid (CSF), have not been studied extensively.<sup>124–126</sup>

Chapter 4 describes a cross-sectional study of blood-based biomarkers, as well as a longitudinal analysis of cerebrovascular hemodynamics in CADASIL patients and controls. Chapter 5 describes that serum NfL levels in CADASIL patients correlate with disease severity, disease progression and survival. Chapter 4 describes a longitudinal analysis of serum NfL over 18 years in CADASIL patients.

## Scope of this thesis

The aim of this PhD-project was to advance CADASIL therapy development, including natural history and biomarker identification. By analyzing a family with naturally occurring *NOTCH3* exon skipping, the first in-human evidence was obtained supporting the hypothesis that 'NOTCH3 cysteine correction' is associated with attenuated NOTCH3 protein aggregation, providing further rational for advancing this therapeutic approach.. An ultrastructural biomarker, a GOM deposit classification system, was developed in the transgenic human *NOTCH3*<sup>Arg182Cys</sup> CADASIL mouse model that can be used as a monitoring or therapeutic marker in pre-clinical therapeutic studies. Further functional characterization of this mouse model was performed to explore other potential pre-clinical biomarkers. In CADASIL patients, multiple candidate blood biomarkers were tested, leading to the identification of Neurofilament Light-chain (NfL) as a biomarker for CADASIL disease severity. The longest follow-up study performed in CADASIL patients to date led to the observation that a subset of patients remain clinically remarkably stable over the course of almost two decades.

## Overview of chapters in this thesis

- In chapter 2, the development of a GOM deposit classification system is described, as well as functional characterisation of the Leiden human *NOTCH3* transgenic mouse model.<sup>90</sup>
- In chapter 3, the first in-human evidence is provided supporting the hypothesis that *NOTCH3* exon skipping reduces mutant NOTCH3<sup>ECD</sup> protein aggregation, and is associated with a milder CADASIL phenotype.<sup>96</sup>
- In chapter 4, a prospective 18-year follow-up study of CADASIL patients is described, showing that disease course can remain relatively stable over almost two decades, and blood biomarkers for CADASIL are evaluated.
- In chapter 5, Neurofilament Light (NfL) levels in blood of CADASIL patients are shown to be associated with disease severity and may therefore function as a biomarker for CADASIL.<sup>127</sup>
- In chapter 6, the findings of the research presented in this thesis are discussed, as well as the implications for future therapy development.

## REFERENCES

- Chabriat, Joutel, Dichgans, Tournier-Lasserre, & Bousser. Cadasil. *Lancet. Neurol.* 8, 643–653 (2009).
- Joutel, Corpechot, Ducros, *et al.* Notch3 mutations in CADASIL, a hereditary adult-onset condition causing stroke and dementia. *Nature* 383, 707–710 (1996).
- Razvi, Davidson, Bone, & Muir. The prevalence of cerebral autosomal dominant arteriopathy with subcortical infarcts and leucoencephalopathy (CADASIL) in the west of Scotland. *J. Neurol. Neurosurg. Psychiatry* 76, 739–741 (2005).
- Kalimo, Ruchoux, Viitanen, & Kalaria. CADASIL: a Common Form of Hereditary Arteriopathy Causing Brain Infarcts and Dementia. *Brain Pathol.* 12, 371–384 (2006).
- Narayan, Gorman, Kalaria, Ford, & Chinnery. The minimum prevalence of CADASIL in northeast England. *Neurology* 78, 1025–1027 (2012).
- Bianchi, Zicari, Carluccio, *et al.* CADASIL in central Italy: a retrospective clinical and genetic study in 229 patients. *J. Neurol.* 262, 134–141 (2015).
- Dichgans, Mayer, Uttner, *et al.* The phenotypic spectrum of CADASIL: Clinical findings in 102 cases. *Ann. Neurol.* 44, 731–739 (1998).
- Desmond, Moroney, Lynch, *et al.* The natural history of CADASIL: A pooled analysis of previously published cases. *Stroke* 30, 1230–1233 (1999).
- Opherk, Peters, Herzog, Luedtke, & Dichgans. Long-term prognosis and causes of death in CADASIL: A retrospective study in 411 patients. *Brain* 127, 2533–2539 (2004).
- Adib-Samii, Brice, Martin, & Markus. Clinical spectrum of CADASIL and the effect of cardiovascular risk factors on phenotype: Study in 200 consecutively recruited individuals. *Stroke* 41, 630–634 (2010).
- Tan, & Markus. CADASIL: Migraine, encephalopathy, stroke and their inter-relationships. *PLoS One* 11, 1–14 (2016).
- Lee, Liu, Chang, *et al.* Population-specific spectrum of NOTCH3 mutations, MRI features and founder effect of CADASIL in Chinese. *J. Neurol.* 256, 249–255 (2009).
- Di Donato, Bianchi, De Stefano, *et al.* Cerebral Autosomal Dominant Arteriopathy with Subcortical Infarcts and Leukoencephalopathy (CADASIL) as a model of small vessel disease: update on clinical, diagnostic, and management aspects. *BMC Med.* 15, 41 (2017).
- Amberla, Wäljas, Tuominen, *et al.* Insidious cognitive decline in CADASIL. *Stroke* 35, 1598–1602 (2004).
- Buffon, Porcher, Hernandez, *et al.* Cognitive profile in CADASIL. *J. Neurol. Neurosurg. Psychiatry* 77, 175–80 (2006).
- Charlton, Morris, Nitkunan, & Markus. The cognitive profiles of CADASIL and sporadic small vessel disease. *Neurology* 66, 1523–1526 (2006).
- Peters, Opherk, Danek, *et al.* The pattern of cognitive performance in CADASIL: A monogenic condition leading to subcortical ischemic vascular dementia. *Am. J. Psychiatry* 162, 2078–2085 (2005).
- Taillia, Chabriat, Kurtz, *et al.* Cognitive alterations in non-demented CADASIL patients. *Cerebrovasc. Dis.* 8, 97–101 (1998).
- Liem, Haan, Neut, *et al.* MRI correlates of cognitive decline in CADASIL. *Neurology* 72, 143–148 (2009).
- Guey, Mawet, Hervé, *et al.* Prevalence and characteristics of migraine in CADASIL. *Cephalalgia* 36, 1038–1047 (2016).
- Singhal, Rich, & Markus. The spatial distribution of MR imaging abnormalities in cerebral autosomal dominant arteriopathy with subcortical infarcts and leukoencephalopathy and their relationship to age and clinical features. *Am. J. Neuroradiol.* 26, 2481–2487 (2005).
- van den Boom, Lesnik Oberstein, Ferrari, Haan, & van Buchem. Cerebral autosomal dominant arteriopathy with subcortical infarcts and leukoencephalopathy: MR imaging findings at different ages--3rd-6th decades. *Radiology* 229, 683–690 (2003).
- Chabriat, Levy, Taillia, *et al.* Patterns of MRI lesions in CADASIL. *Neurology* 51, 452–457 (1998).
- van den Boom, Lesnik Oberstein, van Duinen, *et al.* Subcortical Lacunar Lesions: An MR Imaging Finding in Patients with Cerebral Autosomal Dominant Arteriopathy with Subcortical Infarcts and Leukoencephalopathy. *Radiology* 224, 791–796 (2002).
- Wardlaw, Smith, Biessels, *et al.* Neuroimaging standards for research into small vessel disease and its contribution to ageing and neurodegeneration. *Lancet. Neurol.* 12, 822–38 (2013).
- Lesnik Oberstein, van den Boom, Middelkoop, *et al.* Incipient CADASIL. *Arch. Neurol.* 60, 707–12 (2003).
- O'Sullivan, Jarosz, Martin, *et al.* MRI hyperintensities

- of the temporal lobe CADASIL. *Neurology* 56, 628–634 (2001).
28. Choi, Kang, Kang, & Park. Intracerebral hemorrhages in CADASIL. *Neurology* 67, 2042–2044 (2006).
  29. Markus, Martin, Simpson, *et al.* Diagnostic strategies in CADASIL. *Neurology* 59, 1134–1138 (2002).
  30. Liem, Lesnik Oberstein, Haan, *et al.* Cerebral autosomal dominant arteriopathy with subcortical infarcts and leukoencephalopathy: progression of MR abnormalities in prospective 7-year follow-up study. *Radiology* 249, 964–71 (2008).
  31. Cumurciuc, Guichard, Reizine, *et al.* Dilatation of Virchow-Robin spaces in CADASIL. *Eur. J. Neurol.* 13, 187–190 (2006).
  32. Dichgans, Holtmannspötter, Herzog, *et al.* Cerebral microbleeds in CADASIL: A gradient-echo magnetic resonance imaging and autopsy study. *Stroke* 33, 67–71 (2002).
  33. Lesnik Oberstein, van den Boom, van Buchem, *et al.* Cerebral Microbleeds in CADASIL. *Neurology* 57, 1066–1070 (2001).
  34. Gautam, & Yao. Roles of Pericytes in Stroke Pathogenesis. 1–11 (2018). doi:10.1177/0963689718768455
  35. Lee, Kang, Park, Choi, & Sim. Clinical significance of cerebral microbleeds locations in CADASIL with R544C NOTCH3 mutation. *PLoS One* 10, 1–9 (2015).
  36. Joutel, Corpechot, Ducros, *et al.* Notch3 mutations in CADASIL, a hereditary adult-onset condition causing stroke and dementia. *Nature* 383, 707–710 (1996).
  37. Joutel, Vahedi, Corpechot, *et al.* Strong clustering and stereotyped nature of Notch3 mutations in CADASIL patients. *Lancet* 350, 1511–5 (1997).
  38. Irvin, Zurcher, Nguyen, Weinmaster, & Kornblum. Expression patterns of Notch1, Notch2, and Notch3 suggest multiple functional roles for the Notch-DSL signaling system during brain development. *J. Comp. Neurol.* 436, 167–181 (2001).
  39. Wang, Pan, Moens, & Appel. Notch3 establishes brain vascular integrity by regulating pericyte number. *Development* 141, 307–317 (2014).
  40. Andersson, & Lendahl. Therapeutic modulation of Notch signalling — are we there yet? *Nat. Publ. Gr.* 13, 357–378 (2014).
  41. Domenga, Fardoux, Lacombe, *et al.* Notch3 is required for arterial identity and maturation of vascular smooth muscle cells. *Genes Dev.* 18, 2730–5 (2004).
  42. Henshall, Keller, He, *et al.* Notch3 is necessary for blood vessel integrity in the central nervous system. *Arterioscler. Thromb. Vasc. Biol.* 35, 409–20 (2015).
  43. Machuca-Parra, Bigger-Allen, Sanchez, *et al.* Therapeutic antibody targeting of Notch3 signaling prevents mural cell loss in CADASIL. *J. Exp. Med.* 214, 2271–2282 (2017).
  44. Ando, Wang, Peng, *et al.* Peri-arterial specification of vascular mural cells from naïve mesenchyme requires Notch signaling. *Development* dev.165589 (2019). doi:10.1242/dev.165589
  45. Joutel, Corpechot, Ducros, *et al.* Notch3 mutations in cerebral autosomal dominant arteriopathy with subcortical infarcts and leukoencephalopathy (CADASIL), a mendelian condition causing stroke and vascular dementia. *Ann. N. Y. Acad. Sci.* 826, 213–217 (1997).
  46. Rutten, Haan, Terwindt, *et al.* Interpretation of NOTCH3 mutations in the diagnosis of CADASIL. *Expert Rev. Mol. Diagn.* 14, 593–603 (2014).
  47. Dichgans, Ludwig, Müller-Höcker, Messerschmidt, & Gasser. Small in-frame deletions and missense mutations in CADASIL: 3D models predict misfolding of Notch3 EGF-like repeat domains. *Eur. J. Hum. Genet.* 8, 280–285 (2000).
  48. Cognat, Baron-Menguy, Domenga-Denier, *et al.* Archetypal Arg169Cys Mutation in NOTCH3 Does Not Drive the Pathogenesis in Cerebral Autosomal Dominant Arteriopathy With Subcortical Infarcts and Leukoencephalopathy via a Loss-of-Function Mechanism. *Stroke* 45, 842–849 (2014).
  49. Opherk, Duering, Peters, *et al.* CADASIL mutations enhance spontaneous multimerization of NOTCH3. *Hum. Mol. Genet.* 18, 2761–2767 (2009).
  50. Karlström, Beatus, Dannaeus, *et al.* A CADASIL-mutated Notch 3 receptor exhibits impaired intracellular trafficking and maturation but normal ligand-induced signaling. *Proc. Natl. Acad. Sci. U. S. A.* 99, 17119–17124 (2002).
  51. Rutten, Van Eijsden, Duering, *et al.* The effect of NOTCH3 pathogenic variant position on CADASIL disease severity: NOTCH3 EGF1 1–6 pathogenic variant are associated with a more severe phenotype and lower survival compared with EGF1 7–34 pathogenic variant. *Genet. Med.* 21, 676–682 (2019).
  52. Peters, Opherk, Zacherle, *et al.* CADASIL-associated Notch3 mutations have differential effects both on ligand binding and ligand-induced Notch3 receptor signaling through RBP-Jk. *Exp. Cell Res.* 299, 454–464 (2004).
  53. Joutel, Monet, Domenga, Riant, & Tournier-Lasserre. Pathogenic mutations associated with

- cerebral autosomal dominant arteriopathy with subcortical infarcts and leukoencephalopathy differently affect Jagged1 binding and Notch3 activity via the RBP/JK signaling Pathway. *Am J Hum Genet* 74, 338–347 (2004).
54. Mašek, & Andersson. The developmental biology of genetic Notch disorders. *Development* 144, 1743–1763 (2017).
  55. van Tetering, & Vooijs. Proteolytic cleavage of Notch: 'HIT and RUN'. *Curr. Mol. Med.* 11, 255–69 (2011).
  56. Andersson, Sandberg, & Lendahl. Notch signaling: Simplicity in design, versatility in function. *Development* 138, 3593–3612 (2011).
  57. Haritunians, Boulter, Hicks, *et al.* CADASIL Notch3 mutant proteins localize to the cell surface and bind ligand. *Circ. Res.* 90, 506–508 (2002).
  58. Joutel, Andreux, Gaulis, *et al.* The ectodomain of the Notch3 receptor accumulates within the cerebrovasculature of CADASIL patients. *J. Clin. Invest.* 105, 597–605 (2000).
  59. Duering, Karpinska, Rosner, *et al.* Co-aggregate formation of CADASIL-mutant NOTCH3: a single-particle analysis. *Hum. Mol. Genet.* 20, 3256–65 (2011).
  60. Joutel, Favrole, Labauge, *et al.* Skin biopsy immunostaining with a Notch3 monoclonal antibody for CADASIL diagnosis. *Lancet* 358, 2049–2051 (2001).
  61. Lesnik Oberstein, van Duinen, van den Boom, *et al.* Evaluation of diagnostic NOTCH3 immunostaining in CADASIL. *Acta Neuropathol.* 106, 107–111 (2003).
  62. Ruchoux, Guerouaou, Vandehaute, *et al.* Systemic vascular smooth muscle cell impairment in cerebral autosomal dominant arteriopathy with subcortical infarcts and leukoencephalopathy. *Acta Neuropathol.* 89, 500–512 (1995).
  63. Ruchoux, Domenga, Brulin, *et al.* Transgenic Mice Expressing Mutant Notch3 Develop Vascular Alterations Characteristic of Cerebral Autosomal Dominant Arteriopathy with Subcortical Infarcts and Leukoencephalopathy. *Am. J. Pathol.* 162, 329–342 (2003).
  64. Tikka, Mykknen, Ruchoux, *et al.* Congruence between NOTCH3 mutations and GOM in 131 CADASIL patients. *Brain* 132, 933–939 (2009).
  65. Lewandowska, Dziewulska, Parys, & Pasennik. Ultrastructure of granular osmiophilic material deposits (GOM) in arterioles of CADASIL patients. *Folia Neuropathol.* 49, 174–80 (2011).
  66. Morroni, Marzioni, Ragno, *et al.* Role of Electron Microscopy in the Diagnosis of Cadasil Syndrome: A Study of 32 Patients. *PLoS One* 8, 6–11 (2013).
  67. Brulin, Godfraind, Leteurtre, & Ruchoux. Morphometric analysis of ultrastructural vascular changes in CADASIL: analysis of 50 skin biopsy specimens and pathogenic implications. *Acta Neuropathol.* 104, 241–8 (2002).
  68. Kast, Hanecker, Beaufort, *et al.* Sequestration of latent TGF- $\beta$  binding protein 1 into CADASIL-related Notch3-ECD deposits. *Acta Neuropathol. Commun.* 2, 1–12 (2014).
  69. Monet-Leprêtre, Haddad, Baron-Menguy, *et al.* Abnormal recruitment of extracellular matrix proteins by excess Notch3 ECD: A new pathomechanism in CADASIL. *Brain* 136, 1830–1845 (2013).
  70. Arboleda-Velasquez, Manent, Lee, *et al.* Hypomorphic Notch 3 alleles link Notch signaling to ischemic cerebral small-vessel disease. *Proc. Natl. Acad. Sci.* 108, E128–E135 (2011).
  71. Zellner, Scharrer, Arzberger, *et al.* CADASIL brain vessels show a HTRA1 loss - of - function profile. *Acta Neuropathol.* (2018). doi:10.1007/s00401-018-1853-8
  72. Capone, Cognat, Ghezali, *et al.* Reducing Timp3 or vitronectin ameliorates disease manifestations in CADASIL mice. *Ann. Neurol.* 79, 387–403 (2016).
  73. Capone, Dabertrand, Baron-Menguy, *et al.* Mechanistic insights into a TIMP3-sensitive pathway constitutively engaged in the regulation of cerebral hemodynamics. *Elife* 5, 1–26 (2016).
  74. Kalimo, Viitanen, Amberla, *et al.* CADASIL: Hereditary disease of arteries causing brain infarcts and dementia. *Neuropathol. Appl. Neurobiol.* 25, 257–265 (1999).
  75. Miao, Paloneva, Tuisku, *et al.* Arterioles of the lenticular nucleus in CADASIL. *Stroke* 37, 2242–2247 (2006).
  76. Gatti, Zhang, Korcari, *et al.* Redistribution of Mature Smooth Muscle Markers in Brain Arteries in Cerebral Autosomal Dominant Arteriopathy with Subcortical Infarcts and Leukoencephalopathy. *Transl. Stroke Res.* 10, 160–169 (2019).
  77. Yamamoto, Ihara, Tham, *et al.* Neuropathological correlates of temporal pole white matter hyperintensities in CADASIL. *Stroke* 40, 2004–2011 (2009).
  78. Dong, Ding, Young, *et al.* Advanced intimal hyperplasia without luminal narrowing of leptomeningeal arteries in CADASIL. *Stroke* 44, 1456–1458 (2013).
  79. Rajani, Ratelade, Domenga-Denier, *et al.* Blood

- brain barrier leakage is not a consistent feature of white matter lesions in CADASIL. *Acta Neuropathol. Commun.* 7, 187 (2019).
80. Yamamoto, Craggs, Watanabe, *et al.* Brain microvascular accumulation and distribution of the NOTCH3 ectodomain and granular osmiophilic material in CADASIL. *J. Neuropathol. Exp. Neurol.* 72, 416–431 (2013).
  81. Müller, Courtois, Ursini, & Schwaninger. New Insight Into the Pathogenesis of Cerebral Small-Vessel Diseases. *Stroke* STROKEAHA.116.012888 (2017). doi:10.1161/STROKEAHA.116.012888
  82. Ikawati, Kawaichi, & Oka. Loss of HtrA1 serine protease induces synthetic modulation of aortic vascular smooth muscle cells. 1–22 (2018).
  83. Monet, Domenga, Lemaire, *et al.* The archetypal R90C CADASIL-NOTCH3 mutation retains NOTCH3 function in vivo. *Hum. Mol. Genet.* 16, 982–992 (2007).
  84. Gu, Liu, Fagan, Gonzalez-Toledo, & Zhao. Ultrastructural Changes in Cerebral Capillary Pericytes in Aged Notch3 Mutant Transgenic Mice. *Ultrastruct. Pathol.* 36, 48–55 (2012).
  85. Monet-Lepretre, Bardot, Lemaire, *et al.* Distinct phenotypic and functional features of CADASIL mutations in the Notch3 ligand binding domain. *Brain* 132, 1601–1612 (2009).
  86. Joutel, Monet-Leprêtre, Gosele, *et al.* Cerebrovascular dysfunction and microcirculation rarefaction precede white matter lesions in a mouse genetic model of cerebral ischemic small vessel disease. *J. Clin. Invest.* 120, 433–445 (2010).
  87. Ehret, Vogler, Pojar, *et al.* Mouse model of CADASIL reveals novel insights into Notch3 function in adult hippocampal neurogenesis. *Neurobiol. Dis.* 75, 131–141 (2015).
  88. Wallays, Nuyens, Silasi-Mansat, *et al.* Notch3 Arg170Cys knock-in mice display pathologic and clinical features of the neurovascular disorder cerebral autosomal dominant arteriopathy with subcortical infarcts and leukoencephalopathy. *Arterioscler. Thromb. Vasc. Biol.* 31, 2881–2888 (2011).
  89. Rutten, Klever, Hegeman, *et al.* The NOTCH3 score: a pre-clinical CADASIL biomarker in a novel human genomic NOTCH3 transgenic mouse model with early progressive vascular NOTCH3 accumulation. *Acta Neuropathol. Commun.* 3, 89 (2015).
  90. Gravesteyn, Munting, Overzier, *et al.* Progression and Classification of Granular Osmiophilic Material (GOM) Deposits in Functionally Characterized Human NOTCH3 Transgenic Mice. *Transl. Stroke Res.* 11, 517–527 (2020).
  91. Rutten. NOTCH3 cysteine correction : Developing a rational therapeutic approach for CADASIL. 1–195 (2016).
  92. Ghezali, Capone, Baron-Menguy, *et al.* Notch3 ECD immunotherapy improves cerebrovascular responses in CADASIL mice. *Ann. Neurol.* 84, 246–259 (2018).
  93. Liu, Gonzalez-Toledo, Fagan, *et al.* Stem cell factor and granulocyte colony-stimulating factor exhibit therapeutic effects in a mouse model of CADASIL. *Neurobiol. Dis.* 73, 189–203 (2015).
  94. Rutten, Dauwerse, Peters, *et al.* Therapeutic NOTCH3 cysteine correction in CADASIL using exon skipping: In vitro proof of concept. *Brain* 139, 1123–1135 (2016).
  95. Papasava, Kleanthous, & Lederer. Rare Opportunities: CRISPR/Cas-Based Therapy Development for Rare Genetic Diseases. *Mol. Diagnosis Ther.* 23, 201–222 (2019).
  96. Gravesteyn, Dauwerse, Overzier, *et al.* Naturally occurring NOTCH3 exon skipping attenuates NOTCH3 protein aggregation and disease severity in CADASIL patients. *Hum. Mol. Genet.* (2020). doi:10.1093/hmg/ddz285
  97. Moccia, Mosca, Erro, *et al.* Hypomorphic NOTCH3 mutation in an Italian family with CADASIL features. *Neurobiol. Aging* 36, 547.e5–11 (2015).
  98. Ping, Qiu, Gonzalez-Toledo, Liu, & Zhao. Stem Cell Factor in Combination with Granulocyte Colony-Stimulating Factor reduces Cerebral Capillary Thrombosis in a Mouse Model of CADASIL. *Cell Transplant.* 27, 637–647 (2018).
  99. Ling, De Guio, Jouvent, *et al.* Clinical correlates of longitudinal MRI changes in CADASIL. *J. Cereb. Blood Flow Metab.* 39, 1299–1305 (2019).
  100. Peters, Holtmannspötter, Opherk, *et al.* Brain volume changes in CADASIL: A serial MRI study in pure subcortical ischemic vascular disease. *Neurology* 66, 1517–1522 (2006).
  101. Ling, De Guio, Duering, *et al.* Predictors and Clinical Impact of Incident Lacunes in Cerebral Autosomal Dominant Arteriopathy With Subcortical Infarcts and Leukoencephalopathy. *Stroke* 48, 283–289 (2017).
  102. Chabriat, Hervé, Duering, *et al.* Predictors of clinical worsening in cerebral autosomal dominant arteriopathy with subcortical infarcts and leukoencephalopathy: Prospective cohort study. *Stroke* 47, 4–11 (2016).
  103. Jouvent, Duchesnay, Hadj-Selem, *et al.* Prediction of 3-year clinical course in CADASIL. *Neurology* 87, 1787–1795 (2016).

104. Liem, Van Der Grond, Haan, *et al.* Lacunar infarcts are the main correlate with cognitive dysfunction in CADASIL. *Stroke* 38, 923–928 (2007).
105. Duering, Csanadi, Gesierich, *et al.* Incident lacunes preferentially localize to the edge of white matter hyperintensities: insights into the pathophysiology of cerebral small vessel disease. *Brain* 136, 2717–2726 (2013).
106. Peters, Herzog, Opherk, & Dichgans. A two-year clinical follow-up study in 80 CADASIL subjects: Progression patterns and implications for clinical trials. *Stroke* 35, 1603–1608 (2004).
107. Atkinson, Colburn, DeGruttola, *et al.* Biomarkers and surrogate endpoints: Preferred definitions and conceptual framework. *Clin. Pharmacol. Ther.* 69, 89–95 (2001).
108. FDA-NIH Biomarker Working Group. *BEST (Biomarkers, EndpointS, and other Tools)*. Silver Spring (MD): Food and Drug Administration (US); Bethesda (MD): NIH (US) (2016).
109. Ling, Liu, Song, *et al.* Modeling CADASIL vascular pathologies with patient-derived induced pluripotent stem cells. *Protein Cell* 10, 249–271 (2019).
110. Benjamin, Zeestraten, Lambert, *et al.* Progression of MRI markers in cerebral small vessel disease: Sample size considerations for clinical trials. *J. Cereb. Blood Flow Metab.* 36, 228–240 (2016).
111. Benjamin, Zeestraten, Lambert, *et al.* Progression of MRI markers in cerebral small vessel disease: Sample size considerations for clinical trials. *J. Cereb. Blood Flow Metab.* 36, 228–240 (2016).
112. Holtmannspötter, Peters, Opherk, *et al.* Diffusion magnetic resonance histograms as a surrogate marker and predictor of disease progression in CADASIL a two-year follow-up study. *Stroke* 36, 2559–2565 (2005).
113. Ban, Wang, & Qin. Diffuse Tract Damage in CADASIL Is Correlated with Global Cognitive Impairment. 200011, (2019).
114. Baykara, Gesierich, Adam, *et al.* A Novel Imaging Marker for Small Vessel Disease Based on Skeletonization of White Matter Tracts and Diffusion Histograms. *Ann. Neurol.* 80, 581–592 (2016).
115. Pfefferkorn, von Stuckrad-Barre, Herzog, *et al.* Reduced cerebrovascular CO<sub>2</sub> reactivity in CADASIL: A transcranial Doppler sonography study. *Stroke* 32, 17–21 (2001).
116. Chabriat, Pappata, Ostergaard, *et al.* Cerebral hemodynamics in CADASIL before and after acetazolamide challenge assessed with MRI bolus tracking. *Stroke* 31, 1904–1912 (2000).
117. Huneau, Houot, Joutel, *et al.* Altered dynamics of neurovascular coupling in CADASIL. *Ann. Clin. Transl. Neurol.* 5, 788–802 (2018).
118. Lacombe, Oligo, Domenga, Tournier-Lasserre, & Joutel. Impaired Cerebral Vasoreactivity in a Transgenic Mouse Model of Cerebral Autosomal Dominant Arteriopathy With Subcortical Infarcts and Leukoencephalopathy Arteriopathy. *Stroke* 36, 1053–1058 (2005).
119. Ghosh, Balbi, Hellal, *et al.* Pericytes are involved in the pathogenesis of cerebral autosomal dominant arteriopathy with subcortical infarcts and leukoencephalopathy. *Ann. Neurol.* 78, 887–900 (2015).
120. Gaetani, Blennow, Calabresi, *et al.* Neurofilament light chain as a biomarker in neurological disorders. *J. Neurol. Neurosurg. Psychiatry* 870–881 (2019). doi:10.1136/jnnp-2018-320106
121. Gattringer, Pinter, Enzinger, *et al.* Serum neurofilament light is sensitive to active cerebral small vessel disease. *Neurology* 89, 2108–2114 (2017).
122. Duering, Konieczny, Tiedt, *et al.* Serum Neurofilament Light Chain Levels Are Related to Small Vessel Disease Burden. *J. Stroke* 20, 228–238 (2018).
123. Primo, Graham, Bigger-Allen, *et al.* Blood biomarkers in a mouse model of CADASIL. *Brain Res.* 1644, 118–126 (2016).
124. Dichgans, Wick, & Gasser. Cerebrospinal fluid findings in CADASIL. *Neurology* 53, 233 (1999).
125. Formichi, Parnetti, Radi, *et al.* CSF levels of  $\beta$ -amyloid<sub>1-42</sub>, tau and phosphorylated tau protein in CADASIL. *Eur. J. Neurol.* 15, 1252–55 (2008).
126. Unlü, de Lange, de Silva, Kalara, & St Clair. Detection of complement factor B in the cerebrospinal fluid of patients with cerebral autosomal dominant arteriopathy with subcortical infarcts and leukoencephalopathy disease using two-dimensional gel electrophoresis and mass spectrometry. *Neurosci. Lett.* 282, 149–52 (2000).
127. Gravesteijn, Rutten, Verberk, *et al.* Serum Neurofilament light correlates with CADASIL disease severity and survival. *Ann. Clin. Transl. Neurol.* 6, 46–56 (2019).





# Chapter 2

## Progression and classification of granular osmiophilic material (GOM) deposits in functionally characterized human *NOTCH3* transgenic mice

Gido Gravesteijn  
Leon P. Munting  
Maurice Overzier  
Aat A. Mulder  
Ingrid Hegeman  
Marc Derieppe  
Abraham J. Koster  
Sjoerd G. van Duinen  
Onno C. Meijer  
Annemieke Aartsma-Rus  
Louise van der Weerd  
Carolina R. Jost  
Arn M.J.M. van den Maagdenberg  
Julie W. Rutten\*  
Saskia A.J. Lesnik Oberstein\*

## ABSTRACT

CADASIL is a *NOTCH3*-associated cerebral small vessel disease. A pathological ultrastructural disease hallmark is the presence of *NOTCH3*-protein containing deposits called granular osmiophilic material (GOM), in small arteries. How these GOM deposits develop over time and what their role is in disease progression is largely unknown. Here, we studied the progression of GOM deposits in humanized transgenic *NOTCH3*<sup>Arg182Cys</sup> mice, compared them to GOM deposits in patient material, and determined whether GOM deposits in mice are associated with a functional CADASIL phenotype. We found that GOM deposits are not static, but rather progress in ageing mice, both in terms of size and aspect. We devised a GOM classification system, reflecting size, morphology and electron density. Six-month-old mice showed mostly early stage GOM, whereas older mice and patient vessels showed predominantly advanced stage GOM, but also early stage GOM. Mutant mice did not develop the most severe GOM stage seen in patient material. This absence of end-stage GOM in mice was associated with an overall lack of histological vascular pathology, which may explain why the mice did not reveal functional deficits in cerebral blood flow, cognition and motor function. Taken together, our data indicate that GOM progress over time, and that new GOM deposits are continuously being formed. The GOM staging system we introduce here allows for uniform GOM deposit classification in future mouse and human studies, which may lead to more insight into a potential association between GOM stage and CADASIL disease severity, and the role of GOM in disease progression.

## INTRODUCTION

Deposition of granular osmiophilic material (GOM) is the vascular pathological hallmark of CADASIL, which is the most prevalent hereditary small vessel disease<sup>1</sup> and is caused by missense mutations in the *NOTCH3* gene.<sup>2,3</sup> GOM have been shown to contain NOTCH3 ectodomain (NOTCH3<sup>ECD</sup>) and extracellular matrix proteins,<sup>4–6</sup> and can be visualized ultrastructurally in the tunica media of small arteries and capillaries. These electron dense GOM deposits are located in the basement membrane of mural cells, i.e. vascular smooth muscle cells and pericytes.<sup>7–11</sup> In both manifest and pre-manifest CADASIL patients, GOM deposits are present not only in brain vessels, but also in vessels of other organs, such as the skin.<sup>11–13</sup> Other CADASIL-associated vascular pathology includes mural cell degeneration, smooth muscle actin (SMA)-positive (neo)intima formation, fibrosis, and vessel wall thickening.<sup>14–19</sup> These vascular alterations are associated with compromised cerebrovascular reactivity (CVR)<sup>20,21</sup> and reduced cerebral blood flow (CBF), and eventually lead to mid-adult onset of recurrent strokes, vascular cognitive impairment and ultimately dementia.<sup>1</sup> Brain MRI reveals progressive symmetrical white matter hyperintensities, lacunes, microbleeds and brain atrophy.<sup>1</sup>

We have previously described that our humanized CADASIL transgenic *NOTCH3*<sup>Arg182Cys</sup> mouse model, which overexpresses human mutant NOTCH3 protein from a genomic construct, shows granular NOTCH3<sup>ECD</sup> immunostaining as early as 4 weeks of age, while GOM deposits first appear around 6 months of age.<sup>22</sup> However, little is known about how GOM deposits evolve over time and what their relation is to other CADASIL-associated vascular pathology and vascular dysfunction. Here, we performed a longitudinal study of GOM pathology in the transgenic *NOTCH3*<sup>Arg182Cys</sup> mice. In addition, we assessed cerebrovascular, motor and cognitive function in these mice.

## METHODS

### Mice

Transgenic mice were used that harbour the human full length *NOTCH3* gene (located on a 143 kb BAC construct) in either the wildtype or the mutant (c.544C>T, p.Arg182Cys) form, generated on a C57BL/6J background.<sup>22</sup> Mice were bred at the animal facility of the Leiden University Medical Center and housed individually under standard conditions, i.e. a 12-hour light/dark cycle with food and water available *ad libitum*.

Three different mouse strains were used, with various human *NOTCH3* expression levels: 100% for wildtype mice (tgN3<sup>WT100</sup>), and 100% and 350% for mutant mice (tgN3<sup>MUT100</sup> and tgN3<sup>MUT350</sup>, respectively).<sup>22</sup> Non-transgenic littermates were used as additional controls. A prospective study with 6-8 mice per group was performed to study body weight and motor function at various time points (1.5, 3, 6, 12, 16 and 20 months) and cerebral hemodynamics, cognition and immunohistochemical staining was studied at 20 months. Three mice had to be sacrificed before the end of the study; one due to an eye infection (tgN3<sup>WT100</sup>, at 15 months), one due to having a wound on its back (tgN3<sup>MUT350</sup>, at 19 months), and one due to low body weight (tgN3<sup>MUT100</sup>, at 20 months). In addition to the prospective study, tgN3<sup>MUT350</sup> mice were sacrificed at the age of 1.5 (n=1), 3 (n=1), 6 (n=2), 12 (n=2) and 20 (n=2) months for electron microscopy (EM) studies.

### Electron microscopy

In addition to mouse brain, post-mortem brain tissue was obtained from three CADASIL patients (deceased at age 59, 66, and 69 years) for comparison with human pathology. Mouse (frontal lobe grey matter) and human (frontal lobe grey matter) brain tissue was fixed overnight at 4°C in 1.5% glutaraldehyde and 1% paraformaldehyde (pH=7.4). Tissue blocks of  $\leq 1$  mm<sup>3</sup> were post-fixed for 90 minutes in 2% osmium tetroxide and 2% potassium ferrocyanide after filtrating the post-fixative through a 0.2- $\mu$ m filter. After post-fixation, the tissue was washed for 30 minutes in MilliQ and dehydrated in a series of ethanol (70%, 80% and 90%) for 30 minutes each and twice for 1 hour in 100% ethanol. Blocks were incubated for 10 minutes in propylene oxide, 2 hours in propylene oxide and Epon LX-112 (1:1) and finally for 2 hours in propylene oxide and Epon LX-112 (1:2). Subsequently, the epon was polymerized for 48 hours at 70°C.

One- $\mu$ m thick sections were checked for the presence of blood vessels by light microscopy. Then, areas with high blood vessel density were selected for further analysis with EM, i.e. 80-nm sections were collected on a one hole grid and subsequently stained with uranyl acetate and lead citrate. Images were acquired with a digital camera (One View, Gatan Inc., Pleasanton, CA) mounted on a 120 kV transmission electron microscope (Tecnai T12 with a twin objective lens, Fei Inc, Hillsborough, OR). Overviews of relatively large regions on the specimen that contained abundant numbers of cross-sections of vessels were collected by stitching many individual images together (40,000-60,000 nm<sup>2</sup>) using software described earlier.<sup>23</sup> Stitched images were examined using Aperio ImageScope (version 10.0.35).

### GOM analysis

The number of GOM deposits was counted per vessel and expressed as counts per 100  $\mu$ m vessel circumference. Vessel circumference was approximated using the formula of oval circumference (Ramanujan's approximation for ellipse circumference =  $\pi[3(a+b)$

-  $\sqrt{((3a+b)*(a+3b))}$  where a and b were defined as the major diameter (a) and minor diameter (b) for each vessel between endothelial basement membranes. GOM deposits were studied in vessels with a minor diameter < 8  $\mu\text{m}$ , referred to as microvessels, as these were the most abundant in the stitched images. Twenty-three to 84 microvessels were studied per time point (1.5, 3, 6, 12 and 20 months). Width of the basement membrane was determined averaging 40 measurements in two ntg mice and two tgN3<sup>MUT</sup>350 mice each. In the human brain sample, 21 microvessels were analysed. Also, the GOM deposit area was measured using ImageJ after manually drawn region-of-interests around GOM deposits.

### Immunohistochemistry

Two 5- $\mu\text{m}$  coronal frontal brain sections per mouse (approximately at the height of the infundibulum) and human brain sections of frontal white matter were analysed with immunohistochemistry. NOTCH3<sup>ECD</sup> staining was performed as described before.<sup>22</sup> Smooth muscle actin (SMA) staining was performed after pre-treatment with trypsin for 30 minutes at 37°C and washed three times for 5 min with PBS. The primary antibody (Alpha-Smooth Muscle Actin, 1:4000, goat polyclonal, NB300-978, Novus Biologicals) was incubated overnight at room temperature. The secondary antibody (Rabbit Anti-Goat IgG, biotinylated, 1:400, Jackson Immunoresearch Lab. Inc.) was incubated for 1 hour at room temperature and developed with the Vectastain Elite ABC HRP Kit (PK-6100, Vectorlabs) for 30 min at room temperature. Finally, slices were stained with 0.05% 3,3'-diaminobenzidine (DAB, Sigma) supplemented with 0.0045% H<sub>2</sub>O<sub>2</sub> for 10 min and stained with Harris' hematoxylin solution (diluted 1:3, Merck) for 5 seconds. Sections were Verhoeff-Van Gieson and Periodic Schiff Acid stained using the Artisan Link Pro staining machine (DAKO, Agilent), and Van Gieson stained as described previously.<sup>24</sup> Sections were stained with Klüver-Barrera luxol fast blue to quantify white matter vacuolization (Supplementary Methods 4).

Microscopy imaging was performed with the Keyence BZ-X710 (Keyence). Using 20 times magnification, full colour images were taken of the complete section at 1-ms capture time. Images were stitched by Keyence BZ-X Analyzer software version 1.3.0.3 to obtain one high resolution full brain image per section. The SMA positive area was determined using a Colour Threshold (Hue 0-50; Saturation 0-255; Brightness 0-175) in ImageJ, and expressed as percentage of total brain surface of the section.

### Neuroimaging, cerebrovascular reactivity, cognition and motor function

At the age of 20 months, neuroimaging (T2W, FLAIR, SWI, cerebral hemodynamics) was performed under medetomidine anaesthesia using a 7 Tesla MRI (Bruker PharmaScan), see also Supplementary Methods 1. In short, absolute cerebral blood flow (CBF) was measured using arterial spin labeling (ASL)-MRI during a 7-minute baseline and a 7-minute CO<sub>2</sub> challenge, using the measured signal difference between the labelled and control

images in three brain slices. Absolute CBF at baseline and absolute CBF at challenge were quantified during the last 140 seconds of baseline and challenge, respectively. Absolute CBF increase was calculated as well as the cerebrovascular reactivity (CVR), which was defined as the relative cerebral blood flow (CBF) increase. One non-transgenic mouse was excluded from neuroimaging analysis due to a poor hemodynamic response to anaesthesia.

A Morris Water Maze protocol was used to assess cognitive function in 20-month-old mice, starting 2 weeks before neuroimaging assessment (Supplementary Methods 2.2). In short, during the training phase, mice were trained to find a hidden platform in the north-west quadrant of a circular swimming pool, while at the reversal training phase, mice were retrained to find a hidden platform in the south-east quadrant. Path length of the mice was determined between release in the pool and finding the hidden platform. Motor function was determined by analysing speed on a rotarod, on a beam and during swimming in the Morris water maze (Supplementary Methods 2.3). Motor and cognitive mouse experiments were performed by the same experienced researcher.

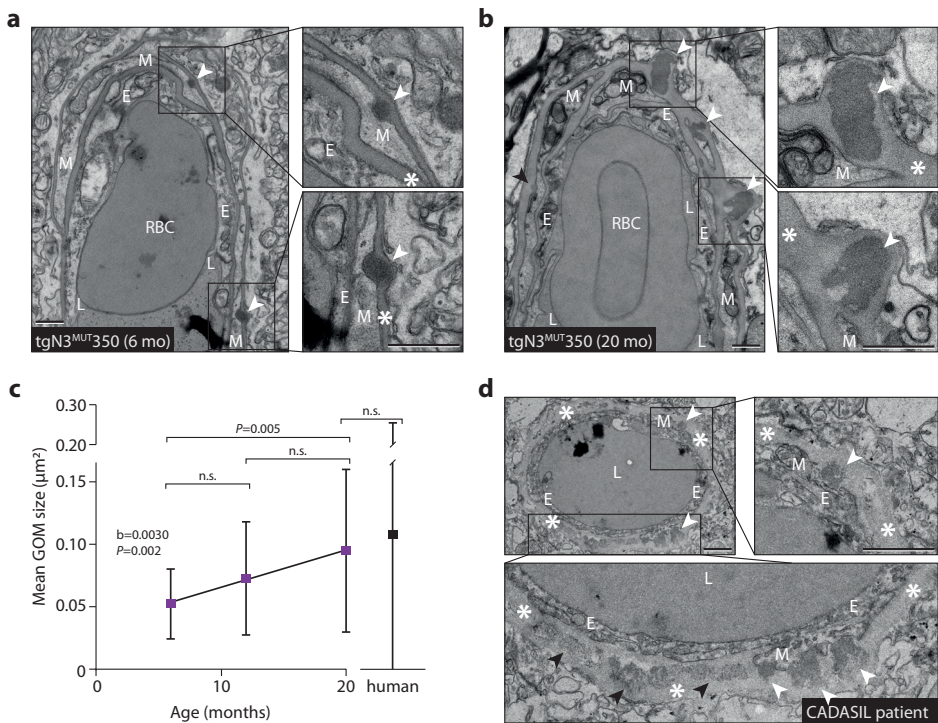
### Statistical analyses

Differences between groups were analysed using one-way ANOVA analyses with Tukey's post-hoc correction. The increase in GOM area over time, as well as the association between baseline CBF and CVR were analysed using simple linear regression. All statistical analyses were two-sided tests with threshold for statistical significance of 0.05, using the IBM SPSS Statistics version 23.0.0.2 software.

## RESULTS

### Temporal GOM assessment

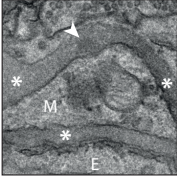
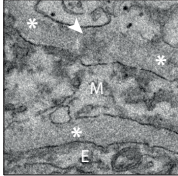
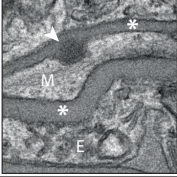
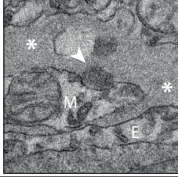
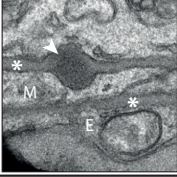
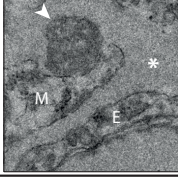
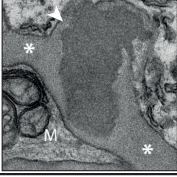
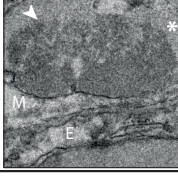
GOM appearance, size and count were studied in brain microvessels of tgN3<sup>MUT</sup>350 mice at the age of 1.5, 3, 6, 12, and 20 months. GOM deposits were first observed at the age of 6 months, appearing as small, round deposits in the basement membrane of mural cells, which were sometimes only slightly more electron dense than the surrounding basement membrane (Figure 2.1a). At 12 months, most GOM deposits were larger and more electron dense. At 20 months, large amorphous GOM deposits were observed, which spanned the full width of the basement membrane (Figure 2.1b). Irrespective of age, GOM deposits were predominantly (85%) located on the abluminal side of mural cells, bulging out the basement membrane and thereby leaving an indentation in the adjacent mural cell. Between 6 and 20 months, GOM size increased ( $b=0.0030 \mu\text{m}^2/\text{month}$ ,  $P=0.002$ ) (Figure 2.1c), GOM count more than doubled (0.9 to 2.4 GOM/100  $\mu\text{m}$ ) and the percentage of GOM-positive vessels increased from 26% to 39%.

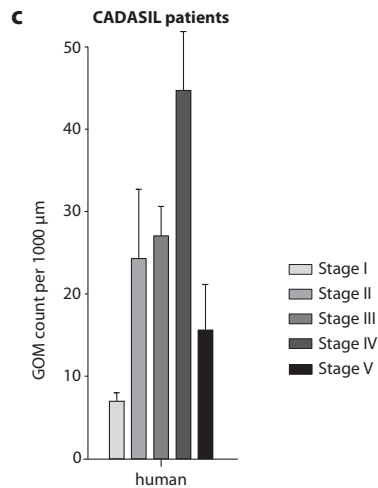
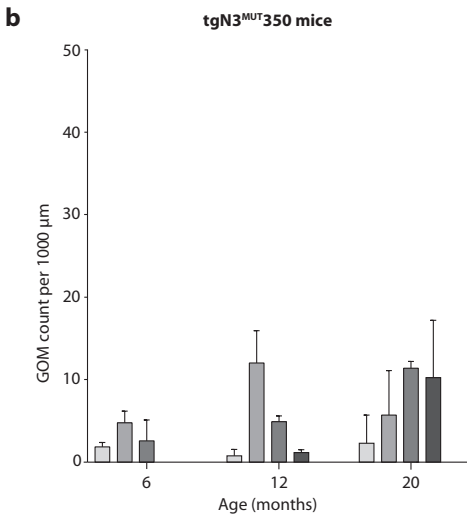


**Figure 2.1: Progression of GOM in brain vessels of CADASIL mice**

(A) Electron microscopy (EM) of brain vessels of tgN3<sup>MUT350</sup> mice at the age of 6 months reveals round, electron dense GOM deposits near mural cells (white arrowheads). (B) EM at the age of 20 months shows larger and amorphous GOM deposits (white arrowheads), but also a small GOM deposit (grey arrowhead). The basement membrane bulges out at the location of a GOM deposit, but is otherwise not thickened in vessels of tgN3<sup>MUT350</sup> mice. Mural cells have a normal aspect, i.e. without electron lucent vacuoles, large intracellular vesicles or a shrunken appearance. (C) Analysis of the size of GOM deposits in mouse brain vessels shows a significant increase in GOM size between the age of 6 and 20 months ( $b=0.0030 \mu\text{m}^2/\text{month}$ ,  $P=0.002$ ). Average GOM size in brain vessels of deceased CADASIL patients ( $0.108 \pm 0.148 \mu\text{m}^2$ ,  $n=292$  GOM deposits) was higher than in mice ( $0.095 \pm 0.065 \mu\text{m}^2$ ,  $n=31$  GOM deposits), but this difference was not statistically significant ( $P=0.634$ ) due to the large variability in GOM size in human brain vessels. (D) Post-mortem analysis of CADASIL brain microvessels ( $n=3$  patients) showed extensive GOM pathology, with deposits in all vessels, both bulging into adjacent mural cells (white arrowheads) and located centrally in the thickened basement membrane further away from mural cells (grey arrowheads). In contrast to mice, GOM deposits in the CADASIL patient had a more granular aspect with heterogeneous electron density. CADASIL patient brain vessels had a thickened basement membrane and mural cells showed signs of degeneration, such as a shrunken appearance. Arrowhead = GOM; Asterisk = basement membrane; E = Endothelial cell; M = Mural cell; n.s. = non significant; RBC = Red blood cell. Bar represents  $1 \mu\text{m}$ . Graph represents mean  $\pm$  SD.

Based on these observations, we categorized GOM deposits into various stages that reflect relative size, morphology, electron density and the GOM deposit-induced bulging of the basement membrane with concomitant indentation of adjacent mural cells (Figure 2.2a).

Stage	tgN3 <sup>MUT350</sup> mouse	CADASIL patient	Description
I			<ul style="list-style-type: none"> <li>- GOM deposits are <i>smaller</i> than normal width of BM</li> <li>- GOM deposits are round or elliptical</li> <li>- Minimal bulging of BM and minimal indentation of mural cell near GOM</li> <li>- GOM deposits are <i>only slightly more electron-dense</i> than surrounding extracellular matrix</li> </ul>
II			<ul style="list-style-type: none"> <li>- GOM deposits are <i>smaller</i> than normal width of BM</li> <li>- GOM deposits are round or elliptical</li> <li>- Bulging of BM with indentation of mural cell near GOM</li> <li>- GOM deposits are electron-dense</li> </ul>
III			<ul style="list-style-type: none"> <li>- GOM deposits are <i>larger</i> than normal width of BM</li> <li>- GOM deposits are round or elliptical</li> <li>- Bulging of BM, and/or overall thickened BM (in human)</li> <li>- Larger indentation of mural cell near GOM</li> <li>- GOM deposits are electron-dense</li> </ul>
IV			<ul style="list-style-type: none"> <li>- GOM deposits are <i>larger</i> than normal width of BM</li> <li>- GOM deposits are <i>amorphous</i> or have <i>bizarre shapes</i></li> <li>- Bulging of BM, and/or overall thickened BM (in human)</li> <li>- Larger indentation of mural cell near GOM</li> <li>- GOM deposits are electron-dense</li> </ul>
V	not observed in mice		<ul style="list-style-type: none"> <li>- Two or more stage IV GOM deposits confluence into a patch of <i>confluent GOM</i></li> <li>- Bulging of BM, and/or overall thickened BM (in human)</li> <li>- Mural cells can have two or more subtle indentations, reflecting two or more GOM deposits</li> </ul>



### ◀ Figure 2.2: A 5-stage GOM classification system for CADASIL

(A) Classification system for GOM deposits based on size, morphology and electron density. Per stage, examples are shown from brain vessels of  $\text{tgN3}^{\text{MUT}350}$  mice and of deceased CADASIL patient. In each example, the bottom of the image points towards the luminal side of the vessel. Cells were denoted as endothelial cells (E) or mural cells (M) based on interpretation of the morphology of cells as a whole within the vessel. (B) Staging of GOM deposits in brain vessels of  $\text{tgN3}^{\text{MUT}350}$  mice. At 6 months of age, stages I-III GOM deposits were present, while at 20 months mainly stages III-IV GOM deposits were observed. (C) Staging of GOM in brain vessels from deceased CADASIL patients. GOM deposits of all stages were observed, but stage IV GOM deposits were most abundant. Overall GOM count in patients was higher than in mice. Arrowhead = GOM; Asterisk = basement membrane; E = Endothelial cell; M = Mural cell.

Stage I GOM deposits are small and slightly electron dense and induce minimal mural cell indentation. Stage II and III GOM deposits are more electron dense, induce basement membrane bulging with mural cell indentation, and are within (II) or extend beyond (III) the normal width of the basement membrane (~150 nm). Stage IV GOM deposits extend beyond the normal width of the basement membrane and are amorphous. At 6 months of age, stage I-III GOM deposits were observed in  $\text{tgN3}^{\text{MUT}350}$  mice. At 12 months, the first stage IV GOM appeared. At 20 months, the majority of the GOM were at stages III and IV (Figure 2.2b), but stage I GOM deposits were also observed. This suggests that new GOM deposits are continuously being formed, and that once formed, the initially small round GOM deposits progress over time into large amorphous deposits.

Next, we compared GOM in brain tissue of three CADASIL patients to GOM in 20-month-old  $\text{tgN3}^{\text{MUT}350}$  mice (Figure 2.1d). Almost all (96%) of the analysed microvessels in the patients contained GOM deposits, whereas GOM deposits were observed in only 39% of microvessels in the mutant mice. In human brain material, like in mice, GOM deposits of all stages were observed, but stage IV GOM deposits were most frequent (Figure 2.2c). In addition, the patients' microvessels contained large confluent patches of GOM (stage V GOM) that were not observed in the mice. Of note, the electron density of GOM deposits in the patients' microvessels was less homogeneous than of GOM in mice. GOM deposits in patient microvessels either bulged out of the basement membrane and thereby left an indentation in the adjacent mural cell, or were located further away from any recognisable mural cells within an overall thickened basement membrane. In contrast, GOM deposits in mice were always located close to the mural cell, often in indentations of the mural cell formed by the GOM deposits.

### Other CADASIL-associated vessel wall and brain parenchyma changes

Despite large GOM deposits and extensive granular *NOTCH3*<sup>ECD</sup> staining at 20 months (Figure 2.3a),  $\text{tgN3}^{\text{MUT}350}$  mice did not show basement membrane thickening ( $\text{tgN3}^{\text{MUT}350}$   $0.145 \pm 0.050 \mu\text{m}$ , *ntg*  $0.148 \pm 0.055 \mu\text{m}$ ,  $P=0.73$ ) and there were no signs of mural

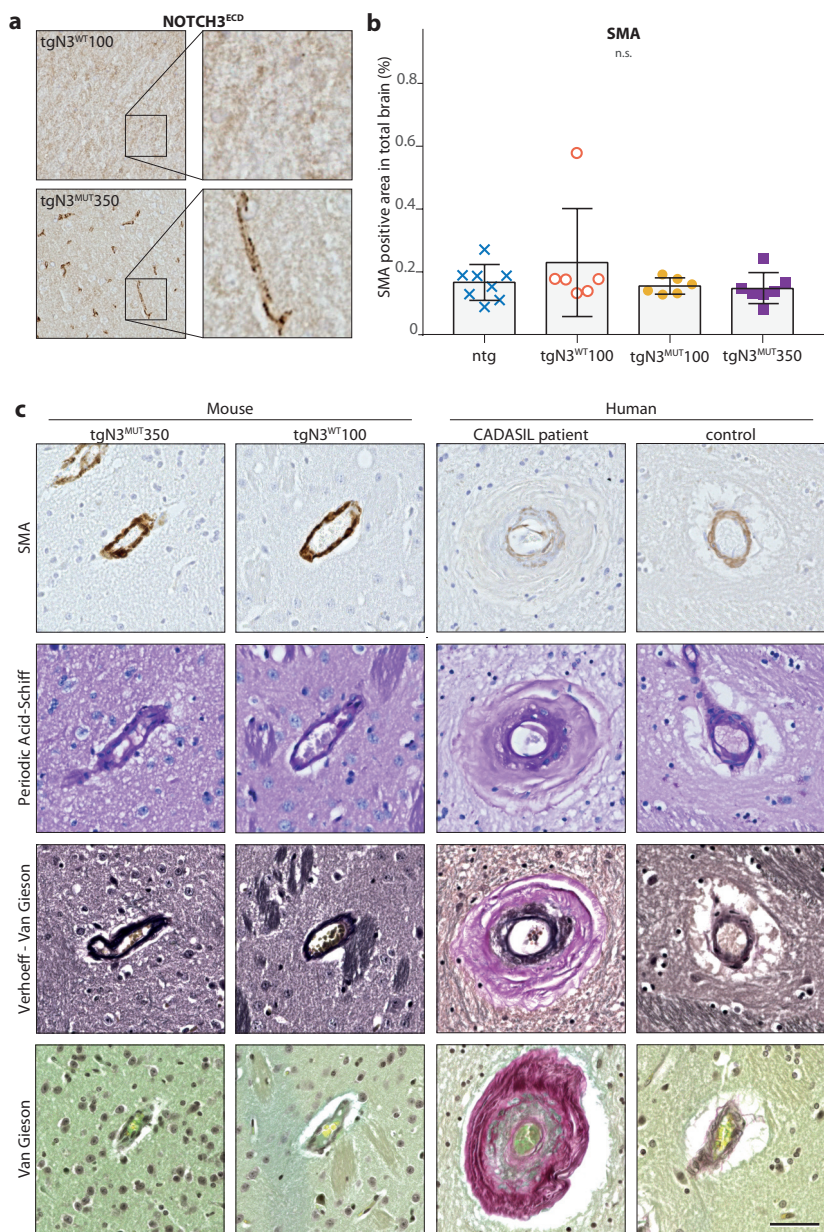


**Figure 2.3: No vessel wall thickening or reduced SMA staining in mice expressing mutant human NOTCH3 protein**  
 (A) Mutant mice (tgN3<sup>MUT350</sup>) show granular NOTCH3<sup>ECD</sup> deposits in brain vessels, which were not observed in wildtype mice (tgN3<sup>WT100</sup>). (B) SMA content in brain was similar in the four mouse strains. One tgN3<sup>WT100</sup> brain section contained a large artery which was longitudinally cleaved, resulting in a high SMA positive area. (C) The pattern of SMA immunoreactivity in the vessel wall was similar between the four groups (only images of the tgN3<sup>MUT350</sup> and tgN3<sup>WT100</sup> strains are shown), while the white matter of CADASIL patients ▶

degeneration, such as electron lucent vacuoles, large intracellular vesicles or a shrunken appearance (Figure 2.1a,b). Also, there was no difference in the amount or pattern of SMA staining between mutant and wildtype mice (Figure 2.3b,c). In addition, Van Gieson's, Verhoeff-Van Gieson's, and Periodic Acid-Schiff staining did not show vessel wall thickening, in contrast to our observations in vessels of the CADASIL patients (Figure 2.3c). There was no difference in white matter vacuolization between wildtype and mutant mice (Supplementary Data 2.2).

### Cerebral blood flow, cerebrovascular reactivity and neuroimaging

Next, we assessed cerebral blood flow (CBF) dynamics in 20-month-old mice using ASL-MRI with CO<sub>2</sub> as vasodilative stimulus (Figure 2.4a). Compared to non-transgenic and wildtype mice, mutant mice (tgN3<sup>MUT</sup>100 and tgN3<sup>MUT</sup>350) did not show a significant difference in CVR, which was defined as relative CBF increase upon challenge (Figure 2.4b,d), absolute CBF increase upon challenge (Figure 2.4c,e), or in CBF at baseline (Figure 2.4f). There was, however, a non-significant trend towards a reduced CVR and a slightly increased baseline CBF in the tgN3<sup>MUT</sup>350 mice. Differences in baseline CBF likely contributed to the observed differences in CVR, as there was an inverse correlation between baseline CBF and CVR ( $s=-0.69$ ,  $P<0.001$ , Supplementary data 2.1). Separate analysis of CBF and CVR for cortex and subcortex showed similar results (Supplementary data 2.3 and 2.4). High-resolution T2w, FLAIR and SWI MRI scans of mouse brains did not show white matter hyperintensities, lacunes, or microbleeds. Also, gadolinium enhancement showed the typical pattern of contrast enhancement in and around the ventricles, but no differences were observed between tgN3<sup>MUT</sup>350 and wildtype mice (Supplementary data 2.5).

### Cognition and motor function

Motor function, as assessed by rotarod running, beam walk and swimming speed, did not differ between mutant and wildtype mice at any of the time points (Supplementary data 2.6). In the Morris water maze tests, mutant mice did not show signs of impaired memory formation. If anything, tgN3<sup>MUT</sup>350 mice performed slightly better at some of the tasks (Figure 2.5).

► showed less and fragmented SMA immunoreactivity, with SMA-positive areas in the intima. PAS, VvG and VG staining showed similar brain vessel staining patterns between the four groups, but the brain vessels of the CADASIL patients showed a clearly thickened vessel wall, with a positive PAS staining (carbohydrates), VvG staining (collagenous material red; elastic material black) and VG staining (collagenous material red). SMA = smooth muscle actin; n.s. = non significant; PAS = Periodic Acid-Schiff staining; VG = Van Gieson's staining; VVG = Verhoeff-Van Gieson's staining. Bar represents 50 µm. Graph represents mean±SD.



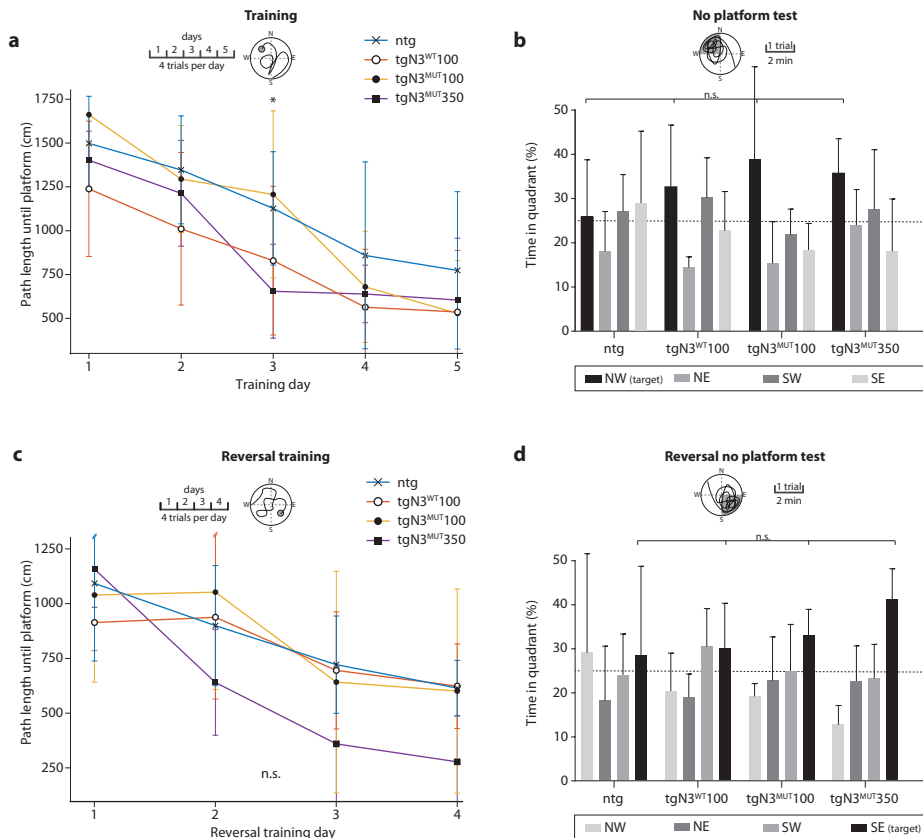


**Figure 2.5: CADASIL mice do not show cognitive dysfunction**

(A) The path length until finding a hidden platform in the water maze was similar for all strains (ntg, tgN3<sup>WT100</sup>, tgN3<sup>MUT100</sup>, tgN3<sup>MUT350</sup>). (B) After the 5 training days, mice underwent one trial without a platform. The time spent in the target quadrant (NW) was similar between the groups ( $P=0.46$ ; ANOVA). (C) A 4-day reversal training phase with the platform hidden in the south-east quadrant showed no significant differences in path length until finding the hidden platform between the groups ( $P=0.14$  on day 4; ANOVA). (D) Time in target quadrant after the reversal training was similar between the groups ( $P=0.09$ ; ANOVA). Graphs represent mean $\pm$ SD; n.s. = non significant; \*  $P<0.05$ .

## DISCUSSION

We investigated the development of GOM deposits over time in a transgenic mouse model of CADASIL, which overexpresses mutant human NOTCH3 protein from a large genomic construct. GOM deposits evolved with respect to size, morphology and number in microvessels of the mutant mouse brain. Here, we propose a 5-stage GOM classification system to facilitate uniform analysis and description of GOM deposits and show that this staging can also be used to systematically classify GOM in vessels of CADASIL patient material.

The GOM deposits observed in aged mice (20 months) included stages I-IV, i.e. from small, circumscribed deposits within the basement membrane (stage I), to large, amorphous GOM that induced bulging of the basement membrane (stage IV). As mice aged 6 months only showed stages I-III GOM, individual GOM deposits seem to increase in size and become increasingly amorphous over time, and new GOM seem to be continuously formed. This is further illustrated by the observation that GOM deposits of stage I and II are also present in post-mortem CADASIL patient brain microvessels, next to the more extensive GOM pathology, including patches of confluent GOM (stage V).<sup>7,25,26</sup>

Although many studies have reported the presence and morphology of GOM in CADASIL patients,<sup>9,11–13,25,27–30</sup> little is known about how GOM deposits progress over time. Brulin *et al.* analyzed GOM in skin biopsies of CADASIL patients of different ages, and found that the number of GOM deposits increase up to 50 years of age, but also found that the number of GOM seems to decrease in elderly patients.<sup>11</sup> The latter may either be attributed to other end-stage vessel wall changes hampering the visualization of GOM, or because GOM seem to become confluent and disintegrate over time.<sup>26</sup> Whether different GOM stages in skin biopsies of CADASIL patients are associated with disease severity and disease progression, therefore, remains to be determined. If so, the proposed GOM classification system may aid future efforts to monitor and predict disease progression at the individual patient level.

In our humanized CADASIL mouse model and in a rat Notch3 CADASIL mouse model, GOM deposits are observed several months after the first signs of NOTCH3<sup>ECD</sup> positive granular immunostaining,<sup>22,30</sup> suggesting that NOTCH3<sup>ECD</sup> granules may act as seeds for GOM development. Since NOTCH3<sup>ECD</sup> aggregates attract extracellular matrix proteins that are components of GOM deposits, such as TIMP3 and clusterin,<sup>4,5</sup> there seems a direct temporal relation between NOTCH3<sup>ECD</sup> aggregates and the formation of GOM deposits. Delineating molecular differences between early- and end-stage GOM deposits may help to understand the sequence of events in CADASIL vascular pathology, and perhaps the identification of early therapeutic targets.

Whereas the CADASIL mice in our study seem to faithfully replicate early signs of disease pathology (*NOTCH3*<sup>ECD</sup> accumulation and GOM deposition), we did not observe other CADASIL-associated disease features which have been observed in other CADASIL mouse models, such as vessel wall thickening, changes in SMA staining, mural cell degeneration and blood brain barrier leakage.<sup>7,9,14,15,17,31</sup> In line with this, we previously showed that our mutant mice do not show brain parenchyma pathology at age 20 months, which we confirmed in this study using high resolution T2W neuroimaging.<sup>22</sup> Furthermore, we extended the characterization of the mice with functional tests, which did not reveal any cognitive or motor dysfunction. Our cerebral blood flow studies showed a small, not significant, reduction in CVR in tgN3<sup>MUT</sup>350 mice, while studies in other, genetically different, CADASIL mouse models did show a reduced CVR.<sup>8,30,32</sup> It may be relevant that we used a different method to anaesthetize mice and also to measure CVR, namely an ASL-based MRI approach. Although less sensitive in detecting small CVR changes, the advantage of ASL-MRI is that it allows for absolute perfusion quantification and detection of differences in baseline CBF. In that way, we found that the slight reduction of CVR in tgN3<sup>MUT</sup>350 mice could at least partially be explained by a higher CBF at baseline. Future research is needed to determine whether the differences in CVR findings between this study and others<sup>8,30,32</sup> can be explained by differences in genetics of the mouse models, by differences in baseline perfusion states, or by differences in the study set-up, including the anaesthesia protocol. Although we did not find evidence for overt functional cerebrovascular deficits in our mouse model, this humanized mouse model captures early markers of CADASIL pathology, making it suitable for therapeutic studies targeting human mutant *NOTCH3*<sup>ECD</sup> accumulation early in the disease course.

In summary, we show progression of GOM deposits in a humanized CADASIL mouse model. We propose a 5-stage GOM classification system for uniform assessment of GOM depositions in translational research. In future pre-clinical studies of therapeutic approaches aimed at reducing or preventing *NOTCH3*<sup>ECD</sup> aggregation, GOM classification may serve as a valuable tool to monitor therapeutic efficiency on an ultrastructural level.

## APPENDIX

### Acknowledgements

We acknowledge the financial support from the Netherlands Brain Foundation (HA2016-02-03). We thank Baudouin Denis de Senneville for his help with the MR image registration; Lydiane Hirschler and Emmanuel Barbier for their help with the pCASL sequence; Sandra van Heiningen and the LUMC animal facility for mouse breeding; and Peter Neeskens for electron microscopy sample preparation.

## Funding

This work was funded by the Netherlands Brain Foundation (HA2016-02-03).

## Ethical approval

All applicable international, national, and/or institutional guidelines for the care and use of animals were followed. Experiments were approved by the local animal ethics committee (code 14073) and conducted in accordance with recommendations of the European Communities Council Directive (2010/63/EU) and ARRIVE guidelines. All efforts were made to minimize animal suffering. Except from using post-mortem material, this article does not contain any studies with human participants performed by any of the authors.

## Disclosures

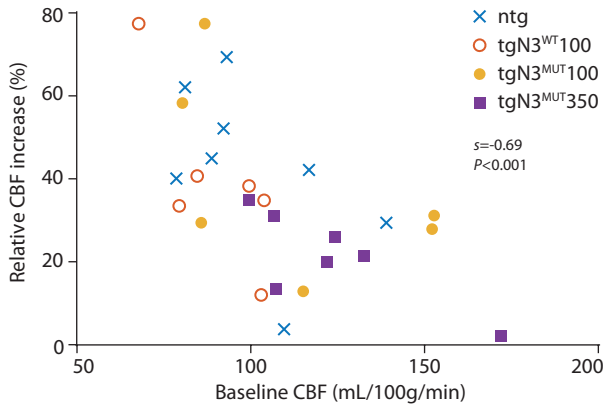
CG, JWR and SAJLO were supported by the Netherlands Brain Foundation (HA2016-02-03). SAJLO is co-inventor on an LUMC owned patent, not related to this work. LPM and LvdW were supported by NWO-VIDI (864.13.014). MO, AAM, IH, MD, AJK, SGvD, OCM, CRJ and AMJMvdM have nothing to disclose. AAR has nothing to disclose related to this work. For full transparency, she discloses being employed by LUMC and being co-inventor on several LUMC owned patents. As such she is entitled to a share of royalties. AAR further discloses being ad hoc consultant for PTC Therapeutics, BioMarin Pharmaceuticals Inc., Global Guidepoint, GLG consultancy, Grunenthal, Eisai, Sarepta Therapeutics and BioClinica, and having been a member of the Duchenne Network Steering Committee (BioMarin) and of the scientific advisory boards of ProQR and Philae Pharmaceuticals. Remuneration for these activities is paid to LUMC. LUMC also received speaker honoraria from PTC Therapeutics and BioMarin Pharmaceuticals.

## REFERENCES

- Chabriat, H., Joutel, A., Dichgans, M., Tournier-Lasserre, E. & Bousser, M.-G. Cadasil. *Lancet. Neurol.* **8**, 643–53 (2009).
- Joutel, A. *et al.* Strong clustering and stereotyped nature of Notch3 mutations in CADASIL patients. *Lancet* **350**, 1511–5 (1997).
- Joutel, A. *et al.* Notch3 mutations in CADASIL, a hereditary adult-onset condition causing stroke and dementia. *Nature* **383**, 707–10 (1996).
- Ishiko, A. *et al.* Notch3 ectodomain is a major component of granular osmiophilic material (GOM) in CADASIL. *Acta Neuropathol.* **112**, 333–339 (2006).
- Monet-Leprêtre, M. *et al.* Abnormal recruitment of extracellular matrix proteins by excess Notch3 ECD: A new pathomechanism in CADASIL. *Brain* **136**, 1830–1845 (2013).
- Arboleda-Velasquez, J. F. *et al.* Hypomorphic Notch 3 alleles link Notch signaling to ischemic cerebral small-vessel disease. *Proc. Natl. Acad. Sci.* **108**, E128–E135 (2011).
- Yamamoto, Y. *et al.* Brain microvascular accumulation and distribution of the NOTCH3 ectodomain and granular osmiophilic material in CADASIL. *J. Neuropathol. Exp. Neurol.* **72**, 416–431 (2013).
- Ghosh, M. *et al.* Pericytes are involved in the

- pathogenesis of cerebral autosomal dominant arteriopathy with subcortical infarcts and leukoencephalopathy. *Ann. Neurol.* **78**, 887–900 (2015).
9. Gu, X., Liu, X.-Y., Fagan, A., Gonzalez-Toledo, M. E. & Zhao, L.-R. Ultrastructural Changes in Cerebral Capillary Pericytes in Aged Notch3 Mutant Transgenic Mice. *Ultrastruct. Pathol.* **36**, 48–55 (2012).
  10. Joutel, A. *et al.* The ectodomain of the Notch3 receptor accumulates within the cerebrovasculature of CADASIL patients. *J. Clin. Invest.* **105**, 597–605 (2000).
  11. Brulin, P., Godfraind, C., Leteurtre, E. & Ruchoux, M.-M. Morphometric analysis of ultrastructural vascular changes in CADASIL: analysis of 50 skin biopsy specimens and pathogenic implications. *Acta Neuropathol.* **104**, 241–8 (2002).
  12. Tikka, S. *et al.* Congruence between NOTCH3 mutations and GOM in 131 CADASIL patients. *Brain* **132**, 933–939 (2009).
  13. Morroni, M. *et al.* Role of Electron Microscopy in the Diagnosis of Cadasil Syndrome: A Study of 32 Patients. *PLoS One* **8**, 6–11 (2013).
  14. Ruchoux, M. M. *et al.* Systemic vascular smooth muscle cell impairment in cerebral autosomal dominant arteriopathy with subcortical infarcts and leukoencephalopathy. *Acta Neuropathol.* **89**, 500–512 (1995).
  15. Kalimo, H. *et al.* CADASIL: Hereditary disease of arteries causing brain infarcts and dementia. *Neuropathol. Appl. Neurobiol.* **25**, 257–265 (1999).
  16. Miao, Q. *et al.* Arterioles of the lenticular nucleus in CADASIL. *Stroke* **37**, 2242–2247 (2006).
  17. Gatti, J. R. *et al.* Redistribution of Mature Smooth Muscle Markers in Brain Arteries in Cerebral Autosomal Dominant Arteriopathy with Subcortical Infarcts and Leukoencephalopathy. *Transl. Stroke Res.* **10**, 160–169 (2019).
  18. Yamamoto, Y. *et al.* Neuropathological correlates of temporal pole white matter hyperintensities in CADASIL. *Stroke* **40**, 2004–2011 (2009).
  19. Dong, H. *et al.* Advanced intimal hyperplasia without luminal narrowing of leptomeningeal arteries in CADASIL. *Stroke* **44**, 1456–1458 (2013).
  20. Pfefferkorn, T. *et al.* Reduced cerebrovascular CO(2) reactivity in CADASIL: A transcranial Doppler sonography study. *Stroke* **32**, 17–21 (2001).
  21. Chabriat, H. *et al.* Cerebral hemodynamics in CADASIL before and after acetazolamide challenge assessed with MRI bolus tracking. *Stroke* **31**, 1904–12 (2000).
  22. Rutten, J. W. *et al.* The NOTCH3 score: a pre-clinical CADASIL biomarker in a novel human genomic NOTCH3 transgenic mouse model with early progressive vascular NOTCH3 accumulation. *Acta Neuropathol. Commun.* **3**, 89 (2015).
  23. Faas, F. G. A. *et al.* Virtual nanoscopy: Generation of ultra-large high resolution electron microscopy maps. *J. Cell Biol.* **198**, 457–469 (2012).
  24. Dodds, H. M. & Clark, G. An improved Van Gieson. *Stain Technol.* **60**, 55 (1985).
  25. Lewandowska, E., Dziewulska, D., Parys, M. & Pasennik, E. Ultrastructure of granular osmiophilic material deposits (GOM) in arterioles of CADASIL patients. *Folia Neuropathol.* **49**, 174–80 (2011).
  26. Lewandowska, E., Felczak, P., Buczek, J., Gramza, K. & Rafałowska, J. Blood vessel ultrastructural picture in a CADASIL patient diagnosed at an advanced age. *Folia Neuropathol.* **4**, 443–451 (2014).
  27. Ruchoux, M. M. *et al.* Transgenic Mice Expressing Mutant Notch3 Develop Vascular Alterations Characteristic of Cerebral Autosomal Dominant Arteriopathy with Subcortical Infarcts and Leukoencephalopathy. *Am. J. Pathol.* **162**, 329–342 (2003).
  28. Monet, M. *et al.* The archetypal R90C CADASIL-NOTCH3 mutation retains NOTCH3 function in vivo. *Hum. Mol. Genet.* **16**, 982–992 (2007).
  29. Monet-Lepretre, M. *et al.* Distinct phenotypic and functional features of CADASIL mutations in the Notch3 ligand binding domain. *Brain* **132**, 1601–1612 (2009).
  30. Joutel, A. *et al.* Cerebrovascular dysfunction and microcirculation rarefaction precede white matter lesions in a mouse genetic model of cerebral ischemic small vessel disease. *J. Clin. Invest.* **120**, 433–445 (2010).
  31. Miao, Q. *et al.* Fibrosis and Stenosis of the Long Penetrating Cerebral Arteries: the Cause of the White Matter Pathology in Cerebral Autosomal Dominant Arteriopathy with Subcortical Infarcts and Leukoencephalopathy. *Brain Pathol.* **14**, 358–364 (2006).
  32. Lacombe, P., Oligo, C., Domenga, V., Tournier-Lasserre, E. & Joutel, A. Impaired Cerebral Vasoreactivity in a Transgenic Mouse Model of Cerebral Autosomal Dominant Arteriopathy With Subcortical Infarcts and Leukoencephalopathy Arteriopathy. *Stroke* **36**, 1053–1058 (2005).

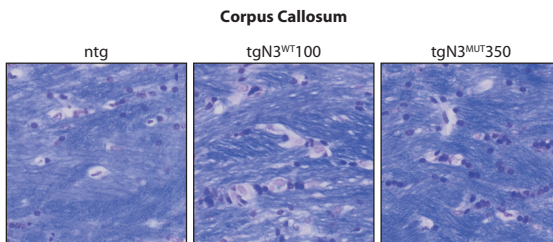
## SUPPLEMENTARY DATA



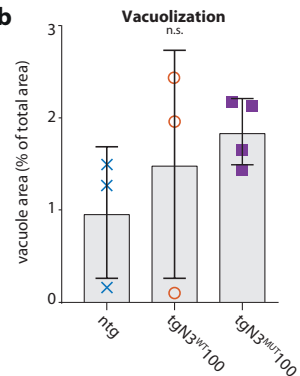
### Supplementary Data 2.1: Baseline CBF correlates with CVR in CADASIL mice

Relative CBF increase (CVR) was determined for all mouse strains (ntg, tgN3<sup>WT</sup>100, tgN3<sup>MUT</sup>100, tgN3<sup>MUT</sup>350). CVR values were negatively associated with baseline CBF values ( $s = -0.69$ ,  $P < 0.001$ ), suggesting that CVR represents differences in both baseline CBF and actual vascular reactivity.

**a**

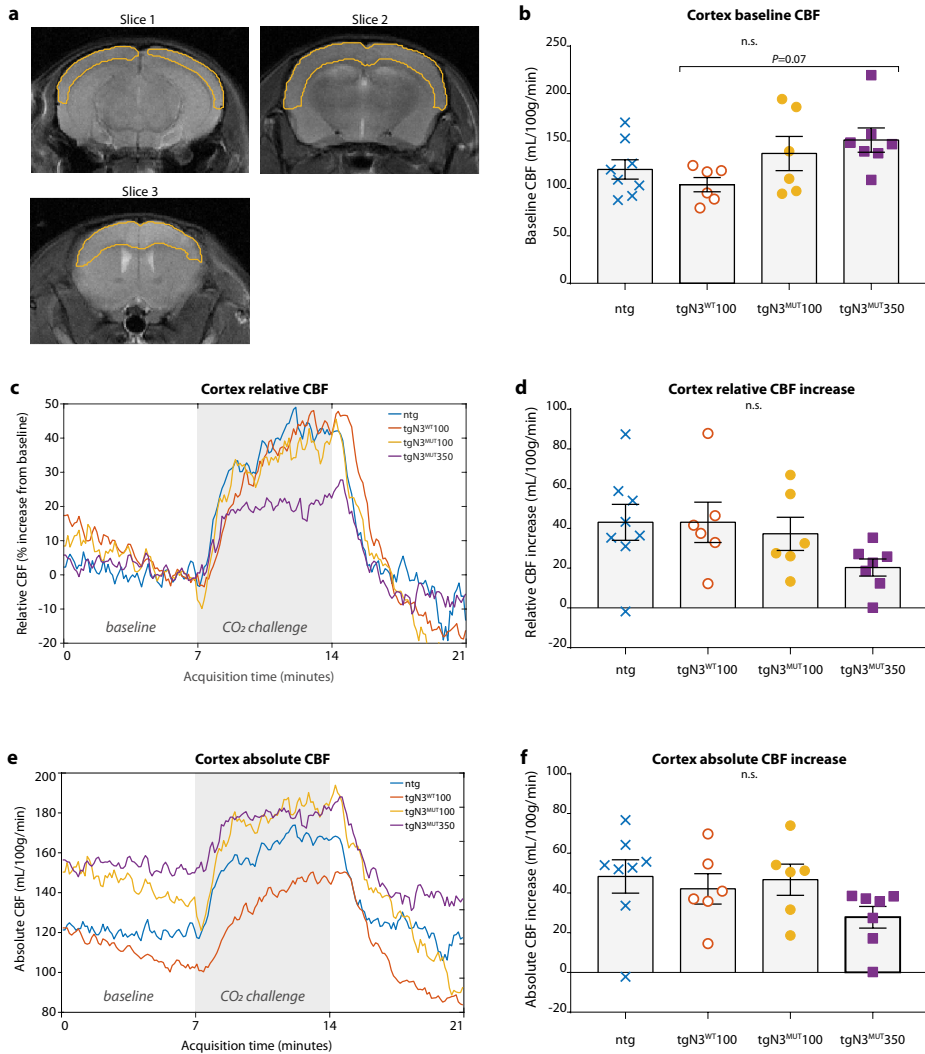


**b**



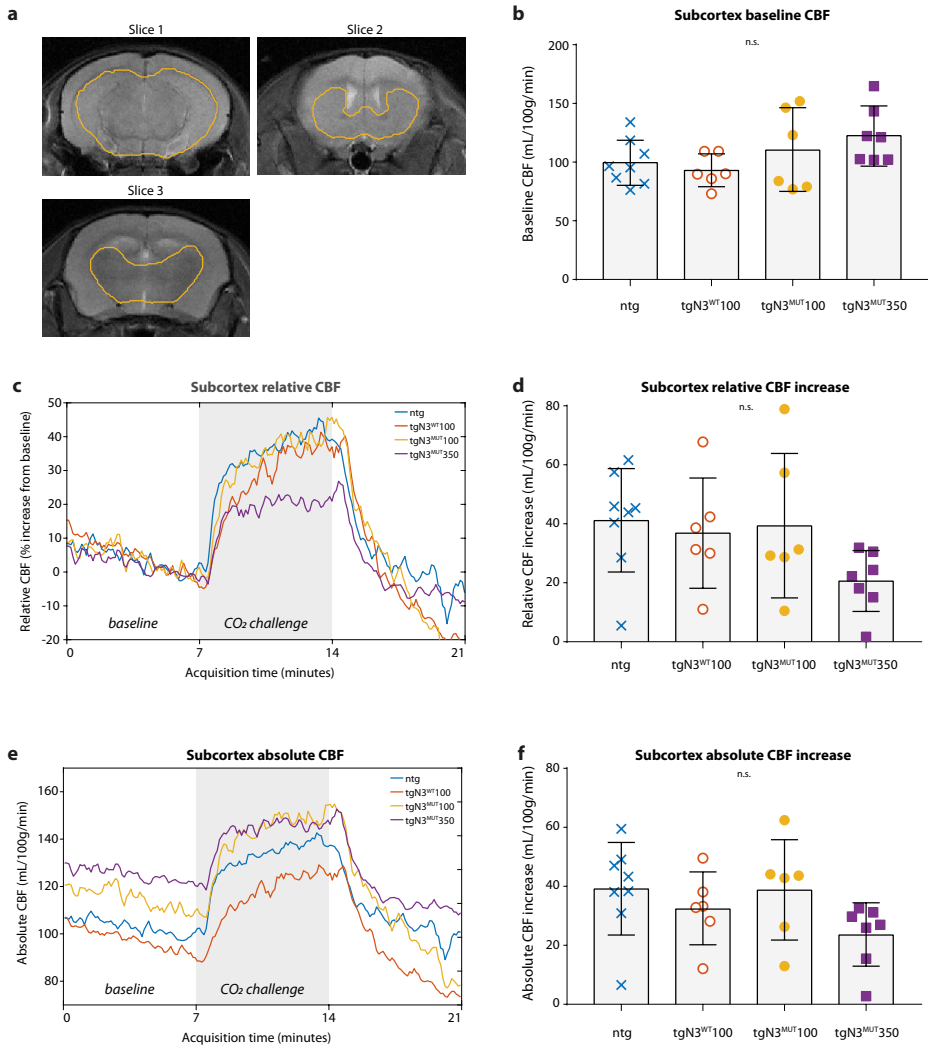
### Supplementary Data 2.2: CADASIL mice do not show increased levels of vacuolization

(A) Representative images of Klüver-Barrera luxol fast blue staining of the corpus callosum in 20-month-old non-transgenic mice (ntg), wildtype mice (tgN3<sup>WT</sup>100) and mutant mice (tgN3<sup>MUT</sup>350). (B) Quantification of the vacuole area in the corpus callosum, showing similar levels of vacuolization (ntg 0.98%±0.71%, tgN3<sup>WT</sup>100 1.51%±0.71%, tgN3<sup>MUT</sup>350 1.86%±0.36%,  $P = 0.40$ , ANOVA). Graph represent mean±SD; n.s. = non significant.



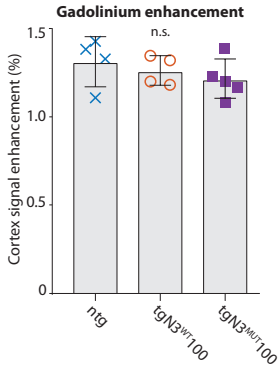
### Supplementary Data 2.3: CADASIL mice do not show altered cortical cerebrovascular reactivity

(A) Region-of-interest of cortex. (B) Baseline CBF in cortex was similar among the groups (ntg, tgN3<sup>WT</sup>100, tgN3<sup>MUT</sup>100, tgN3<sup>MUT</sup>350). (C,D) Average relative CBF profiles over time are shown for cortex. CVR was similar in all groups. (E,F) Average absolute CBF profiles over time. Absolute CBF rise upon CO<sub>2</sub> challenge was similar between the groups. Graphs represent mean or mean±SD; n.s. = non significant.



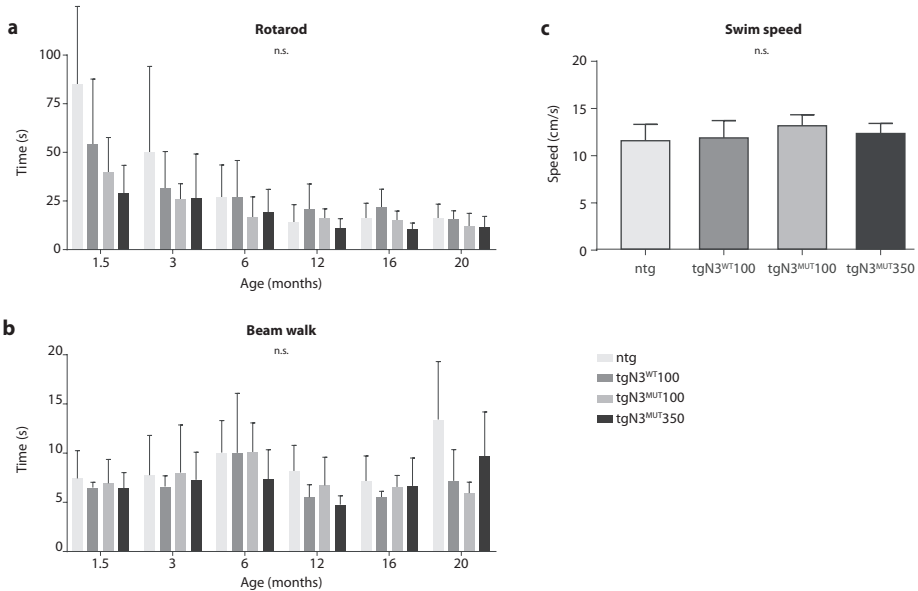
#### Supplementary Data 2.4: CADASIL mice do not show altered subcortical cerebrovascular reactivity

(A) Region-of-interest of subcortex. (B) Baseline CBF in subcortex was similar among the groups (ntg, tgN<sub>3</sub><sup>WT</sup>100, tgN<sub>3</sub><sup>MUT</sup>100, tgN<sub>3</sub><sup>MUT</sup>350). (C,D) Average relative CBF profiles over time are shown for subcortex. CVR was similar in all groups. (E,F) Average absolute CBF profiles over time. Absolute CBF rise upon CO<sub>2</sub> challenge was similar between the groups. Graphs represent mean or mean±SD; n.s. = non significant.



**Supplementary Data 2.5: CADASIL mice do not show blood brain barrier leakage**

Blood brain barrier function was assessed in a second cohort of ntg (n=4), tgN3<sup>WT100</sup> (n=4), and tgN3<sup>MUT350</sup> (n=5) mice at the age of 12 months by determining Gadolinium-induced signal enhancement on brain MRI after injection of Gadolinium. No differences in signal enhancement were observed (ntg 1.31%±0.14%, tgN3<sup>WT100</sup> 1.26%±0.08%, tgN3<sup>MUT350</sup> 1.22%±0.11%, P=0.48, ANOVA).



**Supplementary Data 2.6: CADASIL mice do not show motor dysfunction**

Bar charts showing (A) the time to complete a beam walk and (B) the time without falling of a rotarod for all groups (ntg, tgN3<sup>WT100</sup>, tgN3<sup>MUT100</sup>, tgN3<sup>MUT350</sup>) at various time points. No differences were seen between groups on the beam walk and rotarod motor function tests. (C) Average swimming speed from all trainings and reversal trainings was similar between groups. Graphs represent mean±SD; n.s. = non significant.

### Supplementary Data 2.7: Physiology parameters during cerebral hemodynamic assessment at baseline and at CO<sub>2</sub> challenge in CADASIL mice

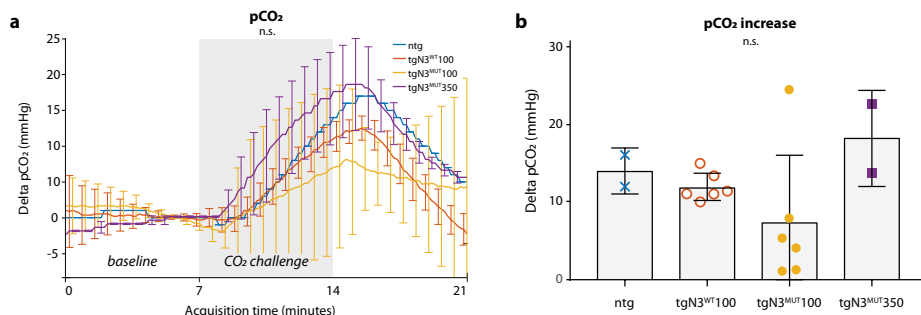
	Baseline mean (sd) <i>P-value</i> <sup>a</sup>	CO <sub>2</sub> challenge mean (sd) <i>P-value</i> <sup>a</sup>	<i>P-value</i> <sup>b</sup>
Body temperature (°C)	n.s.	n.s.	
ntg	35.4 (2.0)	35.3 (2.4)	n.s.
tgN3 <sup>WT</sup> 100	35.3 (0.4)	35.6 (0.5)	n.s.
tgN3 <sup>MUT</sup> 100	34.4 (0.5)	34.5 (0.9)	n.s.
tgN3 <sup>MUT</sup> 350	35.2 (1.3)	35.5 (1.2)	<i>P</i> =0.006
Respiration (/min)	n.s.	n.s.	
ntg	154 (34)	157 (33)	n.s.
tgN3 <sup>WT</sup> 100	125 (32)	127 (45)	n.s.
tgN3 <sup>MUT</sup> 100	112 (45)	131 (37)	n.s.
tgN3 <sup>MUT</sup> 350	160 (28)	191 (50)	<i>P</i> =0.031
Oxygenation (%)	n.s.	n.s.	
ntg	78 (17)	77 (16)	n.s.
tgN3 <sup>WT</sup> 100	72 (15)	72 (18)	n.s.
tgN3 <sup>MUT</sup> 100	74 (15)	85 (4)	n.s.
tgN3 <sup>MUT</sup> 350	86 (11)	90 (7)	n.s.
Heart rate (/min)	n.s.	<i>P</i> =0.009 <sup>c</sup>	
ntg	306 (73)	315 (82) <sup>c</sup>	n.s.
tgN3 <sup>WT</sup> 100	225 (20)	209 (22) <sup>c</sup>	n.s.
tgN3 <sup>MUT</sup> 100	300 (115)	269 (23)	n.s.
tgN3 <sup>MUT</sup> 350	285 (51)	290 (30)	n.s.

<sup>a</sup> *P*-value per tested physiology parameter represent ANOVA *P*-value for testing differences between groups at baseline and differences between groups at challenge.

<sup>b</sup> *P*-value represent paired student's *t*-test between baseline and challenge values of the parameter within the respective mouse strain.

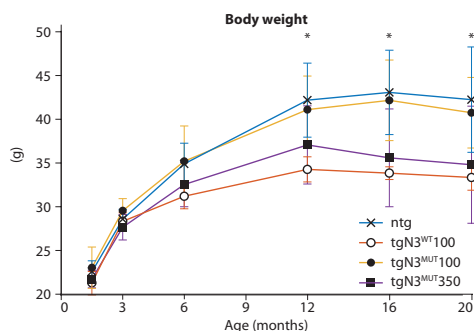
<sup>c</sup> Heart rate during CO<sub>2</sub> challenge was significantly different between the different mouse strains. Post-hoc testing showed that tgN3<sup>WT</sup>100 mice had significantly lower heart rates than ntg (*P*=0.006).

n.s. = non significant.



**Supplementary Data 2.8: pCO<sub>2</sub> in blood increase upon CO<sub>2</sub> challenge**

(A) Absolute pCO<sub>2</sub> increase is plotted over time. pCO<sub>2</sub> levels were normalized to zero at baseline. (B) No significant differences in pCO<sub>2</sub> increase between the mouse strains (ntg, tgN<sub>3</sub><sup>WT100</sup>, tgN<sub>3</sub><sup>MUT100</sup>, tgN<sub>3</sub><sup>MUT350</sup>). Please note that pCO<sub>2</sub> measurements of only a subset of mice is plotted (ntg n=1; tgN<sub>3</sub><sup>WT100</sup> n=6; tgN<sub>3</sub><sup>MUT100</sup> n=6; tgN<sub>3</sub><sup>MUT350</sup> n=2) as the pCO<sub>2</sub> datasets of the other mice were lost due to technical reasons. Graphs represent mean±SD; n.s. = non significant.



**Supplementary Data 2.9: Reduced body weight in tgN<sub>3</sub><sup>MUT350</sup> and tgN<sub>3</sub><sup>WT100</sup> mice compared to ntg and tgN<sub>3</sub><sup>MUT100</sup> mice**

Mice showed similar weights at younger ages, but from the age of 12 months, tgN<sub>3</sub><sup>WT100</sup> mice were significantly lighter than ntg mice, and from the age of 16 months, tgN<sub>3</sub><sup>WT100</sup> and tgN<sub>3</sub><sup>MUT350</sup> mice were significantly lighter than tgN<sub>3</sub><sup>MUT100</sup> and ntg mice (ntg 43.1±4.8 g, tgN<sub>3</sub><sup>WT100</sup> 33.8±0.7 g, tgN<sub>3</sub><sup>MUT100</sup> 42.2±4.6 g, tgN<sub>3</sub><sup>MUT350</sup> 35.6±5.6 g, P=0.003; ANOVA). \*P<0.05. Graph represents mean±SD.

## SUPPLEMENTARY METHODS

### Supplementary Methods 1: Neuroimaging and CVR assessment

#### *Anaesthesia and physiological monitoring during neuroimaging*

Mice were anesthetized with 3.5% isoflurane in medical air enriched with oxygen (75% air, 25% oxygen) for 4 minutes, followed by a continuous flow of 2% isoflurane during positioning of the mouse in the animal bed of the MRI scanner. A subcutaneous catheter was placed to infuse medetomidine (Dexdomitor, Vetoquinol SA, Lure, France [a solution without the inactive enantiomer levomedetomidine]) with a syringe pump (Univentor 802, Univentor High Precision Instruments, Zejtun, Malta). At the beginning of image acquisition, a bolus of 0.15 mg/kg medetomidine was injected, and 10 minutes later followed by a continuous infusion of 0.30 mg/kg/hr medetomidine. During those 10 minutes, the isoflurane concentration was slowly reduced to 0%, while the administration of the air/oxygen mixture was continued. During image acquisition, respiration was registered using a pressure pad placed underneath the animal. Heart rate and pulse oxygenation (both SA instruments, New York, USA) were recorded using an infrared probe around the leg. Changes in transcutaneous (tc)-pCO<sub>2</sub> values were measured using a tc-pCO<sub>2</sub> sensor (TCM radiometer, Zoetermeer, The Netherlands) placed on shaved skin on the flank of the animal. Temperature was maintained using a feedback-controlled waterbed (Medres, Cologne, Germany). Directly after neuroimaging, still under anaesthesia, mice were decapitated and tissue was collected.

#### *MR image acquisition for cerebral hemodynamic assessment*

MR images were acquired with a 7 T Bruker PharmaScan (Ettlingen, Germany) using a 23 mm volume coil. Anatomical T2 Turbo RARE scans were acquired in all three directions for planning of the arterial spin labelling (ASL) scans with the following parameters: TE/TR = 35.0 ms/2,500 ms, 0.7 mm slice thickness without a slice gap, 1 average, matrix of 256 by 256, field of view of 21.55 by 21.55 mm, RARE factor of 8, and a bandwidth of 36.7 kHz. To aid image registration, three slices of 1.5 mm thick with the same imaging parameters as above and the same geometry as the pseudo-continuous arterial spin labeling (pCASL) scans were acquired. The pCASL sequence was used to image the cerebral blood flow (CBF) and cerebrovascular reactivity (CVR, i.e. relative CBF increase). The label and control interpulse-phases of the sequence were optimized beforehand, to correct for off-resonance effects [1]. The labelling plane was placed in the neck, 1.0 cm from isocenter. Three 1.5 mm thick single-shot, spin-echo - Echo Planar Imaging (EPI) slices were used with a slice gap of 1 mm, where the middle slice was placed at isocenter and at -0.75 mm Bregma. The following imaging parameters were used: TE/TR = 16.8 ms/3,520 ms, labelling duration ( $\tau$ ) of 3,000 ms, post-label delay (PLD) of 300 ms, FOV of 21.55 x 21.55 mm and a matrix of 96 x 96. 180 pairs of label/control images (repetitions) were acquired, with a total pCASL imaging duration of 21 minutes. During the challenge, i.e. between minute 7 and 14 and

between repetition 60 to repetition 120, 7.5% CO<sub>2</sub> was added to the gas mixture. T1 maps were acquired using an inversion recovery EPI with 18 inversion times and with the same geometry as the pCASL sequence. Labelling efficiency ( $\alpha$ ) was measured 0.3 cm downstream the labelling plane with a flow-compensated, ASL-encoded FLASH sequence. The latter two sequences were used to support CBF-quantification. After the pCASL scan, three additional anatomical scans were acquired with the following details: (1) a high resolution T2W sequence with TE/TR = 39 ms/2,200 ms, a matrix of 384 x 384, 9 slices with a thickness of 0.7 mm, a 0.3 mm slice gap and 8 averages; (2) a T2W-Fluid-Attenuated Inversion Recovery (FLAIR) sequence with TE/TR = 37 ms/1,000 ms, a matrix of 192 x 192, 9 slices with a thickness of 1.0 mm, without a slice gap and 3 averages; and (3) a Susceptibility-Weighted Imaging (SWI) sequence with TE/TR = 18 ms/350 ms, a matrix of 384 x 384, 9 slices with a thickness of 0.7 mm, a 0.3 mm slice gap and 5 averages. These three sequences were acquired in the same orientation and with the same FOV as the pCASL scan.

#### *MR image registration and processing*

Individual pCASL EPIs and individual inversion recovery EPIs were aligned to the first label magnitude image of the pCASL sequence using a MATLAB monomodal rigid body registration with 300 iterations (MATLAB version R2016a, Mathworks, Natick, USA). The anatomical T2RARE images of one dataset were used to delineate the cortex and the full brain. These regions of interest (ROIs) were automatically propagated to the T2RARE images of the other datasets, and subsequently to the EPIs of every dataset. An edge-based variational method for non-rigid multimodal registration was used to propagate the ROIs [2]. The results of both propagation steps were verified for each dataset by an operator (L.P.M.).

Buxton's general kinetic perfusion model was used to quantify cerebral blood flow (CBF) from the measured difference between label and control acquisition (Buxton et al., *Magn Reson Med.* 1998;40:383-396), *i.e.* the following equation was used:

$$\text{CBF} = [\lambda \cdot \Delta M \cdot \exp(\text{PLD} / T_{1b})] / [2 \cdot \alpha \cdot T_{1T} \cdot (1 - \exp(-\tau / T_{1T}))]$$

Here,  $\Delta M$  is the measured difference between the label and control EPIs,  $T_{1b}$  is the T1 of blood at 7 T, assumed to be 2230 ms [3]. Also, it is assumed that at thermal equilibrium, the magnetization of arterial blood ( $M_{ob}$ ) may be approximated by  $M_{ot}/\lambda$ , where  $M_{ot}$  is the magnetization of tissue and  $\lambda$  is 0.9, the blood–brain partition coefficient of water [4]. Baseline CBF was defined as the mean CBF of the 20 repetitions before the onset of the CO<sub>2</sub> challenge, which is equal to 2 minute 20 seconds before the onset. CBF during CO<sub>2</sub> was defined as the mean of the 20 repetitions before the end of the CO<sub>2</sub>. These two estimates were used to calculate cerebrovascular reactivity (CVR) by using the following equation:  $\text{CVR} (\%) = [\text{mean CBF during challenge} - \text{mean CBF during baseline}] / [\text{mean CBF during baseline}] \cdot 100\%$

### *MR image acquisition for blood brain barrier assessment using Gadolinium*

Blood brain barrier function was assessed in a second cohort of ntg (n=4), tgN3WT100 (n=4), and tgN3MUT350 (n=5) mice at the age of 12 months by determining Gadolinium-induced signal enhancement on brain MRI after injection of Gadolinium. Gadolinium-DOTA (Dotarem, Guerbet, Cedex, France) was administered intra-peritoneally at 10 mmol/kg. MRI was performed using a series of consecutive T1W images with a RARE sequence (TR/TE = 870/11.7 ms, matrix size = 256 x 256, field-of-view = 20 x 20 mm<sup>2</sup>, number of averages = 6, slice thickness = 0.5 mm, coronal slices, RARE factor = 2), both before (1 image) and after (6 images) contrast agent administration. The 6 post-contrast images have been acquired immediately after the contrast agent injection, thus started at 0 min, 12 min, 24 min, 36 min, 48 min, and 60 min post-injection, respectively. Blood brain barrier leakage was calculated as percentage signal enhancement after contrast in a region-of-interest placed on the cortex at Bregma -2 mm. Signal enhancement was calculated as the relative change in signal intensity (SI) between pre- and the last post-contrast T1W image ( $\Delta SI$ ) as per the following equation,  $\Delta SI = [ SI(t) - SI(0) ] / SI(0)$ , where SI(t) is the signal intensity at time t after Gadolinium-DOTA injection and SI(0) is the signal intensity of the selected region-of-interest in the scan prior to Gadolinium-DOTA injection.

### **Supplementary Methods 2: Cognitive assessment**

A Morris water maze protocol was used to assess cognitive function, as it is considered to be a valid measure of hippocampal dependent spatial navigation and reference memory. The swimming pool (diameter 138cm) was filled with opaque white water (by adding non-toxic paint) which was maintained at a temperature of 20-22°C. A platform (diameter 10.8 cm, platform pool ratio 1:163) was placed 5-8 mm under the water surface in the north-west quadrant and south-east quadrant during the training phase and reversal training phase, respectively. Ten cm from the pool, three high contrast figures were placed to facilitate spatial navigation. To prevent praxic and taxic navigation rather than spatial navigation, mice were released from different locations during the experiment.

Three days before starting the training phase, mice were allowed to swim in the pool for 2 min. Mice underwent 4 trials for 5 or 4 days during the training phase or reversal training phase, respectively, where they had a maximum of 120 seconds per trial to locate the hidden platform. After the trial, regardless whether they found the platform, mice were placed on the platform for 15 seconds allowing them to remember the location. Three days after the training phase and reversal training phase, mice were placed for 2 minutes in the swimming pool of which the platform was removed (no platform test and reversal no platform test, respectively). Mice were recorded using the Noldus EthoVision® XT Base software (version 11.5). Path length to platform was used as outcome measure for (reversal) training phase and time per quadrant for the no-platform tests.

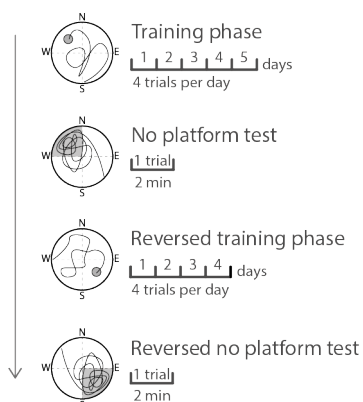


**Figure:** Graphical summary experimental design Morris water maze protocol

### Supplementary Methods 3: Motor function tests

For rotarod tests, mice had to run on a rotating rod (speed gradually increasing up to 45 rpm) for a maximum of 5 minutes. For beam walk tests, time to cross a beam of 80 cm with a diameter of 11 mm was recorded. As we noted that all mice had difficulty performing the task, from the age of 6 months, the diameter of the beam was increased to 17 mm. Mice took three trials per time point and the average time was analysed for both tests. Average swimming speed was calculated based on all MWM trials.

### Supplementary Methods 4: Quantification of vacuolization in mouse brain

Two 5- $\mu$ m brain sections per mouse were analysed after staining them with Klüver-Barrera luxol fast blue staining according to standard protocol. Corpus callosum was captured at 400x with the same capture settings for all sections. Regions-of-interest were manually drawn around the corpus callosum, thereby excluding blood vessel area if vessels were present in the image. Vacuoles were quantified using ImageJ thresholding for the vacuole areas. Vacuole area is expressed as vacuole area percentage compared to total region-of-interest area. Multiple measurements were averaged per mouse.

### Supplementary References

- Hirschler L, Debacker CS, Voiron J, Köhler S, Warnking JM, Barbier EL. Interpulse phase corrections for unbalanced pseudo-continuous arterial spin labeling at high magnetic field. *Magn Reson Med.* 2018;79:1314–24.
- Denis De Senneville B, Zachiu C, Ries M, Moonen C. EVolution: An edge-based variational method for non-rigid multi-modal image registration. *Phys Med Biol.* IOP Publishing; 2016;61:7377–96.
- Dobre MC, Uğurbil K, Marjanska M. Determination of blood longitudinal relaxation time ( $T_1$ ) at high magnetic field strengths. *Magn Reson Imaging.* 2007;25:733–5.
- Herscovitch P, Raichle ME. What is the correct value for the brain–blood partition coefficient for water? *J Cereb Blood Flow Metab.* 1985;5:65–9.



# Chapter 3

## Naturally occurring *NOTCH3* exon skipping attenuates NOTCH3 protein aggregation and disease severity in CADASIL patients

Gido Gravesteyn  
Johannes G. Dauwse  
Maurice Overzier  
Gwendolyn Brouwer  
Ingrid Hegeman  
Aat A. Mulder  
Frank Baas  
Mark C. Kruit  
Gisela M. Terwindt  
Sjoerd G. van Duinen  
Carolina R. Jost  
Annemieke Aartsma-Rus  
Saskia A.J. Lesnik Oberstein\*  
Julie W. Ruten\*

## ABSTRACT

CADASIL is a vascular protein aggregation disorder caused by cysteine altering *NOTCH3* variants, leading to mid-adult onset stroke and dementia. Here, we report individuals with a cysteine altering *NOTCH3* variant that induces exon 9 skipping, mimicking therapeutic *NOTCH3* cysteine correction. The index came to our attention after a coincidental finding on a commercial screening MRI, revealing white matter hyperintensities. A heterozygous *NOTCH3* c.1492G>T, p.Gly498Cys variant was identified using a gene panel, which was also present in four first- and second degree relatives. Although some degree of white matter hyperintensities was present on MRI in all family members with the *NOTCH3* variant, the CADASIL phenotype was mild, as none had lacunes on MRI and there was no disability or cognitive impairment above the age of 60 years. RT-PCR and Sanger sequencing analysis on patient fibroblast RNA revealed that exon 9 was absent from the majority of *NOTCH3* transcripts of the mutant allele, effectively excluding the mutation. *NOTCH3* aggregation was assessed in skin biopsies using electron microscopy and immunohistochemistry and did not show granular osmiophilic material and only very mild *NOTCH3* staining. For purposes of therapeutic translatability, we show that, in cell models, exon 9 exclusion can be obtained using antisense-mediated exon skipping and CRISPR/Cas9-mediated genome editing. In conclusion, this study provides the first in-human evidence that cysteine corrective *NOTCH3* exon skipping is associated with less *NOTCH3* aggregation and an attenuated phenotype, justifying further therapeutic development of *NOTCH3* cysteine correction for CADASIL.

## INTRODUCTION

CADASIL is a hereditary small vessel disease caused by cysteine altering variants in *NOTCH3* (OMIM#125310).<sup>1,2</sup> More than 250 of such variants have been described in CADASIL families,<sup>3</sup> all of which lead to an uneven number of cysteines in one of the epidermal growth factor-like repeat (EGFr) domains of the NOTCH3 ectodomain (NOTCH3<sup>ECD</sup>). These variants cause mutant NOTCH3<sup>ECD</sup> to aggregate in the (cerebro)vasculature. Ultrastructurally, CADASIL-causing *NOTCH3* variants are associated with granular osmiophilic material (GOM) deposits in the blood vessel wall, including vessels of the brain and skin.<sup>4-6</sup> As such, CADASIL is a vascular protein aggregation disorder with secondary central nervous system hypoxia and ischemia, leading to mid-adult onset strokes and cognitive decline.<sup>1</sup> MRI signs include progressive periventricular and deep white matter hyperintensities (WMH), typically but not necessarily including the external capsules and temporal poles, superimposed by lacunes and frequently also microbleeds in later disease stages.<sup>7</sup>

We recently described 'NOTCH3 cysteine correction' as a therapeutic approach for CADASIL, using antisense-mediated exon skipping to exclude mutant exons from the mRNA.<sup>8</sup> Exons were selected in such a way that exclusion from mRNA restores the number of cysteines in the EGFr domains of the NOTCH3<sup>ECD</sup>, with conservation of signalling function and predicted normal protein folding.<sup>8</sup> Many exons harboring CADASIL-causing variants are eligible for this approach, including exon 9.

Here, we describe a family with a unique cysteine altering *NOTCH3* variant in exon 9, which is predicted to cause natural exon 9 skipping. This effectively mimics the therapeutic NOTCH3 cysteine correction approach, allowing us to study the effect of cysteine corrective exon skipping on NOTCH3 protein aggregation and disease severity in humans. Furthermore, we tested exon 9 skipping *in vitro* using antisense oligonucleotides and determined the feasibility of *NOTCH3* cysteine correction using CRISPR/Cas9-mediated gene editing.

## MATERIALS AND METHODS

This study was approved by the Medical Ethics Committee of the Leiden University Medical Center (B19.057). All participants gave written informed consent for publication.

### Phenotype description

Family members were evaluated at the multidisciplinary out-patient clinic for cerebral small vessel disease of our hospital. A neurologist (GMT) and clinical geneticist (SAJLO) with

longstanding expertise in CADASIL took their history and family history. Neuroimaging was performed as part of diagnostic care. MRI scans were re-evaluated by a neuroradiologist with broad expertise in MRI scans of CADASIL patients (MCK). WMH volume was quantified relative to the brain parenchyme volume as described previously.<sup>9</sup> Age-adjusted *z*-score of lacune count (for family member #1, #2, #4, #6) and WMH volume (for family member #1, #2, #6) were calculated using simple linear regression, with a previously published CADASIL cohort as reference.<sup>9</sup> WMH volume in family member #4 could not be quantified because only sagittal brain MRI images were available.

### Genetic variant analysis

In the index patient, a panel of 26 cerebral small vessel disease associated genes (Supplementary Data 3.2) was sequenced by the Leiden Laboratory for Diagnostic Genome Analysis using the Illumina HiSeq platform with the Agilent SureSelectXT Clearseq inherited disease panel target enrichment kit. The complete coding sequence was analysed, including 20 nucleotides in the flanking introns. In the other family members, the presence of the *NOTCH3* variant was determined using Sanger sequencing. *NOTCH3* transcript (NM\_000435.2) was used as reference. The identified *NOTCH3* variant was submitted to the Leiden Open Variant Database (notch3.lovd.nl).<sup>10</sup>

### Qualitative and quantitative analysis of vascular NOTCH3 aggregation in skin biopsies

Skin punch biopsies of all six family members, as well as of 3 CADASIL patients (positive controls with *NOTCH3* variants p.Arg182Cys and p.Cys144Phe located in exon 4, and with *NOTCH3* variant p.Cys446Phe located in exon 8) and 3 unaffected individuals (negative controls), were taken from the lateral upper arm, fixed in formalin and embedded in paraffin. Two 5- $\mu$ m sections were pre-treated with proteinase K and washed three times for 5 minutes with PBS. The primary antibody (rabbit-anti-*NOTCH3*<sup>ECD</sup>, #25070002, Novus, dilution 1:500), was incubated for 2 hours at room temperature. The secondary antibody (swine-anti-rabbit/biotin, Dako, dilution 1:400), was incubated for 30 minutes and developed with the Vectastain Elite ABC HRP Kit (PK-6100, Vectorlabs). Finally, slices were stained with 0.05% 3,3'-diaminobenzidine (DAB, Sigma Aldrich) supplemented with 30% H<sub>2</sub>O<sub>2</sub> for 10 minutes. To validate immunohistochemistry results, sections were also stained with another primary mouse anti-*NOTCH3*<sup>ECD</sup> antibody (clone 1E4, Millipore, dilution 1:1000; data not shown).

For quantification of vascular *NOTCH3* aggregation, full colour images were obtained with the Keyence BZ-X710 microscope (Keyence, Itasca, USA) at 1-ms capture time using 20 $\times$  magnification. Ten images in the *z*-axis (pitch 1  $\mu$ m) per location were made and stitched into one high resolution, full focus image by the Keyence BZ-X Analyzer software version 1.3.0.3. Regions-of-interest were drawn manually around vessel wall inner and outer

boundaries. A median of 40 vessels per individual was analysed (minimally 13 vessels per family member). The NOTCH3<sup>ECD</sup> positive area was determined using a Colour Threshold (Hue 0-50; Saturation 0-255; Brightness 0-175) in ImageJ, and expressed as percentage of vessel wall area.

For electron microscopy, skin tissue blocks of  $\leq 1$  mm<sup>3</sup> were post-fixed for 90 minutes in 2% osmium tetroxide and 2% potassium ferrocyanide. After dehydration, tissue blocks were polymerized in Epon LX-112 for 48 hours at 70°C. 80-nm sections were stained with uranyl acetate and lead citrate. Images were acquired on a digital camera (One View, Gatan Inc., Pleasanton, USA) mounted on a 120 kV transmission electron microscope (Tecnai T12 with a twin objective lens, Fei, Eindhoven, The Netherlands). Overlapping images were collected and stitched together into one image, as previously described.<sup>11</sup> The presence of GOM in the walls of skin vessels was evaluated by independent observers (GG, AAM, CRJ) in 5-14 vessels per individual, in all family members with the *NOTCH3* variant, in two positive control CADASIL patients and in one healthy control.

### Analysis of exon 9 skipping in fibroblast RNA

To obtain patient-derived fibroblasts, part of the skin biopsy was washed in PBS and incubated for 30 minutes at room temperature in collagenase A (0.42 units/mL, Roche). Primary fibroblast culture was performed in DMEM/F12 GlutaMAX supplement medium (Gibco Life Technologies, The Netherlands), supplemented with 10% heat inactivated fetal calf serum (FCS) (Gibco), 2  $\mu$ M MEM sodium pyruvate (Gibco), 0.5 U/mL penicillin and 0.5  $\mu$ g/mL streptomycin (Gibco). Fibroblast RNA was isolated from  $\sim 1 \times 10^6$  cells according to the manufacturer's instruction using the High Pure RNA Isolation Kit (Roche Diagnostics, Almere, The Netherlands). cDNA was synthesized from 1  $\mu$ g RNA with the transcriptase first strand cDNA synthesis kit according to the manufacturer's protocol (Roche). RT-PCR was performed using a 10 $\times$  PCR buffer with 1.5 mM MgCl<sub>2</sub> (Roche) supplemented with 0.2 mM dNTP, 0.2 pmol/ $\mu$ L *NOTCH3* exon 7 forward primer and exon 11 reverse primer with an annealing temperature of 60°C (Supplementary Data 3.3), and 1 U FastStart Taq DNA polymerase (Roche). PCR products were then excised from gel and DNA was extracted using the Zymoclean Gel DNA Recovery kit (Zymo Research, Irvine, USA) and analysed using Sanger sequencing (Macrogen Europe, Amsterdam, The Netherlands).

### 3D modelling of NOTCH3 <sup>$\Delta$ exon9</sup>

3D modelling of EGFR domains was performed with the online Swiss-Model tool (<https://swissmodel.expasy.org/>), using the sequence of NOTCH3 EGFR domains and a model template 5fma.1.A from the NOTCH1 protein. EGFR domains were visualised using Chimera software version 1.11.2.

### Generation of NOTCH3 cDNA constructs

cDNA constructs (NOTCH3<sup>G498C</sup>, NOTCH3<sup>Y465C</sup>, NOTCH3<sup>Δexon9</sup>) were generated by adapting previously generated cDNA construct pTThN3FL and pSEhN3.<sup>8</sup> pSEhN3 was trimmed by removing exons 20–33 by *HindIII* digestion. Inverse PCR was performed on this clone using specific primer sets (Supplementary Data 3.3) and Q5 High-Fidelity DNA Polymerase (New England Biolabs) to introduce the pathogenic variants in exon 9 or to delete exon 9. Following the PCR, the mixture was digested using *DpnI* to remove the methylated input DNA and purified using the GenElute™ PCR Clean-Up Kit (Sigma-Aldrich, Saint Louis, USA). The products were ligated and subsequently NEB5α cells were transformed with the ligation mixes. Clones were verified using Sanger sequencing (Macrogen). The *KpnI*-*HindIII* fragment of the clones carrying the modification was transferred to the pTThN3FL *KpnI*-*HindIII* backbone. Plasmids were isolated using Nucleospin Plasmid Quickpure kit according to the manufacturer's protocol (Macherey-Nagel, Düren, Germany).

### Protein expression, processing and signalling function of NOTCH3<sup>Δexon9</sup>

Control fibroblasts were transfected with wildtype, NOTCH3<sup>Δexon9</sup> and empty vector constructs, and stained for NOTCH3<sup>ECD</sup> to assess cellular localisation as described previously.<sup>8</sup> In short, cells were either fixed and permeabilized with 4% paraformaldehyde and 0.1% Triton X-100, or only fixed without permeabilization using 4% paraformaldehyde and stained with a mouse anti-NOTCH3<sup>ECD</sup> antibody (clone 1E4, Millipore, dilution 1:10,000). To determine the signalling activity of NOTCH3<sup>Δexon9</sup>, a CBF1 responsive luciferase assay was performed as described previously.<sup>8</sup> In short, NIH 3T3 cells were transfected with NOTCH3 cDNA constructs together with the Renilla luciferase expression vector.<sup>12,13</sup> One day after transfection, cells were co-cultured with 3T3 cells expressing the NOTCH3 ligand human JAGGED1, or with mock transfected 3T3 cells. Luciferase activity of NOTCH3<sup>Δexon9</sup> was compared to NOTCH3 with a deletion of the ligand binding domain (LBD), NOTCH3<sup>C183R</sup>, NOTCH3<sup>Y465C</sup>, NOTCH3<sup>G498C</sup> and NOTCH3<sup>WT</sup>. Seven independent luciferase experiments were performed, with four technical replicates per experiment. Signalling values were normalized to unstimulated wildtype NOTCH3 signalling activity.

### Antisense oligonucleotide (ASO)-mediated exon 9 skipping

Antisense oligonucleotides (ASOs) targeting NOTCH3 exon 9 were designed according to guidelines for ASO development using Human Splice Finder ([www.umd.be/HSF](http://www.umd.be/HSF)) (Supplementary Data 3.4). 14,15 ASOs consisted of 2'-O-methyl riboses and contained a full length phosphorothioate backbone (2'-O-MePS). ASOs were tested on primary control arachnoid vascular smooth muscle cells (VSMCs).<sup>8</sup> Cultures of 1×10<sup>5</sup> cells were transfected with a final concentration of 100 nM ASO complexed with Lipofectamine2000 (ratio 2.67:1, Life Technologies) in serum free medium. Exon 9 skipping was analysed 24 hours after transfection using RT-PCR analysis with an exon 7 forward and exon 11 reverse primer. Results of the most efficient ASO are shown.

### CRISPR/Cas9-induced exon 9 and exon 4-5 genomic deletions

To obtain a genomic exon 9 or exon 4-5 deletion, using CRISPR/Cas9 genome editing, guide RNAs were designed targeting NOTCH3 introns 8 and 9, and introns 3 and 5 with the online tool of the Zhang lab (<https://zlab.bio/guide-design-resources>), Guide RNAs were cloned into a modified pSQT1313 vector (Addgene #53370), with both guide RNAs flanked by Csy4 recognition sites. HEK293 cells and VSMCs were transfected during 4 hours with 0.5 µg DNA encoding the guide RNAs and 3.5 µg DNA of a modified eSpCas9(1.1) (Addgene #71814), expressing both the SpCas9 protein and the Csy4 RNase, together with Lipofectamine2000 (DNA:Lipofectamine ratio 1:2.5) in serum free medium. Two days after transfection, DNA and RNA were isolated and the deletion of exon 9 was assessed by PCR using primers in introns 8 and 9, and by RT-PCR using primers in exon 7 and 11, respectively. The deletion of exon 4-5 was assessed by RT-PCR using primers in exon 3 and 6.

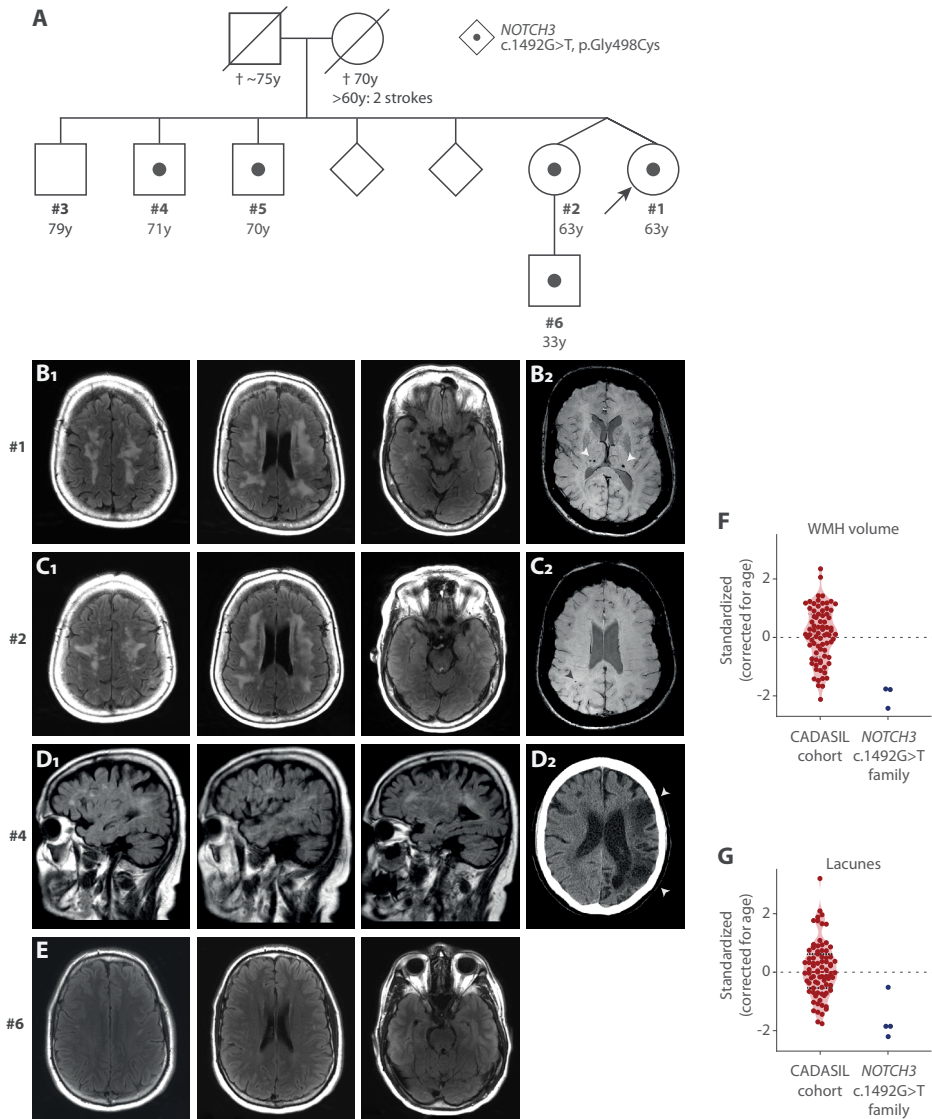
### Statistical analysis

Differences between groups were compared using one-way ANOVA analysis with Bonferroni's post-hoc correction in the immunohistochemistry analysis, and with Dunnett's post-hoc correction relative to the wildtype condition in the NOTCH3 signalling assay. Ligand-dependent increase in luciferase activity was tested per condition using independent samples *t*-tests. Normality of the data was assessed using histograms and could be assumed. All statistical analyses were two-sided tests with threshold for statistical significance of 0.05, using the IBM SPSS Statistics version 23.0.0.2 software.

## RESULTS

### Clinical characteristics of family members with the *NOTCH3* c.1492G>T variant

A 63-year-old female (index, #1, Figure 3.1a) was referred to the hereditary small vessel disease clinic of our hospital because of confluent white matter hyperintensities (WMH) seen on a commercial brain scan. This scan was performed at her own initiative when her twin sister was found to have WMH. She had a history of non-migraine headaches, short lasting attacks of vertigo and tinnitus, but an otherwise unremarkable neurological and neuropsychiatric medical history. Her vascular risk factors included a smoking history of 6 pack years and hypertension, for which she was treated since age 45, with good response. She was living independently and worked until age 60 years. Since age 62 years she noticed some short term memory impairment. Neurological examination revealed a rest tremor and mild dysdiadochokinesia left more than right, which was explained by right-more-than-left nigrostriatal degeneration shown on a DAT-scan. Global neuropsychological



examination was normal. MRI performed in our hospital showed bilateral supratentorial confluent WMH in the frontal and parietal lobes, as well as in the anterior temporal lobes, external capsules and in the basal ganglia: a pattern and extension suggestive of CADASIL, although mild for her age. There were no lacunes, which are typically present in CADASIL patients in their sixties, but some microbleeds were observed in the thalamus (Figure 3.1b).

Family history was remarkable for a large vessel stroke in a brother with a history of chronic alcohol abuse (#4) and depression in a sibling (#3). No siblings had a history of lacunar stroke or vascular cognitive decline. Except for the brother with large vessel stroke in the left medial cerebral artery with hemiparesis, all were living independently and physically able, with at most complaints of mild short term memory impairment. Both parents were deceased and their mother had experienced two strokes and cognitive decline in her 7<sup>th</sup> decade (Figure 3.1a).

A gene panel of 28 genes for small vessel disease and adult-onset leukoencephalopathy was performed in the index patient, revealing a previously unreported cysteine altering heterozygous missense *NOTCH3* variant (NM\_000435.2: c.1492G>T, p.(Gly498Cys)). The variant alters the number of cysteines in an EGFr domain of *NOTCH3* (EGFr 12), which is typical for a CADASIL-associated variant. However, this variant is remarkable for the fact that it is located adjacent to the exon 9 donor splice site. In silico analyses predict that this variant results in exon 9 skipping, thereby excluding the missense variant from the mature mRNA (Figure 3.2). This variant was also found to be present in her twin sister (#2) and in 2 other siblings (#4 and #5), as well as in a nephew (#6). One tested sibling did not have the variant (#3). Neuroimaging was performed, showing confluent WMH in all siblings, but no lacunes and a few microbleeds in only one individual (Figure 3.1c,d). The 33-year-old nephew had a few small focal WMH in the frontal deep white matter (Figure 3.1e), but not the more extensive (periventricular and temporal pole) WMH often seen in CADASIL patients in the fourth decade<sup>16</sup>. The sibling without the *NOTCH3* variant (#3) had a normal MRI scan. Family members with the *NOTCH3* variant had a lower age-adjusted WMH volume and lacune lesion load compared to a cohort of CADASIL patients. (Figure 3.1f,g and Supplementary Data 3.1).

► left medial cerebral artery (arrowheads). (E) MRI of the nephew (#6) showing minimal focal WMH in the frontal deep white matter. No brain MRI was available for one brother (#5). (F) Violin plot showing age-adjusted standardized WMH scores of the index (#1), her twin sister (#2) and the nephew (#6) compared to a cohort of CADASIL patients. (G) Violin plot showing age-adjusted standardized lacune count scores in the family members #1, #2, #4 and #6. None of the family members had lacunes. The differences the standardized score for lacunes between family members are due to the differences in age (see Supplementary Data 3.1).

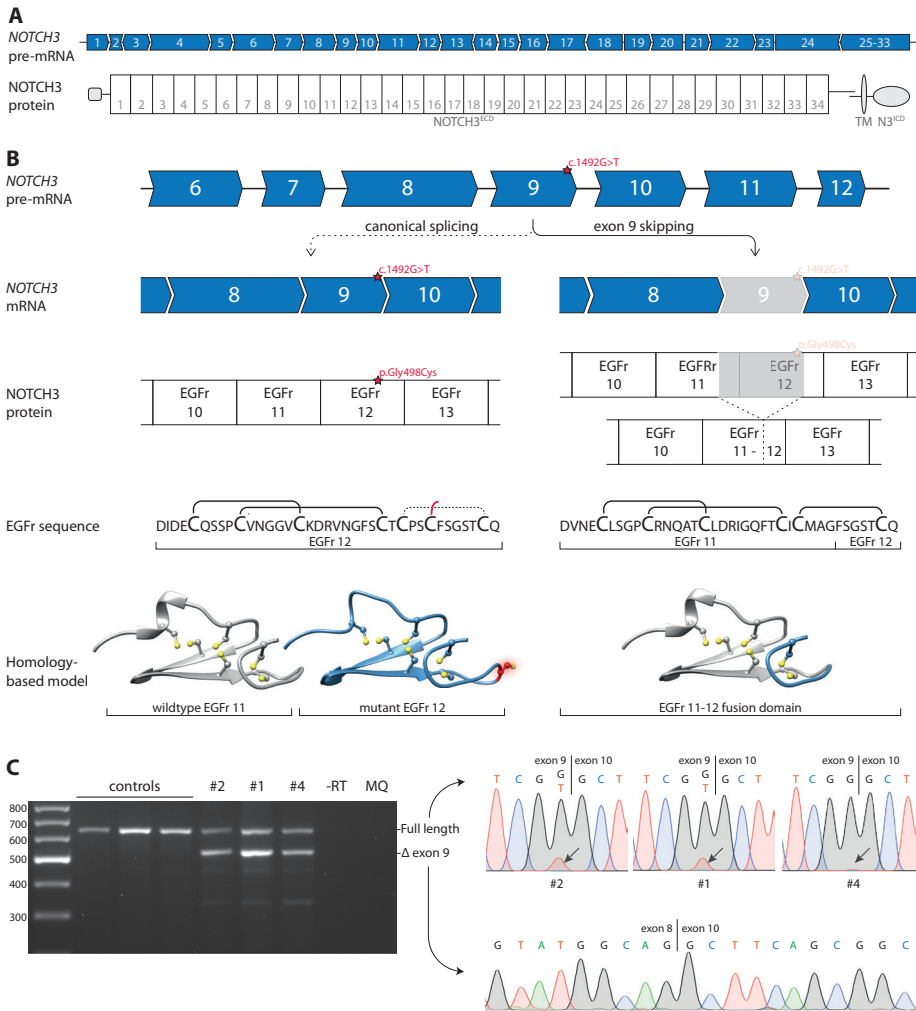


**Figure 3.2: Exon 9 skipping and predicted effect on NOTCH3 protein of NOTCH3 c.1492G>T variant**

(A) The *NOTCH3* gene contains 33 exons, of which exon 2-24 encode the 34 epidermal growth factor-like repeat (EGFr) domains in the ectodomain of the NOTCH3 protein (NOTCH3<sup>ECD</sup>). One exon can encode one or more, complete or partial EGFr domains. (B) The *NOTCH3* c.1492G>T variant is located adjacent to the splice donor site of exon 9. Upon canonical splicing of the *NOTCH3* transcript, the c.1492G>T variant results in an additional cysteine residue in EGFr domain 12. However, because the c.1492G>T variant is located adjacent to the splice donor site, it is predicted to result in exon 9 skipping. Exon 9 encodes part of EGFr 11 and part of EGFr 12; the remaining parts of EGFr 11 and EGFr 12 encoded by exon 8 and exon 10 respectively, are predicted to form an EGFr 11-12 fusion domain, with the correct number of and spacing of cysteine residues. Homology-based models show the predicted structure of EGFr domains. (C) RT-PCR and Sanger sequencing analysis showing exon 9 skipping in fibroblast RNA from individuals with the *NOTCH3* c.1492G>T variant. The full length band predominantly contained the wildtype transcript, but also some mutant transcripts, as indicated by the relatively low mutant T-peak in the sequence. No exon 9 skipping was seen in controls. RT-PCR and Sanger sequencing were performed in two independent experiments. NOTCH3<sup>ECD</sup> = NOTCH3 extracellular domain; EGFr = Epidermal growth factor-like repeat.

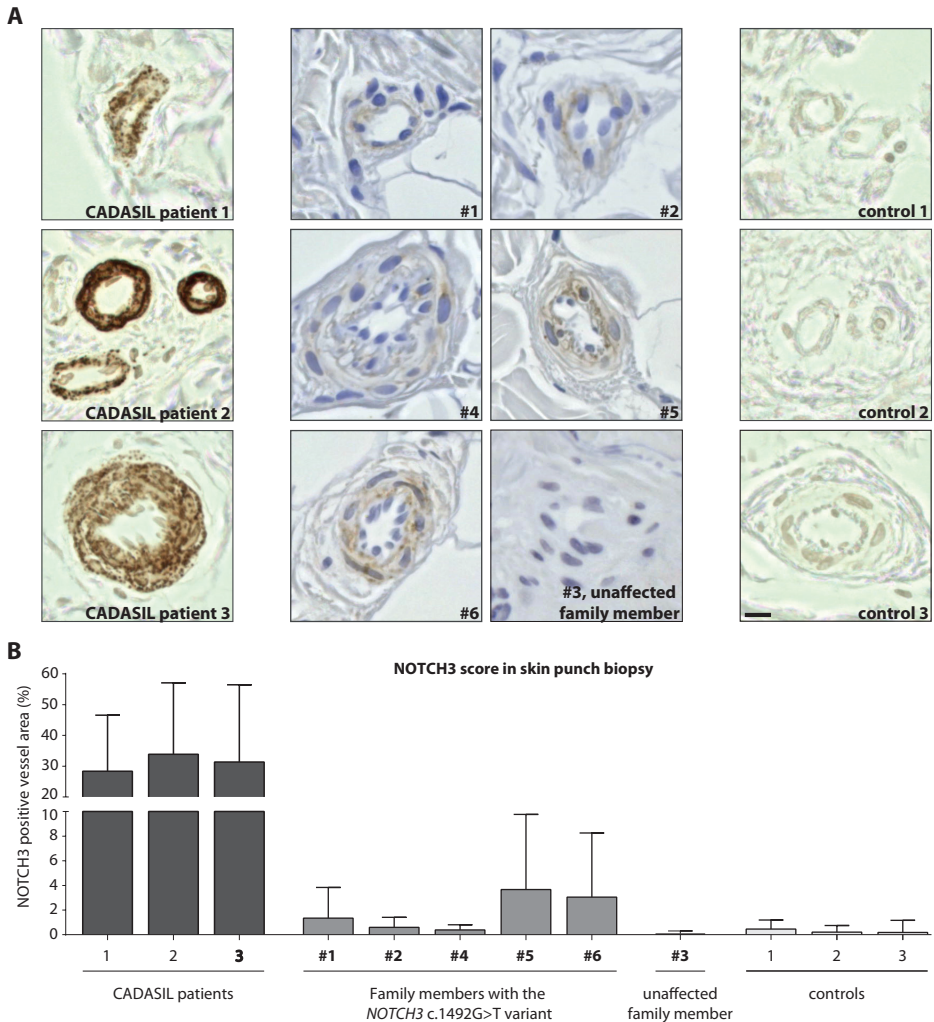


**Figure 3.3: Individuals with the *NOTCH3* c.1492G>T variant show much less granular *NOTCH3*<sup>ECD</sup> staining in skin vasculature than CADASIL patients**

(A) Representative images of *NOTCH3*<sup>ECD</sup> staining in blood vessels of skin punch biopsies: CADASIL patients, individuals with the *NOTCH3* c.1492G>T variant and controls. All family members with the *NOTCH3* c.1492G>T variant had minimal granular *NOTCH3*<sup>ECD</sup> staining, which was much less compared to *NOTCH3*<sup>ECD</sup> staining typically seen in CADASIL patients. No *NOTCH3*<sup>ECD</sup> staining was seen in the brother without the *NOTCH3* variant (#3) or in controls. (B) Quantification of the area of *NOTCH3*<sup>ECD</sup> immunostaining within the vessel wall showed that individuals with the *NOTCH3* c.1492G>T variant have significantly less *NOTCH3*<sup>ECD</sup> staining compared to CADASIL patients ( $1.81\% \pm 1.48$  versus  $31.2\% \pm 2.75$  *NOTCH3*<sup>ECD</sup> positive area within vessel wall boundaries, ANOVA,  $P < 0.001$ ). Bar represents 10  $\mu\text{m}$ . Mean  $\pm$  standard deviation.

Skin punch biopsies were taken to determine whether CADASIL-associated vessel wall pathology was present. NOTCH3 immunohistochemistry using two NOTCH3<sup>ECD</sup> antibodies showed only very slight positive, but typically granular, NOTCH3 staining compared to positive controls. There was no granular staining present in negative controls, nor in the sibling lacking the *NOTCH3* variant (Figure 3.3). Exhaustive electron microscopic analysis did not reveal CADASIL-associated GOM deposits in the vessel walls of any of the family members with the *NOTCH3* c.1492G>T variant, while many GOM deposits were observed in vessel walls of CADASIL patients (Supplementary Data 3.6).

### Characterisation of the NOTCH3 cysteine altering splice variant

To confirm that the *NOTCH3* c.1492G>T variant impairs exon 9 inclusion during the splicing process, RT-PCR analysis was performed on RNA from skin fibroblasts from three family members, which confirmed exon 9 skipping in all three individuals. Exon 9 skipping was highly efficient, with only a minority of mutant transcripts escaping exon skipping and therefore still harbouring the cysteine altering missense variant (Figure 3.2c). Skipping of exon 9 leaves the open reading frame intact and is predicted to result in the production of a slightly shorter internally deleted NOTCH3 protein. Exon 9 encodes part of EGFr 11 and part of EGFr 12, and these parts are therefore excluded from the exon 9 skipped NOTCH3 protein; the remaining parts of EGFr 11 and EGFr 12 encoded by exon 8 and exon 10, respectively, are predicted to form an EGFr 11-12 fusion domain. This EGFr fusion domain resembles a wildtype EGFr domain, with six canonically spaced cysteine residues (Figure 3.2b), mimicking NOTCH3 cysteine correction<sup>8</sup>. There is one notable difference with other *NOTCH3* exons eligible for cysteine corrective exon skipping, such as exon 4-5 skipping, namely that the exon 9 skipped protein lacks a small part of EGFr 11 which is part of the putative NOTCH3 ligand binding domain (i.e. EGFr 10 and 11).

To assess translation, processing and signalling of the exon 9 skipped NOTCH3 protein, we transfected control fibroblasts and NIH 3T3 cells with cDNA constructs lacking exon 9 (NOTCH3<sup>Δexon9</sup>). NOTCH3<sup>Δexon9</sup> was expressed at the cell surface of fibroblasts, comparable to wildtype NOTCH3 (Figure 3.4a). However, ligand-dependent signalling was impaired, comparable to the protein lacking the entire NOTCH3 ligand binding domain (NOTCH3<sup>ΔLBD</sup>) (Figure 3.4b and Supplementary Data 3.5).

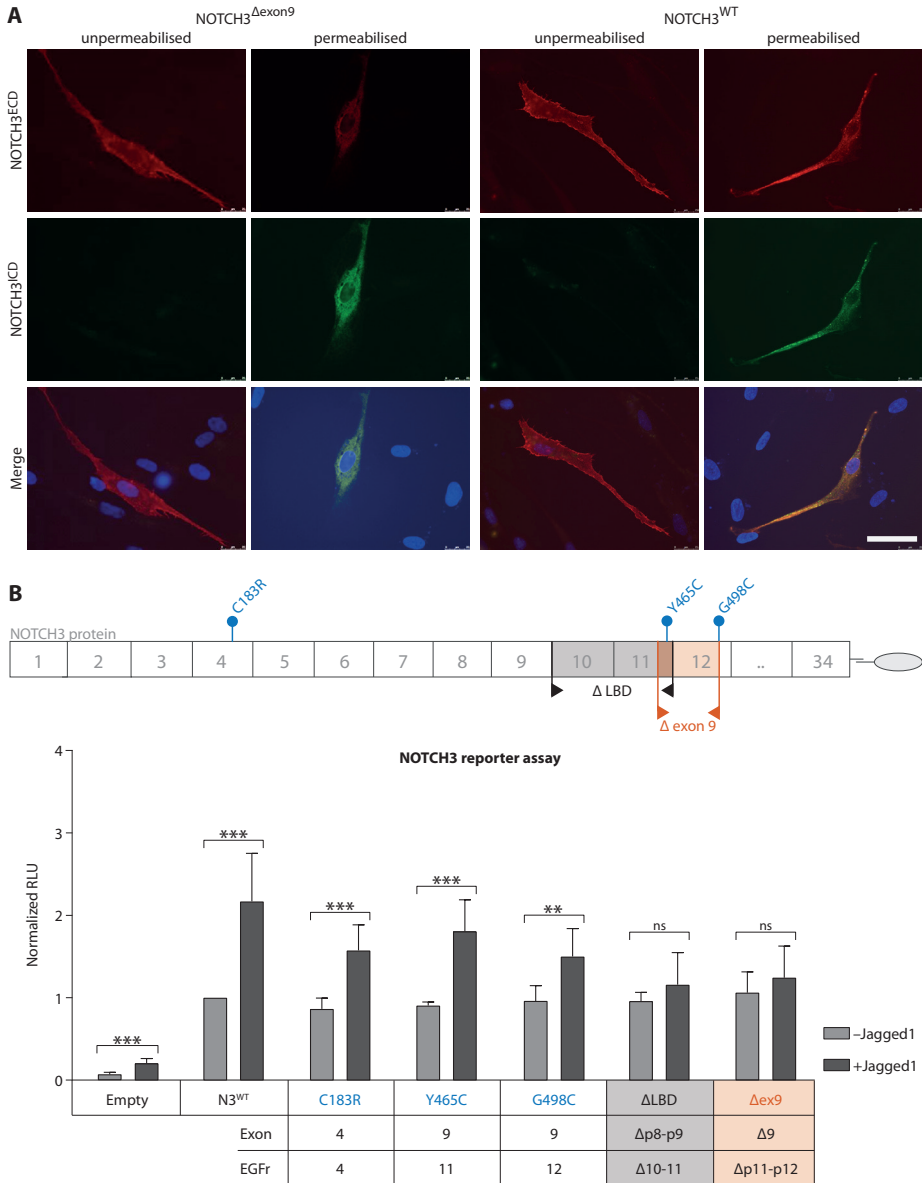


**Figure 3.4:** NOTCH3<sup>Δexon9</sup> protein has normal cellular localisation but has reduced signalling properties *in vitro*

(A) Immunocytochemistry of fibroblasts transfected with NOTCH3 cDNA constructs shows that the NOTCH3<sup>Δexon9</sup> protein is translated and expressed on the cell surface similar to NOTCH3<sup>WT</sup>, as indicated by NOTCH3<sup>ECD</sup> staining of the cell membrane in unpermeabilized cells. (B) NOTCH3 signalling in a CBF1 reporter assay with and without JAGGED1 stimulation. JAGGED1 significantly activated NOTCH3 signalling in NOTCH3<sup>WT</sup>, NOTCH3<sup>Y465C</sup> and NOTCH3<sup>G498C</sup>, but not in NOTCH3<sup>Δexon9</sup> and NOTCH3<sup>ΔLBD</sup> (independent samples *t*-test; see Supplementary Data 3.5 for details). LBD = ligand binding domain; RLU = relative luciferase units; N3<sup>WT</sup> = NOTCH3 wildtype protein; NOTCH3<sup>Δexon9</sup> = NOTCH3 exon 9 skip protein; NOTCH3<sup>ECD</sup> = NOTCH3 ectodomain; scale bar represents 50 μm. Mean ± standard deviation of 7 independent experiments. \*\* *P* < 0.01; \*\*\* *P* < 0.001.

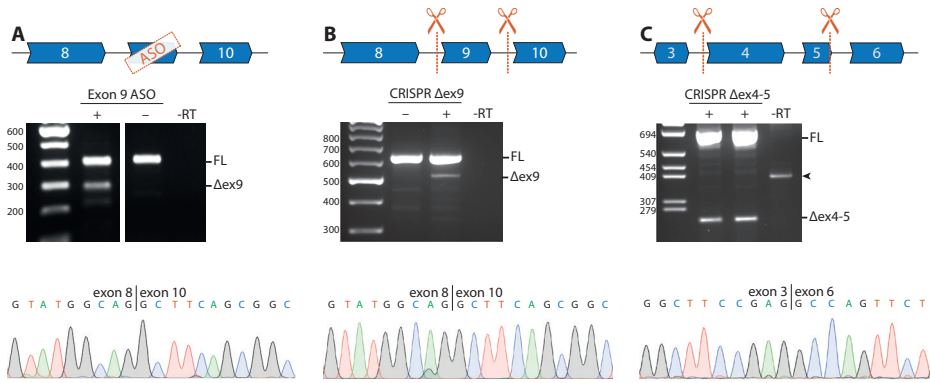


**Figure 3.5: Targeted *NOTCH3* exon exclusion using antisense oligonucleotides and CRISPR/Cas9 *in vitro***

(A) RT-PCR analysis of VSMCs after transfection with an ASO targeting exon 9, showing a band at ~300 bp, corresponding to the expected fragment size after exon 9 skipping, which was confirmed to be a correct exon 9 skip with Sanger sequencing. (B) Guide RNAs targeting *NOTCH3* intron 8 and 9 were used to delete exon 9 from the genomic DNA of HEK293 cells. RT-PCR analysis confirmed exon 9 exclusion at the RNA level. (C) Guide RNAs targeting intron 3 and intron 5 were used to delete exon 4 and exon 5 from the genomic DNA from control (left lane) and CADASIL patient-derived VSMCs (right lane), which was confirmed with Sanger sequencing. ASO = antisense oligonucleotide; FL = full length; -RT = condition without reverse transcriptase; Δex9 = PCR product lacking exon 9; Δex4-5 = PCR product lacking exon 4-5; arrowhead = aspecific genomic PCR product.

### Targeted *NOTCH3* exon exclusion *in vitro* using antisense oligonucleotides and CRISPR/Cas9

For purposes of translatability, we assessed whether it was possible to induce exon 9 antisense-mediated skipping or an exon 9 genomic deletion in control cell cultures. Exon 9 skipping was induced in VSMCs transfected with ASOs targeting exon 9 (Figure 3.5a,b). Using CRISPR/Cas9-mediated gene editing with guide RNAs targeting introns 8 and 9, exon 9 was deleted from genomic DNA in HEK293 cells (Figure 3.5c,d), with mRNA transcripts showing a correct exon 8-10 boundary similar to the mRNA transcript expressed after ASO-mediated exon 9 skipping. We also tested whether we could delete *NOTCH3* exons 4 and 5, as this cysteine corrective exon skipping would ensure a single treatment approach for most CADASIL patients<sup>8</sup>. Genome editing with guide RNAs targeting introns 3 and 5 resulted in a correct genomic exon 4-5 deletion in VSMCs and mRNA transcripts with a correct exon 3-6 boundary (Figure 3.5e,f).

## DISCUSSION

Here, we present a family with a unique cysteine altering *NOTCH3* variant that leads to exon 9 skipping, effectively excluding the mutant exon and correcting the number of cysteines in the EGFr domains of the NOTCH3<sup>ECD</sup>. This mimics the 'NOTCH3 cysteine correction' therapeutic strategy for CADASIL we previously described,<sup>8</sup> offering the unique opportunity to study the effect of cysteine correction on NOTCH3 protein aggregation and disease severity in humans. We show that exon 9 skipping is associated with strongly reduced levels of vascular NOTCH3<sup>ECD</sup> aggregation, and that individuals with exon 9 skipping have a milder small vessel disease phenotype compared to most CADASIL patients, although CADASIL can also be variable.<sup>17</sup> Furthermore, we show that NOTCH3 cysteine correction can be accomplished at the RNA level using ASOs<sup>9</sup> and at the DNA level using CRISPR/Cas9-mediated gene editing.

All family members with naturally occurring exon 9 skipping had only minimal levels of NOTCH3<sup>ECD</sup> protein aggregation in their skin vasculature, suggesting that the exon 9 skipped NOTCH3 protein does not aggregate. The minimal aggregation that was seen is likely due to the low levels of mutant NOTCH3 proteins containing exon 9, translated from the low levels of unskipped mutant transcripts. In line with this, the individual with the most efficient exon 9 skipping, had the least vascular NOTCH3<sup>ECD</sup> positive staining in skin biopsy. Notably, none of the individuals with the *NOTCH3* c.1492G>T variant had CADASIL-associated GOM deposits. In CADASIL mouse models, it has been shown that progressive NOTCH3 aggregation precedes GOM formation, showing that GOM are likely only formed once a certain threshold of NOTCH3 aggregation has been reached.<sup>18,19</sup> Thus, we cautiously pose that the natural cysteine correction that occurs in these patients strongly reduces progressive NOTCH3 aggregation, such that the GOM stage is not reached, vessel wall integrity is better preserved and therefore there is a milder later-onset disease course. Cysteine altering *NOTCH3* variants are known to be associated with a variable disease severity, part of which is explained by mutation position<sup>17</sup> and environmental factors,<sup>20,21</sup> but other genetic factors are widely held to play a role,<sup>21–23</sup> of which this naturally occurring exon skipping may be a rare example.

We have previously shown that NOTCH3 cysteine corrected proteins with EGFr fusion domains retain signalling function comparable to wildtype.<sup>8</sup> Here, we show that the exon 9 skipped NOTCH3 protein has expression and localisation properties comparable to wildtype, but that ligand-induced signalling properties are strongly reduced, comparable to complete lack of the ligand binding domain (EGFr domains 10 and 11). Whether reduced NOTCH3 signalling may contribute to the phenotype in this family is unclear, as the role of heterozygous loss-of-function variants in CADASIL or CADASIL-like small vessel disease

is still subject of debate.<sup>17,24,25</sup> Of note, we found that NOTCH3<sup>Y465C</sup>, located in EGFr domain 11, has similar JAGGED1-induced signalling capacity as variants located outside the ligand binding domain, as opposed to the NOTCH3<sup>C455R</sup> variant in EGFr 11 which has been shown to impair JAGGED1-induced signalling.<sup>12</sup> As the NOTCH3<sup>Y465C</sup> variant is located in the second-to-last amino acid of EGFr domain 11, this suggests that the distal part of EGFr domain 11 is not involved in binding to JAGGED1.

We previously showed that cysteine altering variants associated with a severe CADASIL phenotype, i.e. those located EGFr domains 1-6, are also eligible for cysteine correction by skipping exons 4 and 5 simultaneously using ASOs.<sup>8</sup> Here, we showed that CRISPR/Cas9-mediated genome editing to exclude exons 4 and 5 or exon 9 from genomic DNA is feasible, and thereby may be a potential future alternative for ASO-based cysteine correction. Therapeutic genome editing has the potential of a single treatment approach, instead of the potentially lifelong repeated ASO administration, which would be necessary for an RNA-based exon skipping approach. However, before *in vivo* genome editing of VSMCs can be applied in CADASIL patients, major hurdles need to be taken, including delivery, immunogenicity and off-target effects,<sup>26</sup> whereas ASO-mediated RNA modifications are already FDA-approved for the treatment of a number of neurodegenerative disorders,<sup>27</sup> for both intrathecal and systemic administration.<sup>28,29</sup>

In conclusion, we provide the first in-human evidence that cysteine corrective *NOTCH3* exon skipping is associated with only minimal vascular NOTCH3<sup>ECD</sup> aggregation and a relatively mild later-onset phenotype. These findings support continuing efforts in developing NOTCH3 cysteine correction for treatment of CADASIL patients..

## APPENDIX

### Acknowledgements

We acknowledge H.M. van der Klift and N. Lamzira-Arichi for their assistance in the variant analysis. We thank A.M. van Opstal for the quantification of the WMH. This work was funded by the Netherlands Brain Foundation (HA2016-02-03; BG2015-2).

### Conflict of Interest Statement

MO, GB, IH, AAM, SGvD, MCK, GMT and CRJ report no conflict of interest. GG, JWR and SAJLO were financially supported by the Netherlands Brain Foundation (HA2016-02-03; BG2015-2). NOTCH3 antisense therapies have been patented by the Leiden University Medical Center. As co-inventors on this patent JGD, AAR and SAJLO are entitled to a share

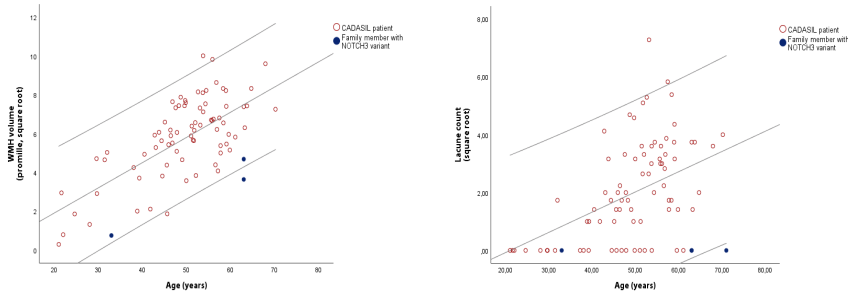
of potential royalties. FB is employed by LUMC and named inventor on patents related to neuroregeneration and is founder of Complement Pharma BV. He receives funding for contract research from WAVE technologies and is a member of scientific advisory board of CMTA USA. Renumeration is paid to LUMC. AAR discloses being employed by LUMC which has patents on exon skipping technology, including NOTCH3. As co-inventor of these patents AAR is entitled to a share of royalties. For full transparency (not related to this work) AAR discloses being ad hoc consultant for PTC Therapeutics, Sarepta Therapeutics, CRISPR Therapeutics, Summit PLC, Alpha Anomeric, BioMarin Pharmaceuticals Inc., Eisai, Astra Zeneca, Santhera, Audentes, Global Guidepoint and GLG consultancy, Grunenthal, Wave and BioClinica, having been a member of the Duchenne Network Steering Committee (BioMarin) and being a member of the scientific advisory boards of ProQR and Philae Pharmaceuticals. Remuneration for these activities is paid to LUMC. LUMC also received speaker honoraria from PTC Therapeutics and BioMarin Pharmaceuticals and funding for contract research from Italpharmaco and Alpha Anomeric.

## REFERENCES

- Chabriat, H., Joutel, A., Dichgans, M., Tournier-Lasserre, E. & Bousser, M.-C. Cadasil. *Lancet. Neurol.* **8**, 643–53 (2009).
- Joutel, A. *et al.* Notch3 mutations in CADASIL, a hereditary adult-onset condition causing stroke and dementia. *Nature* **383**, 707–10 (1996).
- Rutten, J. W. *et al.* Interpretation of NOTCH3 mutations in the diagnosis of CADASIL. *Expert Rev. Mol. Diagn.* **14**, 593–603 (2014).
- Bruhin, P., Godfraind, C., Leteurtre, E. & Ruchoux, M.-M. Morphometric analysis of ultrastructural vascular changes in CADASIL: analysis of 50 skin biopsy specimens and pathogenic implications. *Acta Neuropathol.* **104**, 241–8 (2002).
- Joutel, A. *et al.* Skin biopsy immunostaining with a Notch3 monoclonal antibody for CADASIL diagnosis. *Lancet* **358**, 2049–2051 (2001).
- Lesnik Oberstein, S. A. J. *et al.* Evaluation of diagnostic NOTCH3 immunostaining in CADASIL. *Acta Neuropathol.* **106**, 107–111 (2003).
- Schoemaker, D., Quiroz, Y. T., Torrico-Teave, H. & Arboleda-Velasquez, J. F. Clinical and research applications of magnetic resonance imaging in the study of CADASIL. *Neurosci. Lett.* (2019). doi:10.1016/j.neulet.2019.01.014
- Rutten, J. W. *et al.* Therapeutic NOTCH3 cysteine correction in CADASIL using exon skipping: In vitro proof of concept. *Brain* **139**, 1123–1135 (2016).
- Liem, M. K. *et al.* MRI correlates of cognitive decline in CADASIL. *Neurology* **72**, 143–148 (2009).
- Fokkema, I. F. A. C. *et al.* LOVD v.2.0: The next generation in gene variant databases. *Hum. Mutat.* **32**, 557–563 (2011).
- Faas, F. G. A. *et al.* Virtual nanoscopy: Generation of ultra-large high resolution electron microscopy maps. *J. Cell Biol.* **198**, 457–469 (2012).
- Peters, N. *et al.* CADASIL-associated Notch3 mutations have differential effects both on ligand binding and ligand-induced Notch3 receptor signaling through RBP-Jk. *Exp. Cell Res.* **299**, 454–464 (2004).
- Karlström, H. *et al.* A CADASIL-mutated Notch 3 receptor exhibits impaired intracellular trafficking and maturation but normal ligand-induced signaling. *Proc. Natl. Acad. Sci. U. S. A.* **99**, 17119–17124 (2002).
- Aartsma-Rus, A. *et al.* Functional analysis of 114 exon-internal AONs for targeted DMD exon skipping: indication for steric hindrance of SR protein binding sites. *Oligonucleotides* **15**, 284–97 (2005).
- Aartsma-Rus, A. *et al.* Theoretic applicability of antisense-mediated exon skipping for Duchenne muscular dystrophy mutations. *Hum. Mutat.* **30**, 293–299 (2009).
- van den Boom, R., Lesnik Oberstein, S. a J., Ferrari, M. D., Haan, J. & van Buchem, M. a. Cerebral autosomal dominant arteriopathy with subcortical infarcts and leukoencephalopathy: MR imaging findings

- at different ages—3rd–6th decades. *Radiology* **229**, 683–690 (2003).
17. Rutten, J. W. *et al.* The effect of NOTCH3 pathogenic variant position on CADASIL disease severity: NOTCH3 EGFr1–6 pathogenic variant are associated with a more severe phenotype and lower survival compared with EGFr7–34 pathogenic variant. *Genet. Med.* **21**, 676–682 (2019).
  18. Rutten, J. W. *et al.* The NOTCH3 score: a pre-clinical CADASIL biomarker in a novel human genomic NOTCH3 transgenic mouse model with early progressive vascular NOTCH3 accumulation. *Acta Neuropathol. Commun.* **3**, 89 (2015).
  19. Joutel, A. *et al.* Cerebrovascular dysfunction and microcirculation rarefaction precede white matter lesions in a mouse genetic model of cerebral ischemic small vessel disease. *J. Clin. Invest.* **120**, 433–445 (2010).
  20. Mykkänen, K. *et al.* Different clinical phenotypes in monozygotic cadasil twins with a novel notch3 mutation. *Stroke* **40**, 2215–2218 (2009).
  21. Singhal, S., Bevan, S., Barrick, T., Rich, P. & Markus, H. S. The influence of genetic and cardiovascular risk factors on the CADASIL phenotype. *Brain* **127**, 2031–2038 (2004).
  22. Opherck, C. *et al.* Genome-wide genotyping demonstrates a polygenic risk score associated with white matter hyperintensity volume in CADASIL. *Stroke* **45**, 968–972 (2014).
  23. Opherck, C. *et al.* Heritability of MRI lesion volume in CADASIL: Evidence for genetic modifiers. *Stroke* **37**, 2684–2689 (2006).
  24. Arboleda-Velasquez, J. F. *et al.* Hypomorphic Notch 3 alleles link Notch signaling to ischemic cerebral small-vessel disease. *Proc. Natl. Acad. Sci.* **108**, E128–E135 (2011).
  25. Moccia, M. *et al.* Hypomorphic NOTCH3 mutation in an Italian family with CADASIL features. *Neurobiol. Aging* **36**, 547.e5–11 (2015).
  26. Rahman, S., Datta, M., Kim, J. & Jan, A. T. CRISPR/Cas: An intriguing genomic editing tool with prospects in treating neurodegenerative diseases. *Semin. Cell Dev. Biol.* **96**, 22–31 (2019).
  27. Wurster, C. D. & Ludolph, A. C. Antisense oligonucleotides in neurological disorders. *Ther. Adv. Neurol. Disord.* **11**, 175628641877693 (2018).
  28. Luu, K. T. *et al.* Population Pharmacokinetics of Nusinersen in the Cerebral Spinal Fluid and Plasma of Pediatric Patients With Spinal Muscular Atrophy Following Intrathecal Administrations. *J. Clin. Pharmacol.* **57**, 1031–1041 (2017).
  29. Geary, R. S., Norris, D., Yu, R. & Bennett, C. F. Pharmacokinetics, biodistribution and cell uptake of antisense oligonucleotides. *Adv. Drug Deliv. Rev.* **87**, 46–51 (2015).

## SUPPLEMENTARY DATA



### Supplementary Data 3.1: Scatter plots WMH volume and lacune count

Scatter plots showing WMH volume and lacune count in the family members with the *NOTCH3* c.1492G>T variant (blue, filled dots), compared to a cohort of CADASIL patients (red, open dots)

### Supplementary Data 3.2: Small vessel disease gene panel

Gene	Reference sequence
<i>NOTCH3</i> , exon 2-24	NM_000435.2
<i>APP</i> , exon 16-17	NM_00484.3
<i>TREX1</i>	NM_016381.3
<i>HTRA1</i>	NM_002775.4
<i>ABCD1</i>	NM_000033.3
<i>AUH</i>	NM_001698.2
<i>CBS</i>	NM_000071.2
<i>CLCN2</i>	NM_004366.5
<i>COL4A1</i>	NM_001845.4
<i>COL4A2</i>	NM_001846.2
<i>CSF1R</i>	NM_005211.3
<i>CST3</i>	NM_000099.3
<i>CYP27A1</i>	NM_000784.3
<i>CTSA</i>	NM_000308.2
<i>DARS2</i>	NM_018122.4
<i>GBE1</i>	NM_000158.3
<i>GFAP</i>	NM_002055.4
<i>GLA</i>	NM_000169.2
<i>GSN</i>	NM_000177.4
<i>ITM2B</i>	NM_021999.4
<i>LMNB1</i>	NM_005573.3
<i>MMACHC</i>	NM_015506.2
<i>TREM2</i>	NM_018965.3
<i>TTR</i>	NM_000371.3
<i>TYMP</i>	NM_001257988.1; NM_001257989.1
<i>TYROBP</i>	NM_003332.3

Analysis was performed on the sequence of the coding exons of the target genes, including 20 nucleotides in the flanking introns. Analysis was performed by the Leiden Laboratory for Diagnostic Genome Analysis (LDGA).

## Supplementary data 3.3: List of PCR primers and RNA guides

Gene	F/R	Sequence (5'–3')	Product size	Product size $\Delta$ exon 9	Application
NOTCH3	Fw, exon 7	GGATGTGGACGAGTGCTCTATC	635 bp	521 bp	RT-PCR
	Rv, exon 11	CCACCAGTCTAGGCATTTG			
NOTCH3	Fw, exon 8	AACCCCTGCGAGCACTTG	403 bp	289 bp	RT-PCR
	Rv, exon 10	CACAGCGGCACTCGTAGC			
NOTCH3	Fw, intron 8	GGATTGTGCGATGAGTAGGAA	424 bp		gDNA PCR
	Rv, intron 9	CAGAAAGGGTGAGAGCAGTACAC			
NOTCH3	Fw, exon 3	CCGATTCTCATGCCGGTGC	581 bp	119 bp	RT-PCR, Sanger
	Rv, exon 6	CCAGCGTGTGAAGCAGGT			
NOTCH3	Fw	p-TGCTTCAGCGGCTCCACC			Inverse PCR <sup>a</sup>
	Rv	CGAGGGGAGGTGCAGCT			NOTCH3 <sup>C498C</sup>
NOTCH3	Fw	p-GTTGCGAGGTGGACATTGACGAG			Inverse PCR <sup>a</sup>
	Rv	AGTTTCTGTGAAGCCTGCCAT			NOTCH3 <sup>Y465C</sup>
NOTCH3	Fw	p-GCTTCAGCGGCTCCACGTGT			Inverse PCR <sup>a</sup>
	Rv	CTGCCATACAGATACAGGTGAAC			NOTCH3 <sup><math>\Delta</math>exon9</sup>
NOTCH3	Fw, exon 9	TCAGACTAGCCCTGTGTCA			Sanger <sup>b</sup>
NOTCH3	Intron 8	TGCACCCCGTTCACACCATA			RNA guides
	Intron 9	TTGTAAGTTATCCGCTAACG			exon 9 deletion

<sup>a</sup> For the inverse PCR, the forward primer was phosphorylated at the 5' side of the primer.

<sup>b</sup> Sanger: Sanger Sequencing.

## Supplementary Data 3.4: List of tested ASOs targeting NOTCH3 exon 9

ASO Sequence (5'–3')	Multimerization <sup>a</sup>	<i>In vitro</i> skip efficiency <sup>b</sup>
AUUGACUCGGUCCUUGCAGA	No	~40%
AUGUCCACCUCGCAAUAGGU	No	~30%
ACUCUGACACUCGUCAAUGU	No	~15%

<sup>a</sup> Multimerization was tested at 37°C.

<sup>b</sup> *In vitro* skip efficiency was assessed in cultured control fibroblasts. Quantification of exon skip efficiency was performed by Lab-on-a-Chip analysis after RT-PCR with 30 cycles.

### Supplementary Data 3.5: NOTCH3 signaling in a CBF1 reporter assay with and without Jagged1 stimulation to assess ligand-induced signaling in *NOTCH3* variants

	RLU with and without JAGGED1 stimulation			RLU fold induction upon Jagged1 stimulation	
	-Jagged1 Mean $\pm$ SD	+Jagged1 Mean $\pm$ SD	P-value <sup>a</sup>	Mean $\pm$ SD	P-value <sup>b</sup>
NOTCH3 <sup>WT</sup>	1.00	2.16 $\pm$ 0.58	<0.001	2.17 $\pm$ 0.58	<i>Reference</i>
NOTCH3 <sup>C183R</sup>	0.86 $\pm$ 0.13	1.57 $\pm$ 0.31	<0.001	1.84 $\pm$ 0.37	0.541
NOTCH3 <sup>Y465C</sup>	0.90 $\pm$ 0.04	1.80 $\pm$ 0.38	<0.001 <sup>c</sup>	1.99 $\pm$ 0.37	0.966
NOTCH3 <sup>G498C</sup>	0.96 $\pm$ 0.19	1.50 $\pm$ 0.34	0.003	1.58 $\pm$ 0.31	0.044
NOTCH3 <sup><math>\Delta</math>exon9</sup>	0.96 $\pm$ 0.11	1.16 $\pm$ 0.39	0.216	1.22 $\pm$ 0.43	<0.001
NOTCH3 <sup><math>\Delta</math>LBD</sup>	1.06 $\pm$ 0.25	1.24 $\pm$ 0.38	0.317	1.17 $\pm$ 0.19	<0.001

<sup>a</sup> P-value represents difference between unstimulated versus Jagged1 stimulated condition (independent samples *t*-test).

<sup>b</sup> P-value represents RLU fold induction compared to NOTCH3<sup>WT</sup> (ANOVA with Dunnett's post-hoc correction relative to the wildtype condition).

LBD = ligand binding domain; RLU = relative luciferase units.

### Supplementary Data 3.6: Results of ultrastructural GOM deposit analysis in skin blood vessels

Patient	Number of GOM deposits	Number of vessels assessed
Family member #1	0	14
Family member #2	0	5
Family member #4	0	9
Family member #5	0	6
Family member #6	0	6
Healthy control	0	10
CADASIL patient 1	85	9
CADASIL patient 2	17	10



# Chapter 4

## Long-term disease progression in CADASIL: an 18-year follow-up study

Gido Gravesteijn  
Remco J. Hack  
Anna M. van Opstal  
Bastian J. van Eijsden  
Maurice Overzier  
Joseph F. Arboleda-Velasquez  
Huub A.M. Middelkoop  
Mar D.M. Rodriguez Gironde  
Charlotte E. Teunissen  
Annemieke Aartsma-Rus  
Jeroen van de Grond  
Julie W. Rutter\*  
Saskia A.J. Lesnik Oberstein\*

Submitted

# ABSTRACT

## Objective

To gain more insight into long-term disease progression and survival in CADASIL patients, we performed a prospective clinical and neuroimaging 18-year follow-up study, including cerebral hemodynamics and blood biomarkers.

## Methods

Forty-one CADASIL patients and 21 unaffected family members were characterised at baseline, including MRI, functional independence and neuropsychological testing. Cerebral hemodynamics were measured using PC-MRA and functional MRI. At 18-year follow-up, 15 patients and 9 controls re-visited our hospital for the same battery of tests. Blood levels of Neurofilament-Light-chain (NfL) were measured using single molecule array. HTRA1, Endostatin, IGF-BP1 and TGF- $\beta$  were quantified using ELISA.

## Results

Half of the patients (22/41) were still alive after 18 years. Lacune load and disability at baseline were significantly associated with survival. Eight of the 15 patients who were able to participate in the follow-up study still had no significant disability, executive dysfunction or global cognitive impairment after 18 years (age range 40-63 years). At baseline and follow-up these relatively stable patients had significantly less lacunes than the severely affected patients. Of the tested blood biomarkers, only serum NfL levels were associated with disease severity at both time points, but its 18-year increase did not significantly differ between patients and controls. Patients and controls did not differ in longitudinal hemodynamic changes.

## Conclusion

CADASIL patients can remain clinically relatively stable over almost two decades. Disease severity, disease progression and survival are most strongly associated with lacune load. NfL was the only blood biomarker associated with disease severity at both time points.

## INTRODUCTION

CADASIL is the most prevalent monogenic cerebral small vessel disease and is caused by *NOTCH3* mutations.<sup>1</sup> These mutations lead to aggregation of the *NOTCH3* ectodomain (*NOTCH3*<sup>ECD</sup>) in the vessel wall of small arteries, which is associated with impaired cerebrohemodynamics, leading to recurrent stroke and vascular cognitive impairment.<sup>2–5</sup> Disease severity is increasingly recognized to be highly variable in CADASIL, partially attributable to modifiers such as mutation position<sup>6</sup> and classical cardiovascular risk factors.<sup>7,8</sup> There are only a few prospective studies in CADASIL cohorts, of which the longest is a seven year follow-up.<sup>9–14</sup>

Here, we performed a prospective 18-year follow-up study in CADASIL patients and unaffected family members to gain more insight into long-term disease progression and survival. Longitudinal assessment included functional independence, a neuropsychological test battery and structural neuroimaging, as well as cerebral hemodynamics and blood withdrawal for the analysis of potential blood biomarkers, including Neurofilament Light-chain (NfL).<sup>15–18</sup>

## METHODS

### Cohort

In 2000, 41 genetically confirmed CADASIL patients and 22 unaffected family members were recruited from the Dutch CADASIL registry and enrolled in the baseline study.<sup>19</sup> The participants came from 15 families, of which 10 families had 2 or more participants in the study. *NOTCH3* sequence analysis showed that most of the patients had mutations in exon 4 (n=32), while the other nine patients had a mutation in exon 8 (n=1), exon 11 (n=1), exon 19 (n=4) or exon 20 (n=3).

### Study procedure

A full medical history was taken, blood was withdrawn and neuropsychological tests and brain MRI were performed.<sup>19</sup> In 2018, survival data were obtained from the Dutch population registry from all participants. All living patients were re-invited for the 18-year follow-up study for the same battery of tests. Medical information was collected for patients who could not participate on-site and for those who were deceased. Cause of death could be obtained from seven deceased patients. Patients not participating in the follow-up study were considered to have had a stroke when patients were deceased during the follow-up or when a stroke was reported by a neurologist. Relevant disease progression was

defined as an increased modified Ranking Scale score, but not counting the increase from stage 0 to 1. Both studies were approved by the medical ethics committee of the Leiden University Medical Center (P80.89; P17.170). Written informed consent of each participant was obtained at each visit.

### Neuroimaging

MRI at baseline was performed on a 1.5 Tesla MR system, as described previously.<sup>12,20</sup> At 18-year follow-up, MRI was performed on a whole body magnetic resonance system with a 3 Tesla field strength (Philips Medical Systems, Best, Netherlands). Neuroimaging follow-up was available for 13/15 patients: one did not undergo MRI due to severe claustrophobia and one had a contra-indication for MRI. We obtained three dimensional T<sub>1</sub>-weighted images (echo time [TE] 4.6ms, repetition time [TR] 9ms, Flip 8°, field of view [FOV] = 224 × 177 × 168mm, scan duration ~5mins), T<sub>2</sub>-weighted images (TE/TR/Flip: 80ms/4.2s/90°, 40 slices, FOV 224 × 180 × 144mm, slice thickness 3.6mm, matrix size 448 × 320), fluid-attenuated inversion recovery (TE/TR/Flip angle: 125ms/11.0s/90°, slices 25, FOV 252 × 179.76 × 250mm, matrix size 224 × 224, scan duration 293s) and susceptibility-weighted images (TE/TR/Flip angle: 31ms/45ms/13°, 125 slices, matrix size: 250 × 175 × 112mm voxel size: 0.78 × 0.78 × 0.8mm). Phase-contrast quantitative flow scans (PC-MRA) were acquired using 2 localizer angiograms in the sagittal and coronal planes (TR=11ms; TE 7.5ms; flip angle=10°; slice thickness=5mm; field of view 150 × 103mm; voxel size 1.17 × 1.17mm; velocity sensitivity=200cm/s, 20 signal averages). The visually stimulated blood-oxygen-level-dependent (BOLD) fMRI scans were acquired with a TE/TR: 31ms/1499ms, FOV 220 × 75 × 220mm, matrix 80 × 80mm, slices 25, 130 dynamics, scan duration 201sec. Lacunar infarcts of presumed vascular origin (lacunes) were re-counted for the baseline scans and counted for the follow-up scans using the definition of the STRIVE criteria.<sup>21</sup> Volumetric analyses of MR images at baseline were described previously<sup>12,20</sup> and volumetric analysis of MR images at 18-year follow-up was performed using FMRIB Software Library (FSL) version 5.0.8 (Analysis Group, FMRIB, Oxford, UK).<sup>22</sup> Brain parenchymal fraction (BPF) was calculated at each time-point by dividing brain parenchymal volume over intracranial volume. Absolute white matter hyperintensity (WMH) volume was analysed at baseline as described previously<sup>13</sup> and for 18-year follow-up, FSL was used to quantify WMH automatically as described before.<sup>23</sup> WMH volume was normalized to brain parenchymal volume in order to obtain normalized WMH volume (WMH<sub>v</sub>). In order to correct for potential differences in WMH<sub>v</sub> quantification methods at baseline and follow-up, WMH were also quantified on MRI scans made in a 7-year follow-up study of the same cohort,<sup>12,20</sup> using similar methods to the baseline scans,<sup>12,20</sup> as well as using FSL similar to the 18-year follow-up scans.<sup>23</sup> Baseline WMH<sub>v</sub> were then normalized to the quantification method used for the 7- and 18-year follow-up studies, using mixed model linear regression with random intercepts, with quantification method and time point as

variables. WMH were also classified semi-quantitatively using the Fazekas scale for deep white matter hyperintensities.<sup>24</sup>

### Neuropsychological and functional ability tests

Disability was assessed using the modified Rankin Scale (mRS). Global cognition was assessed using the Cambridge Cognitive Examination (CAMCOG) and Mini-Mental State Examination (MMSE).<sup>25,26</sup> Global memory was determined using the Wechsler Memory Scale.<sup>27</sup> Executive function was assessed using the symbol substitution test of the Wechsler Adult Intelligence Scale (WAIS; Pearson, London, UK) and the Trail Making Test part A (TMT-A) and part B (TMT-B).<sup>28</sup>

### CVR and BOLD procedure

At 18-year follow-up, blood-oxygen-level dependent (BOLD) fMRI studies were performed in patients participating in the 18-year follow-up study, as well as in seven additional CADASIL patients and 10 additional healthy controls in order to increase sample size for the BOLD analyses (extended cohort). A visual stimulus, consisting of 16 blocks of an 8 Hz flashing radial black and white checkerboard pattern was shown for 20 seconds, alternated with 28 seconds of grey screen, as used in an earlier study in cerebral amyloid angiopathy.<sup>29</sup> BOLD fMRI scans were analysed for BOLD amplitude, time to peak and time to baseline as described before.<sup>29,30</sup>

At baseline and follow-up, cerebrovascular reactivity (CVR) measurements were performed using a gradient-echo phase-contrast technique (PC-MRA) before and after administration of 14 mg/kg acetazolamide, as described previously.<sup>31</sup> At 18-year follow-up, cerebral blood flow was measured in the internal carotid and basilar arteries using the Dicom viewing software Osirix with region of interest measurement tools. In addition to the patients and controls participating in the 18-year follow-up study, seven additional CADASIL patients and 10 additional healthy controls were enrolled in order to increase sample size (extended cohort). Flow was measured for basilar artery and both internal carotid arteries separately. Total cerebral blood flow was calculated as the sum of the flow of all three vessels. CVR was defined as  $(\text{CBF}_{\text{challenge}} - \text{CBF}_{\text{resting}}) / \text{CBF}_{\text{resting}} \times 100\%$ .

### Blood biomarkers

Serum and plasma samples were taken at baseline and 18-year follow-up, centrifuged at 2750g, aliquoted and stored at -80°C until analysis. Commercially available enzyme-linked immunosorbent assays (ELISA) were used to quantify levels of Endostatin (DNSTO, R&D Systems, USA; plasma diluted 1/50), HTRA1 (SEL604Hu, American Research Products, USA; plasma diluted 1/50), IGF-BP1 (DGB100, R&D; plasma diluted 1/2.5) and TGF-β (DB100B, R&D; serum diluted 1/80), according to manufacturer's instructions. All

standard curves had  $r^2 > 0.99$ . The previously reported home-brew NOTCH3<sup>ECD</sup> ELISA<sup>17</sup> was adapted for determining NOTCH3<sup>ECD</sup> levels in human samples, by using 4  $\mu$ L horse radish peroxidase-streptavidin complex in 100  $\mu$ L volume per well and by using a 1/20 dilution of plasma samples. Serum NfL levels at baseline were previously determined.<sup>16</sup> Only NfL and Endostatin levels were measured in 18-year follow-up samples, as the other blood biomarkers showed no differences between patients and controls at baseline. In baseline and follow-up samples, the levels of serum NfL were measured as previously reported,<sup>16</sup> and the levels of Endostatin were measured using ELISA (DNSTO, R&D Systems).

### Statistics

Independent samples *t*-test and independent samples Mann-Whitney U test were used to compare baseline differences between the whole cohort and the cohort that completed the 18-year follow-up study, to compare baseline differences in 18-year change between patients and controls, and to compare patients with  $mRS \geq 2$  versus patients with  $mRS \leq 1$ . The median age at first stroke was calculated using Kaplan Meier stroke-free survival analysis. Kaplan Meier analysis was also used to analyse 18-year overall survival with log-rank using the factors lacunes (0; 1-10; >10), stroke (yes/no), and mRS (0-2; 3-5). Age-corrected *P*-values for survival were calculated using Cox regression models. The difference in age-dependent increase in disease measures and biomarkers between patients and controls was modelled with linear mixed models with random slopes (which showed lower AIC values than random intercepts) with correction for sex. Non-normally distributed data were transformed for this analysis to obtain plausible normal distributions: WMH<sub>v</sub> was square root transformed; CAMCOG and MMSE were quadratic transformed; TMT-A and -B were  $\log_{10}$  transformed; microbleed count was  $\log_{10}(1+x)$  transformed; and NfL was natural log transformed. For exploring which vascular risk factors at baseline were associated with changes in disease measures over 18-years (stroke count, lacune count, mRS, CAMCOG), linear regression models were used with correction for age. Differences in cerebral hemodynamics and blood biomarkers were tested using ANCOVA with correction for age and Bonferroni correction for multiple testing. Associations with NfL levels in patients were performed using simple linear regression and forward linear regression with covariates lacunes, WMH<sub>v</sub>, BPF, mRS, CAMCOG and age. All statistical analyses were performed in IBM SPSS Statistics version 25.0. All statistical tests were two-sided and the threshold for statistical significance was 0.05.

### Data availability

With the permission of the authors and their institutions, all data used for analysis will be shared after ethics approval if requested by other investigators for reasonable purposes of replicating procedures and results.

**Table 4.1: Patient characteristics at baseline and at 18-year follow-up**

18-year follow-up data of the whole cohort			
	Baseline	18-year follow-up	P-value <sup>d</sup>
N	41	37 <sup>a</sup>	
Age, y (mean, SD)	45.8 (10.4)	- <sup>b</sup>	
Female	22 (54%)	20 (54%)	
History of stroke	23 (56%)	29 (78%) <sup>c</sup>	0.03 <sup>*</sup>
mRS			
score 0-2	30 (73%)	13 (35%)	
score 3-5	11 (27%)	5 (14%)	
score 6 (deceased)	-	19 (51%)	
Patients who visited the study site after 18 years			
	Baseline	18-year follow-up	P-value <sup>d</sup>
N	15	15	
Age, y (mean, SD)	39.6 (8.9) <sup>†e</sup>	57.6 (8.8) <sup>e</sup>	
Female	9 (60%)	9 (60%)	
History of stroke	4 (27%)	9 (60%)	0.06
Disability			
score 0-2	15 (100%) <sup>†</sup>	12 (80%)	0.25
score 3-5	0	3 (20%)	
<i>Neuroimaging measures (N)</i>	13 <sup>f</sup>	13 <sup>f</sup>	
Lacunae	0 (0-7) <sup>†</sup>	4 (0-16)	0.008 <sup>**</sup>
yes	6 (46%)	11 (85%)	0.06
no	7 (54%)	2 (15%)	
WMH <sub>v</sub> (‰)	13.76 (0.63-55.22) <sup>†</sup>	39.7 (19.3-92.1)	<0.001 <sup>***</sup>
BPF (%)	83.3 (3.2)	78.1 (3.5)	n/a <sup>g</sup>
Microbleeds	0 (0-0) <sup>†</sup>	3 (0-37)	0.046 <sup>*</sup>
yes	0 (0%)	8 (62%)	0.008 <sup>**</sup>
no	13 (100%)	5 (38%)	
<i>Cognitive measures (N)</i>	15	15	
CAMCOG	96.3 (4.1) <sup>†</sup>	89.6 (7.4)	0.03 <sup>*</sup>
MMSE	28.1 (1.5)	28.7 (1.2)	0.19
WMS	69.3 (11.0)	62.6 (11.8)	0.47
WAIS substitution	53.7 (12.1)	45.6 (18.2)	0.54
TMT-A (s)	33 (10-48)	37 (12-156)	0.19
TMT-B (s)	64 (36-140)	76 (43-383)	0.48

Summary statistics are shown as count (%), mean (SD) or mean (range).

<sup>†,‡</sup> For the indicated measures, the fifteen patients participating at 18-year follow-up were significantly younger and less severely affected at baseline (<sup>†</sup>  $P < 0.05$ , <sup>‡</sup>  $P < 0.01$ ).

<sup>a</sup> Four patients were lost to follow-up.

<sup>b</sup> No average age could be calculated since part of the patients were deceased at follow-up.

<sup>c</sup> All patients deceased at follow-up due to CADASIL were considered to have had a stroke.

<sup>d</sup> P-value represents the change over 18 years of the respective variable in patients, compared to controls. Significance level of 0.05, 0.01 and 0.001 is indicated by asterisks (\*, \*\*, \*\*\*, respectively). For dichotomous variables, P-value represents McNemar test for the difference in proportion at baseline and follow-up.

<sup>e</sup> The age range was 22-51 years at baseline and 40-70 years at follow-up.

<sup>f</sup> For two patients neuroimaging was not available due to claustrophobia and an MRI contra-indication.

<sup>g</sup> Due to technical differences between baseline and follow-up, BPF at the two time points could not be compared.

## RESULTS

### 18-year disease progression

Of the 41 patients who participated in the baseline study, 19 (46%) were deceased at the time of the 18-year follow-up study. The mean age at death of these 19 patients was  $62.4 \pm 7.1$  years, the overall mean survival estimate was 66.5 years (95%-CI 63.7–69.3 years). One patient was deceased due to stroke, and the majority of the other patients was deceased due to secondary complications of CADASIL, including swallowing difficulties and pneumonia. Mortality was associated with the following variables at baseline: age ( $P=0.005$ ), prior stroke ( $P=0.02$ ), presence of lacunes ( $P<0.001$ ) and disability ( $P<0.001$ ) (Figure 4.1). Patients without any disability (mRS 0) at baseline had a 85% (11/13) survival rate. Of the 22 patients who were still alive, fifteen visited the study site after 18 years for a complete assessment including MRI and neuropsychological testing. Three additional patients could not visit the study site, but did give consent for medical record retrieval and hetero-anamnesis via their spouse. Four patients were completely lost to follow-up.

During the 18-year follow-up, 29/37 (78%) patients had at least one incident or recurrent stroke (Table 4.1). Of these 29 patients, 23 (79%) had prior stroke at baseline. Three patients who had prior stroke at baseline did not have recurrent stroke during the 18-year follow-up. The mean age at first stroke was 49.5 years (95%-CI: 45.5–53.5 years, range 31–73 years). In our cohort, the total stroke incidence was 5.5 per 100 person years.

In the fifteen patients and nine controls from the baseline study who visited the study site after 18 years, the mean follow-up time was  $18.1 \pm 0.3$  years. Compared to all patients, the 15 patients for whom 18-year follow-up data were available were younger ( $39.6 \pm 8.9$  versus  $45.8 \pm 10.4$  years,  $P=0.044$ ) and less severely affected at baseline (mRS  $0.5 \pm 0.6$  versus  $1.6 \pm 1.5$ ,  $P=0.006$ ). Eight of the fifteen patients remained clinically relatively stable over 18 years: they had no relevant disability (mRS  $\leq 1$ ) and also no significant cognitive impairment at 18-year follow-up (Table 4.2). Compared to the seven patients who showed disease progression over 18-years (increase of 1 unit on the mRS, except going from mRS 0 to 1) and who had significant disability at follow-up (mRS  $\geq 2$ ), the eight patients with mRS  $\leq 1$ , differed in baseline characteristics only with respect to age and lacune count (Table 4.2). Three of the 8 patients who remained stable had an incident stroke during follow-up, whereas incident or recurrent stroke occurred in 6/7 patients who progressed. WMH<sub>v</sub> increase was similar between the patients that remained stable and those who progressed. Patients who progressed showed a stronger deterioration on CAMCOG and WAIS compared those who remained stable, but not on the other cognitive measures (Table 4.2). For the whole group of 15 patients, the only cognitive test that showed deterioration compared to controls

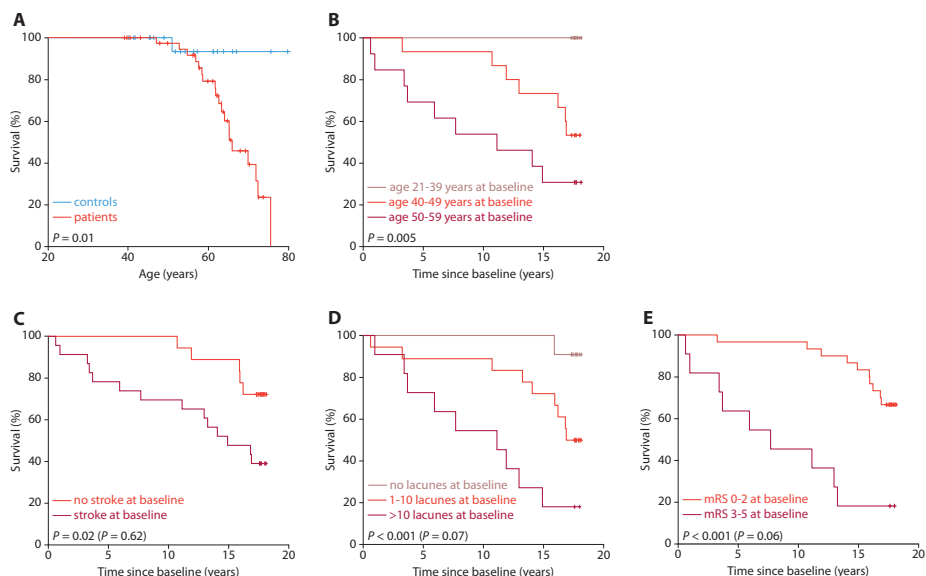


**Figure 4.1: Association between disease severity at baseline and 18-year survival**

(A) Overall mean survival of CADASIL patients was 66.5 years (95%-CI 63.7–69.3 years). (B) Age at baseline was associated with survival (log-rank  $P=0.005$ ). (C) Prior stroke at baseline was associated with a higher mortality before correction for age (HR 3.1,  $P=0.02$ ; after correction for age: HR 1.31,  $P=0.62$ ). Median survival time for patients with prior stroke at baseline was 14.9 years (95%-CI: 9.3–20.5). (D) The presence of lacunes at baseline was associated with a higher mortality (log-rank  $P<0.001$ , age-corrected log-rank  $P=0.07$ ) (>10 lacunes HR 21.6,  $P=0.004$ , age-corrected HR 6.9,  $P=0.07$ ; and 1-10 lacunes HR 6.9,  $P=0.07$ , age-corrected HR 3.1,  $P=0.28$ , compared to patients without lacunes). Median survival time for patients with >10 lacunes at baseline was 11.1 years (95%-CI: 4.7–17.6). (E) Patients with mRS  $\geq 3$  at baseline had a median survival time of 7.7 years (95%-CI: 0–15.7) with a HR of 5.8 ( $P<0.001$ , age-corrected HR 2.7,  $P=0.05$ ), compared to patients with mRS  $\leq 2$  at baseline (log-rank  $P<0.001$ , age-corrected log-rank  $P=0.06$ ).  $P$ -values in figures represent log-rank test for differences between survival curves, and  $P$ -values in brackets represent age-corrected  $P$ -values.

was the CAMCOG (Table 4.1, Figure 4.2). There was no association between 18-year disease progression and vascular risk factors (smoking, hypertension, hyperlipidaemia, Diabetes Mellitus type II and ApoE4 genotype).

There were some striking differences in disease progression, even in patients who were the same age at baseline. This is clearly illustrated by two siblings in their forties at baseline who were two years apart in age. One sibling was already more severely affected at baseline and had a rapid disease progression, while the other sibling was mildly affected at baseline and had hardly progressed at 18-year follow-up (Figure 4.3).

Table 4.2: Disease progression in the subset of patients studied at 18-year follow-up

	At baseline			Delta over 18-years		
	mRS 0-1 at FU18	mRS $\geq 2$ at FU18	P-value	mRS 0-1 at FU18	mRS $\geq 2$ at FU18	P-value for difference in 18-year delta between groups
Age	34.8 (22.1–45.7)	46.0 (38.9–51.7)	0.009 <sup>***</sup>	-	-	-
Stroke count	0 (0–0)	1 (0–3)	0.07	0 (0–1)	1 (0–3)	0.04 <sup>*</sup>
Lacune count	0 (0–1)	1 (0–7)	0.02 <sup>*</sup>	2 (0–9)	6.5 (1–12)	0.07
BPF (%)	82.9 (4.1)	83.7 (2.0)	0.69	n/a <sup>a</sup>	n/a <sup>a</sup>	n/a <sup>a</sup>
WMH <sub>v</sub> (%)	8.5 (0.6–21.6)	29.9 (4.0–55.2)	0.07	27.5 (15.1–36.2)	23.9 (15.2–38.9)	0.95
Microbleed count	0 (0–0)	0 (0–0)	0.99	0 (0–11)	5 (0–37)	0.14
mRS	0 (0–1)	1 (0–2)	0.05	0 (0–1)	2 (1–2)	0.001 <sup>**</sup>
CAMCOG	98 (93–100)	96 (87–101)	0.46	-4 (-7–3)	-8 (-16 – -5)	0.004 <sup>**</sup>
MMSE	28 (25–30)	28 (26–29)	0.99	1.1 (1.3)	0 (1.6)	0.17
WMS	71.5 (9.9)	66.8 (12.4)	0.43	-4.0 (8.2)	-8.2 (6.1)	0.31
WAIS-substitution	58.5 (10.0)	48.1 (12.5)	0.10	-1.5 (7.3)	-18.3 (9.9)	0.003 <sup>**</sup>
TMT-A (s)	26 (10–39)	37 (30–48)	0.05	2.5 (-17–19)	22 (-17–108)	0.19
TMT-B (s)	60 (36–140)	77 (44–102)	0.23	10 (-13–27)	67.5 (-42–315)	0.14
NfL (pg/mL)	6.1 (2.2–16.2)	7.7 (6.8–22.2)	0.07	4.4 (-0.3–5.5)	5.2 (0–33.5)	0.28
CVR	69.1 (20.4)	52.7 (16.2) <sup>b</sup>	0.34	-3.14 (36.1)	-0.45 (n/a) <sup>c</sup>	n/a
Resting CBF	642 (120)	548 (118) <sup>d</sup>	0.18	-52 (170)	-220 (100) <sup>e</sup>	0.11

Depending on whether normal distribution could be assumed, data is shown as mean (SD) or median (range). Group were based on mRS at follow-up, with patients with mRS 0-1 (n=7 for neuroimaging measures, n=8 for other measures unless otherwise stated) and patients with mRS $\geq 2$  (n=6 for neuroimaging measures, n=7 for other measures unless otherwise stated).

<sup>a</sup> Due to technical differences between baseline and follow-up, BPF at the two time points could not be compared.

<sup>b,c,d,e</sup> Not all patients consented to acetazolamide challenge, resulting in a group size of n=2, n=1, n=6, n=4, respectively.

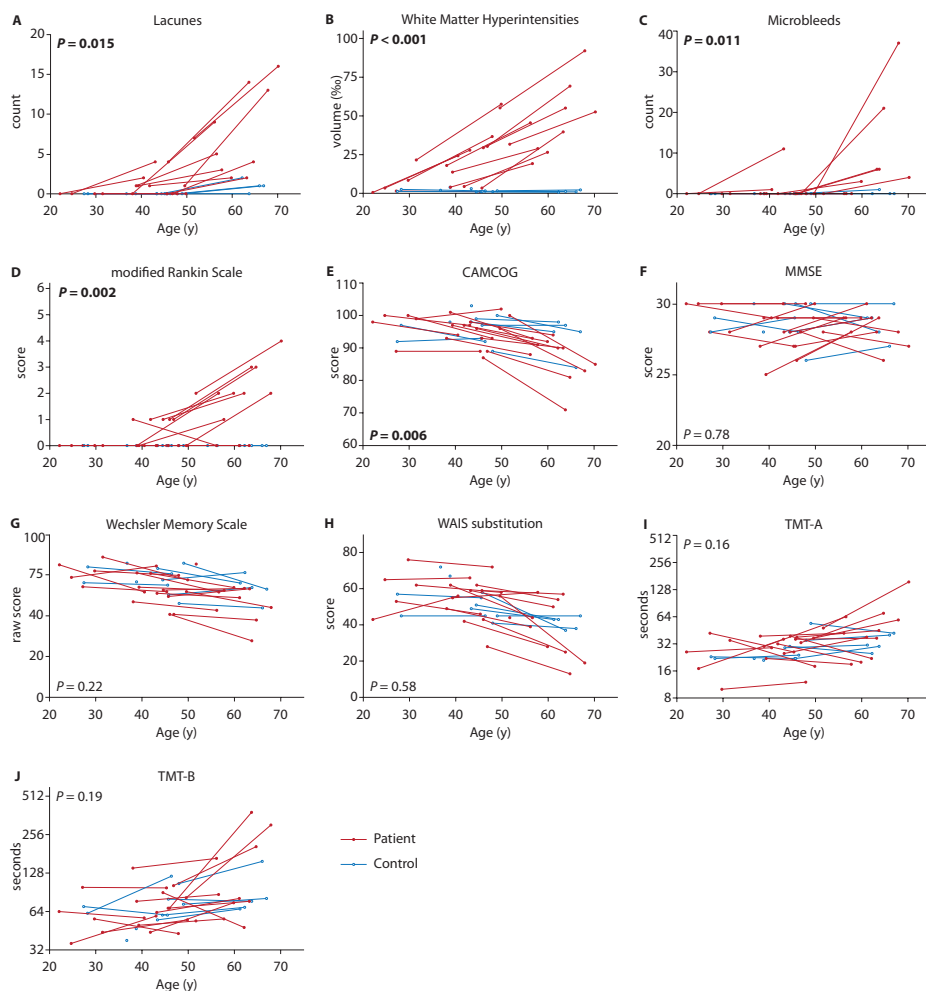


**Figure 4.2: Changes in disease measures over 18 years in CADASIL patients versus controls**

Graphs showing the age-dependent difference between patients and controls for neuroimaging measures, disability and cognitive measures. Each line represents patient (red) or control (blue), with measurements at baseline and 18-year follow-up. (A) Lacunes mainly start to appear on MRI from the age of 40 onwards, although some patients do not have lacunes at the age of 60 years. Three controls had lacunes on MRI. (B,C) WMH<sub>v</sub> and microbleed count significantly increase in patients compared to controls. (D-J) Only disability (mRS) and global cognition measured by CAMCOG show a steeper age-dependent deterioration in patients than in controls, whilst other measures (for global cognition [MMSE], global memory [WMS] and executive function [WAIS substitution, TMT-A, TMT-B]) do not. *P*-values represent the difference in age-dependent change between patients and controls. Graphs with the *P*-value located in the upper corner represent a higher-is-worse covariate.

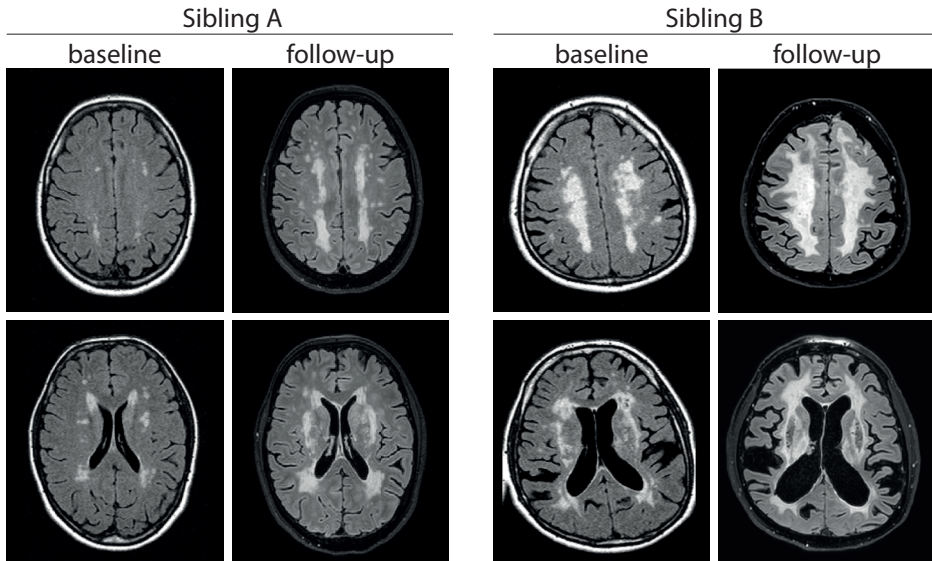


**Figure 4.3: Differences in disease severity and disease progression between two siblings**

(A) FLAIR MRI images of sibling A (aged between 40 and 45 years), with only white matter hyperintensities (Fazekas grade II) and no lacunes. Over 18 years, WMH increased to Fazekas grade III, but there were still no lacunes or microbleeds. Clinically, there was no significant decline in cognitive function (CAMCOG). (B) Sibling B, differing 2 years in age from sibling A, was already much more severely affected at baseline with Fazekas grade III, brain atrophy, and 4 lacunes. There was significant progression at follow-up, both clinically and on MRI. Neither sibling had a history of hypertension, hyperlipidemia or diabetes. Sibling A was an ex-smoker (6 pack years).

### Cerebral hemodynamics

Next, we assessed functional neuroimaging measures. Age-corrected resting CBF and CVR did not differ between patients and controls participating at follow-up (Figure 4.4a,d). Longitudinal analysis of CBF and CVR did also not show a steeper age-dependent decrease in patients than in controls (Figure 4.4b,e). CBF at baseline was associated with survival, but not after correction for age (Figure 4.4c), while CVR at baseline was not associated with survival (Figure 4.4f).

In order to increase sample size, seven additional patients (mean age 56 years (range 50 – 66 years), 4/7 had a history of stroke, 5/7 had lacunes, and 4/7 had  $mRS_{\geq 2}$ ) and ten additional controls (mean age 56 years (range 46 – 64 years), 0/10 had history of stroke, 1/10 had lacunes, and 0/10 had  $mRS_{\geq 2}$ ) were enrolled for the CBF and CVR analyses, as well as for BOLD analysis of the vascular reactivity analysis of the visual cortex. The level of disability was included in the analyses ( $mRS_{\leq 1}$  versus  $mRS_{\geq 2}$ ). Only patients with  $mRS_{\geq 2}$  had a significant lower resting cerebral blood flow (CBF) than controls (Figure 4.4g). No differences were found in CVR, BOLD amplitude, BOLD time-to-peak and BOLD time-to-baseline (Figure 4.4h-j).

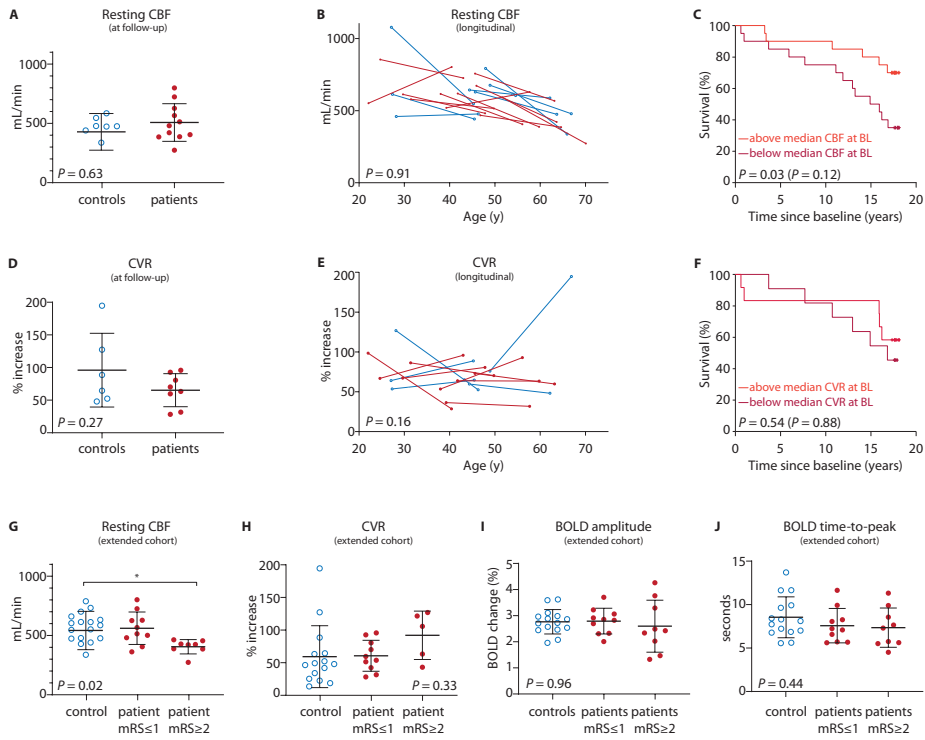


**Figure 4.4: Cerebral hemodynamics**

(A) At follow-up, resting CBF was similar in patients and controls. (B) Longitudinal analysis of resting CBF in the whole brain did also not show statistical differences between patients and controls. Lines connect measurements of individuals at baseline and follow-up. (C) Above median CBF at baseline was associated with higher survival ( $P=0.03$ , age-corrected  $P=0.12$ ). (D) Whole brain CVR upon acetazolamide challenge was similar in patients and controls at follow-up. (E) Longitudinal CVR analysis showing no statistical differences between patients and controls. (F) CVR at baseline was not associated with long-term survival. (G-J) In order to increase sample size at follow-up, seven additional CADASIL patients and ten additional controls were recruited. Together with the participants of the follow-up study, they are called the 'extended cohort'. (G) Resting CBF was lower in the patients with disability compared to controls, but not in patients without disability. (H) CVR showed no difference between patients with and without disability in the extended follow-up cohort. (I, J) BOLD response of the occipital cortex was measured during a visual stimulus, showing no difference between patients and controls in BOLD amplitude, time-to-peak and time-to-baseline (latter not shown). All analyses are corrected for age unless otherwise stated.

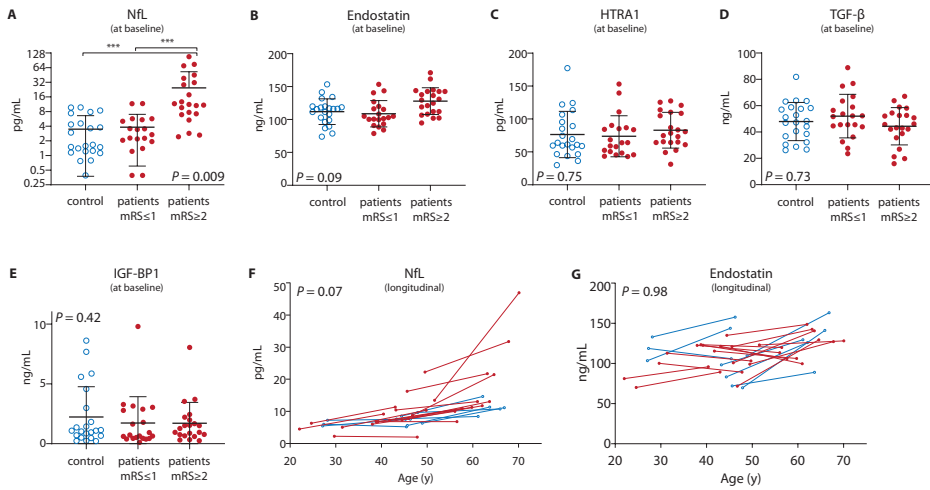


**Figure 4.5: Blood biomarkers**

(A,F) At baseline, blood levels of NfL were significantly elevated in patients with  $mRS \geq 2$  (median 11.22 pg/mL, range 2.43–107.7 pg/mL) compared to patients with  $mRS \leq 1$  (2.68 pg/mL, 0.39–11.67 pg/mL) and controls (1.62 pg/mL, range 0.39–9.73 pg/mL,  $P=0.009$ ). Serum NfL levels show a steeper age-dependent increase in patients than in controls, although this effect did not reach significance ( $P=0.07$ ). The six highest values all belong to patients with lacunes. (B-E) Five potential blood biomarkers were tested in blood withdrawn at baseline, showing no differences between patients and controls, nor in patients with and without disability. (B,C) As there seemed to be slightly higher Endostatin levels in patients with  $mRS \geq 2$  (mean 110.5 ng/mL  $\pm$  SD 15.4 ng/mL) than in patients with  $mRS \leq 1$  (91.6 ng/mL  $\pm$  20.5 ng/mL) and controls (98.1 ng/mL  $\pm$  20.4 ng/mL,  $P=0.09$ ), we assessed Endostatin levels longitudinally, showing no differences between patients and controls ( $P=0.98$ ). All analyses are corrected for age.

## Blood biomarkers

Of the potential serum biomarkers that were tested in the baseline samples (HTRA1, IGF-BP1, TGF-β, Endostatin and NfL), only serum NfL levels were elevated in patients with  $mRS \geq 2$  (Figure 4.5a-e). Serum NfL was associated with lacune count at baseline and at 18-year follow-up. The 18-year changes in serum NfL levels also correlated with the increase in lacune count before correction for age (St.β 0.63,  $P=0.02$ ). NfL showed a tendency to increase in patients compared to age-matched controls ( $P=0.07$ , Figure 4.5f); there were four patients who had a strong increase in serum NfL. Three of these four patients had a high increase in lacune count (range 4–12). However, there were also four patients with an increased lacune count (range 4–10) who had NfL levels similar to controls. We were not able to optimize the homebrew NOTCH3<sup>ECD</sup> ELISA in order to get consistent data. Endostatin levels were not significantly higher in patients with  $mRS \geq 2$  after correction for age ( $P=0.09$ , Figure 4.5b). Longitudinal profiles of Endostatin at baseline and follow-up did not differ between patients and controls ( $P=0.98$ , Figure 4.5g).

## DISCUSSION

Here, we describe an 18-year follow-up study in a cohort of CADASIL patients, thereby providing insight into long-term disease progression and survival. In addition, we assessed cerebral hemodynamics longitudinally and we tested candidate blood biomarkers.

Such a prospective long follow-up study has never been performed in CADASIL patients and gives new insights into the differences in long-term disease progression. Most remarkably, we found that a subset of patients remained clinically relatively stable and were still only mildly affected after 18 years, even those who were already in their forties at baseline. In line with this, patients without lacunes or disability (mRS 0) at baseline had high long-term survival rates, namely more than 80% over 18 years. On the other hand, patients with moderate-severe disability (mRS 3-5) had estimated median survival rates of 7.7 years. Secondary complications to CADASIL are the major cause of death in CADASIL patients, such as pneumonia and generalized weakness.<sup>32</sup>

In line with previous studies, cognitive impairment and disability at 18-year follow-up was associated with lacune count at baseline.<sup>8,10,11,33</sup> Although age is strongly associated with disease progression, there is still a notable variation even between patients of the same age, with some patients remaining stroke-free until their sixties, while others were already deceased in their fifties. These findings underline that disease modifiers play an important role in CADASIL.<sup>7,8,34-36</sup> In this study we found no association between disease progression and classical vascular risk factors, which may be attributable to the relatively small sample size. This study was also too small to take the effect of the *NOTCH3* mutation position into account.<sup>6</sup> Larger cohort studies are needed to further determine the association between long-term disease progression and both known and novel genetic and environmental modifiers.<sup>6-8,34-36</sup> Development of CADASIL disease prediction models, incorporating these modifiers, is imperative for tailored prognosis for CADASIL patients.

In the subset of patients who were able to participate in the 18-year follow-up study, there was a significant increase in lacune count, WMH<sub>v</sub>, and a decrease in global cognition (CAMCOG). Several cross-sectional studies have reported that executive dysfunction is one of the earliest domains of cognitive deterioration in CADASIL patients, even preceding first stroke.<sup>37-39</sup> In this long-term follow-up, we found no significant difference in deterioration on executive function profiles in patients compared to controls.

Cerebral hemodynamics were studied at baseline and 18-year follow-up, as cerebral blood flow and cerebrovascular reactivity have been shown to be reduced in most studies.<sup>4,5,15,40-47</sup> CBF at baseline<sup>15</sup> and follow-up was reduced in patients with more advanced disease

compared to controls, but remarkably, there was no difference in CBF changes over time between patients and controls. This may be partially due to the fact that patients able to participate in the 18-year follow-up study were inherently less severely affected and therefore may have had a better preservation of cerebral hemodynamics. We could not determine changes in CBF specifically in the subcortex or in WMH,<sup>5,15,40,41</sup> due to technical limitations inherent to the study set-up using 18-year old data. Cerebrovascular reactivity (CVR) changes over time also did not significantly differ between patients and controls and, moreover, we also found no association between CVR and disease severity at baseline<sup>15</sup> or follow-up. Previous studies on CVR in CADASIL show contradictory findings, with reduction of CVR in some studies<sup>4,41,47</sup> and no reduction in others.<sup>15,42,44,45</sup> In line with previous studies, we also did not find a reduction in BOLD signal between patients and controls.<sup>42,45</sup> Studies in which CVR reduction was not found, including the current study, may be due to small sample sizes and techniques used, as CVR and CBF changes have been detected using region-specific analyses or by assessing temporal hemodynamics.<sup>40,46,47</sup>

Of the potential blood biomarkers which were previously described in a pre-clinical study<sup>17,18</sup>, none showed differences in blood levels between patients and controls, including levels of Endostatin, which was found to be enriched in CADASIL vessels.<sup>48</sup> However, ELISA might not be sensitive enough to detect small differences between patients and controls with our relatively small sample size. Using a more sensitive single molecule analysis approach, we and others previously showed that NfL blood levels correlate with disease severity in CADASIL.<sup>16,49</sup> The fact that we could longitudinally study blood biomarker levels only in the milder subset of 15 patients who participated at follow-up might explain why we found no statistically significant differences in serum NfL level changes over 18 years between patients and controls. Nevertheless, in patients, 18-year increase in NfL levels was correlated with increase in lacune count. However, not all patients with an increase in lacune count had high NfL levels, likely explained by NfL levels rising upon axonal damage after a recent stroke and returning to normal in approximately a year.<sup>16,49,50</sup>

The strength of our study is the very long follow-up time of patients and controls, but the long follow-up time also has inherent limitations e.g. new consensus guidelines and technical equipment. Differences between baseline and follow-up in measuring WMH<sub>v</sub> were overcome by using a statistical correction approach, and lacunes were re-counted using STRIVE criteria. Differences in BPF measurements could not be overcome, so this could only be assessed cross-sectionally at both time points.

In conclusion, although survival rate of our cohort of CADASIL patients was 54% over 18 years, here we show that a subset of CADASIL patients remain remarkably stable over the course of 18 years.

## APPENDIX

### Acknowledgments

The authors thank all the CADASIL patients and their family members who participated in the study. We acknowledge Merve Atli, Lesse Tieman, Hella Janssen, Annick den Hartog and Yvette Knaap for conducting the neuropsychological assessments.

### Funding

This work was funded by the Netherlands Brain Foundation (HA2016-02-03; BG2015-2).

### Contribution

Study design and conceptualization by BJvE, JvdG, JWR and SAJLO. Data acquisition by GG, RJH, AMvO, BJvE, MO, JFAV, HAMM, CET, JvdG, JWR and SAJLO. Data analysis by GG, AMvO, MDMRG, JWR and SAJLO. Data interpretation by GG, AMvO, MDMRG, AAR, JRW and SAJLO. Manuscript drafted by GG and SAJLO. Manuscript edited and/or reviewed by all authors.

### Disclosures

GG was funded by the Netherlands Brain Foundation (HA2016-02-03; BG2015-2). Part of the experiments were made possible by the Dutch Alzheimer Society and the Leiden University Fund. NOTCH3 antisense therapies have been patented by the Leiden University Medical Center. As co-inventors on this patent AAR and SAJLO are entitled to a share of potential royalties. RJH was funded by Dutch National Institutes of Health (ZonMW, reference 91717325). JFAV is funded by NS110048 grant from the United States National Institute on Aging and the National Institutes of Neurological Disorders and Stroke. CET is supported by the European Commission (Marie Curie International Training Network, JPND), Health Holland, the Dutch Research Council (ZonMW), The Weston Brain Institute, Alzheimer Netherlands. CET has a collaboration contract with ADx Neurosciences, performed contract research or received grants from Probiodrug, AC Immune, Biogen-Esai, CogRx, Toyama, Janssen prevention center, Boehringer, AxonNeurosciences, Fujirebio, EIP farma, PeopleBio, Roche. AAR reports being employed by LUMC which has patents on exon skipping technology, some of which has been licensed to BioMarin and subsequently sublicensed to Sarepta. As co-inventor of some of these patents AAR is entitled to a share of royalties. AAR further discloses being ad hoc consultant for PTC Therapeutics, Sarepta Therapeutics, CRISPR Therapeutics, Summit PLC, Alpha Anomeric, BioMarin Pharmaceuticals Inc., Eisai, Astra Zeneca, Santhera, Audentes, Global Guidepoint and GLG consultancy, Grunenthal, Wave and BioClinica, having been a member of the Duchenne Network Steering Committee (BioMarin) and being a member of the scientific advisory boards of ProQR, hybridize therapeutics, silence therapeutics, Sarepta therapeutics and Philae Pharmaceuticals. Remuneration for these activities is paid to LUMC. LUMC also received speaker honoraria from PTC Therapeutics and BioMarin Pharmaceuticals and funding for contract research from Italpharmaco and Alpha Anomeric. AMvO, BJvE, MO, HAM, MDMRG and JvdG report no disclosures.

## REFERENCES

- Chabriat, Joutel, Dichgans, Tournier-Lasserre, & Boussier. Cadasil. *Lancet. Neurol.* 8, 643–653 (2009).
- Ruchoux, Guerouaou, Vandenhaute, *et al.* Systemic vascular smooth muscle cell impairment in cerebral autosomal dominant arteriopathy with subcortical infarcts and leukoencephalopathy. *Acta Neuropathol.* 89, 500–512 (1995).
- Kalimo, Viitanen, Amberla, *et al.* CADASIL: Hereditary disease of arteries causing brain infarcts and dementia. *Neuropathol. Appl. Neurobiol.* 25, 257–265 (1999).
- Pfefferkorn, von Stuckrad-Barre, Herzog, *et al.* Reduced cerebrovascular CO(2) reactivity in CADASIL: A transcranial Doppler sonography study. *Stroke* 32, 17–21 (2001).
- Mellies, Baumer, Muller, *et al.* SPECT study of a German CADASIL family: A phenotype with migraine and progressive dementia only. *Neurology* 50, 1715–1721 (1998).
- Rutten, Van Eijdsden, Duering, *et al.* The effect of NOTCH3 pathogenic variant position on CADASIL disease severity: NOTCH3 EGFr 1–6 pathogenic variant are associated with a more severe phenotype and lower survival compared with EGFr 7–34 pathogenic variant. *Genet. Med.* 21, 676–682 (2019).
- Singhal, Bevan, Barrick, Rich, & Markus. The influence of genetic and cardiovascular risk factors on the CADASIL phenotype. *Brain* 127, 2031–2038 (2004).
- Ling, De Guio, Duering, *et al.* Predictors and Clinical Impact of Incident Lacunes in Cerebral Autosomal Dominant Arteriopathy With Subcortical Infarcts and Leukoencephalopathy. *Stroke* 48, 283–289 (2017).
- Viswanathan, Godin, Jouvent, *et al.* Impact of MRI markers in subcortical vascular dementia: a multimodal analysis in CADASIL. *Neurobiol. Aging* 31, 1629–36 (2010).
- Chabriat, Hervé, Duering, *et al.* Predictors of clinical worsening in cerebral autosomal dominant arteriopathy with subcortical infarcts and leukoencephalopathy: Prospective cohort study. *Stroke* 47, 4–11 (2016).
- Jouvent, Duchesnay, Hadj-Selem, *et al.* Prediction of 3-year clinical course in CADASIL. *Neurology* 87, 1787–1795 (2016).
- Liem, Lesnik Oberstein, Haan, *et al.* Cerebral autosomal dominant arteriopathy with subcortical infarcts and leukoencephalopathy: progression of MR abnormalities in prospective 7-year follow-up study. *Radiology* 249, 964–71 (2008).
- Liem, Haan, Neut, *et al.* MRI correlates of cognitive decline in CADASIL. *Neurology* 72, 143–148 (2009).
- Ling, De Guio, Jouvent, *et al.* Clinical correlates of longitudinal MRI changes in CADASIL. *J. Cereb. Blood Flow Metab.* 39, 1299–1305 (2019).
- van den Boom, Lesnik Oberstein, Spilt, *et al.* Cerebral hemodynamics and white matter hyperintensities in CADASIL. *J. Cereb. Blood Flow Metab.* 23, 599–604 (2003).
- Gravesteijn, Rutten, Verberk, *et al.* Serum Neurofilament light correlates with CADASIL disease severity and survival. *Ann. Clin. Transl. Neurol.* 6, 46–56 (2019).
- Primo, Graham, Bigger-Allen, *et al.* Blood biomarkers in a mouse model of CADASIL. *Brain Res.* 1644, 118–126 (2016).
- Machuca-Parra, Bigger-Allen, Sanchez, *et al.* Therapeutic antibody targeting of Notch3 signaling prevents mural cell loss in CADASIL. *J. Exp. Med.* 214, 2271–2282 (2017).
- Lesnik Oberstein, van den Boom, van Buchem, *et al.* Cerebral Microbleeds in CADASIL. *Neurology* 57, 1066–1070 (2001).
- van den Boom, Lesnik Oberstein, Ferrari, Haan, & van Buchem. Cerebral autosomal dominant arteriopathy with subcortical infarcts and leukoencephalopathy: MR imaging findings at different ages—3rd–6th decades. *Radiology* 229, 683–690 (2003).
- Wardlaw, Smith, Biessels, *et al.* Neuroimaging standards for research into small vessel disease and its contribution to ageing and neurodegeneration. *Lancet. Neurol.* 12, 822–38 (2013).
- Jenkinson, Beckmann, Behrens, Woolrich, & Smith. FSL. *Neuroimage* 62, 782–790 (2012).
- Van Rooden, Van Den Berg-Huysmans, Croll, *et al.* Subjective Cognitive Decline Is Associated with Greater White Matter Hyperintensity Volume. *J. Alzheimer's Dis.* 66, 1283–1294 (2018).
- Fazekas, Chawluk, & Alavi. MR signal abnormalities at 1.5 T in Alzheimer's dementia and normal aging. *Am. J. Neuroradiol.* 8, 421–426 (1987).
- Roth, Tym, Mountjoy, *et al.* CAMDEX. A standardised instrument for the diagnosis of mental disorder in the elderly with special reference to the early

- detection of dementia. *Br. J. Psychiatry* 149, 698–709 (1986).
26. Folstein, Folstein, & McHugh. 'Mini-mental state'. A practical method for grading the cognitive state of patients for the clinician. *J. Psychiatr. Res.* 12, 189–198 (1975).
  27. Wechsler. A Standardized Memory Scale for Clinical Use. *J. Psychol.* 19, 87–95 (1945).
  28. Reitan. The relation of the trail making test to organic brain damage. *J. Consult. Psychol.* 19, 393–4 (1955).
  29. van Opstal, van Rooden, van Harten, *et al.* Cerebrovascular function in presymptomatic and symptomatic individuals with hereditary cerebral amyloid angiopathy: a case-control study. *Lancet Neurol.* 16, 115–122 (2017).
  30. Dumas, Dierksen, Guro, *et al.* Functional magnetic resonance imaging detection of vascular reactivity in cerebral amyloid angiopathy. *Ann. Neurol.* 72, 76–81 (2012).
  31. Liem, Lesnik Oberstein, Haan, *et al.* Cerebrovascular reactivity is a main determinant of white matter hyperintensity progression in CADASIL. *Am. J. Neuroradiol.* 30, 1244–1247 (2009).
  32. Opherk, Peters, Herzog, Luedtke, & Dichgans. Long-term prognosis and causes of death in CADASIL: A retrospective study in 411 patients. *Brain* 127, 2533–2539 (2004).
  33. Liem, Van Der Grond, Haan, *et al.* Lacunar infarcts are the main correlate with cognitive dysfunction in CADASIL. *Stroke* 38, 923–928 (2007).
  34. Mykkänen, Junna, Amberla, *et al.* Different clinical phenotypes in monozygotic cadasil twins with a novel notch3 mutation. *Stroke* 40, 2215–2218 (2009).
  35. Opherk, Gonik, Duering, *et al.* Genome-wide genotyping demonstrates a polygenic risk score associated with white matter hyperintensity volume in CADASIL. *Stroke* 45, 968–972 (2014).
  36. Opherk, Peters, Holtmannspötter, *et al.* Heritability of MRI lesion volume in CADASIL: Evidence for genetic modifiers. *Stroke* 37, 2684–2689 (2006).
  37. Amberla, Wäljas, Tuominen, *et al.* Insidious cognitive decline in CADASIL. *Stroke* 35, 1598–1602 (2004).
  38. Buffon, Porcher, Hernandez, *et al.* Cognitive profile in CADASIL. *J. Neurol. Neurosurg. Psychiatry* 77, 175–80 (2006).
  39. Taillia, Chabriat, Kurtz, *et al.* Cognitive alterations in non-demented CADASIL patients. *Cerebrovasc. Dis.* 8, 97–101 (1998).
  40. Yin, Zhou, Yan, & Lou. Effects of cerebral blood flow and white matter integrity on cognition in CADASIL patients. *Front. Psychiatry* 10, 1–6 (2019).
  41. Chabriat, Pappata, Ostergaard, *et al.* Cerebral hemodynamics in CADASIL before and after acetazolamide challenge assessed with MRI bolus tracking. *Stroke* 31, 1904–1912 (2000).
  42. Reddy, De Stefano, Mortilla, Federico, & Matthews. Functional reorganization of motor cortex increases with greater axonal injury from CADASIL. *Stroke* 33, 502–508 (2002).
  43. Tuominen, Miao, Kurki, *et al.* Positron emission tomography examination of cerebral blood flow and glucose metabolism in young CADASIL patients. *Stroke* 35, 1063–1067 (2004).
  44. Singhal, & Markus. Cerebrovascular reactivity and dynamic autoregulation in nondemented patients with CADASIL (cerebral autosomal dominant arteriopathy with subcortical infarcts and leukoencephalopathy). *J. Neurol.* 252, 163–167 (2005).
  45. Cheema, Switzer, McCreary, *et al.* Functional magnetic resonance imaging responses in CADASIL. *J. Neurol. Sci.* 375, 248–254 (2017).
  46. Moreton, Cullen, Delles, *et al.* Vasoreactivity in CADASIL: Comparison to structural MRI and neuropsychology. *J. Cereb. Blood Flow Metab.* 38, 1085–1095 (2018).
  47. Huneau, Houot, Joutel, *et al.* Altered dynamics of neurovascular coupling in CADASIL. *Ann. Clin. Transl. Neurol.* 5, 788–802 (2018).
  48. Arboleda-Velasquez, Manent, Lee, *et al.* Hypomorphic Notch 3 alleles link Notch signaling to ischemic cerebral small-vessel disease. *Proc. Natl. Acad. Sci.* 108, E128–E135 (2011).
  49. Duering, Konieczny, Tiedt, *et al.* Serum Neurofilament Light Chain Levels Are Related to Small Vessel Disease Burden. *J. Stroke* 20, 228–238 (2018).
  50. Gatteringer, Pinter, Enzinger, *et al.* Serum neurofilament light is sensitive to active cerebral small vessel disease. *Neurology* 89, 2108–2114 (2017).



# Chapter 5

## Serum Neurofilament Light correlates with CADASIL disease severity and survival

Gido Gravesteijn  
Julie W. Rutten  
Inge M.W. Verberk  
Stefan Böhringer  
Michael K. Liem  
Jeroen van der Grond  
Annemieke Aartsma-Rus  
Charlotte E. Teunissen  
Saskia A.J. Lesnik Oberstein

# ABSTRACT

## Objective

To validate whether serum Neurofilament Light-chain (NfL) levels correlate with disease severity in CADASIL, and to determine whether serum NfL predicts disease progression and survival.

## Methods

Forty-one (pre-)manifest individuals with CADASIL causing *NOTCH3* mutations and 22 healthy controls were recruited from CADASIL families. At baseline, MRI-lesion load and clinical severity was determined and serum was stored. Disease progression was measured in 30/41 patients at 7-year follow-up, and survival of all individuals was determined at 17-year follow-up. Serum NfL levels were quantified using an ultra-sensitive molecule array. Generalized estimated equation regression (GEE) was used to analyse association between serum NfL, MRI-lesion load, disease severity and disease progression. With GEE-based Cox regression, survival was analysed.

## Results

At baseline, serum NfL levels correlated with MRI-lesion load [lacune count ( $s=0.64$ ,  $P=0.002$ ), brain atrophy ( $r=-0.50$ ,  $P=0.001$ ), and microbleed count ( $s=0.48$ ,  $P=0.044$ )], cognition [CAMCOG ( $s=-0.45$ ,  $P=0.010$ ), MMSE ( $r=-0.61$ ,  $P=0.003$ ), GIT ( $r=-0.61$ ,  $P<0.001$ ), TMT-A ( $r=0.70$ ,  $P<0.001$ )] and disability (mRS ( $r=0.70$ ,  $P=0.002$ )). Baseline serum NfL predicted 7-year changes in disability ( $B=0.34$ ,  $P<0.001$ ) and cognition (CAMCOG  $B=-4.94$ ,  $P=0.032$ ), as well as 17-year survival. Higher NfL levels were associated with increased mortality (HR=1.8 per 2-fold increase in NfL levels,  $P=0.006$ ).

## Interpretation

Serum NfL levels correlate with disease severity, disease progression and 17-year survival in CADASIL patients. Serum NfL is a promising biomarker to monitor and predict disease course in CADASIL, as well as potentially assessing therapeutic response in future clinical trials.

## INTRODUCTION

CADASIL (cerebral autosomal dominant arteriopathy with subcortical infarcts and leukoencephalopathy) is the most prevalent hereditary form of cerebral small vessel disease (SVD), and is caused by mutations in the *NOTCH3* gene.<sup>1</sup> CADASIL patients suffer from recurrent ischemic strokes with a mean age at onset of 45-50 years, although age at first stroke is highly variable.<sup>1</sup> Cognitive decline is a main but also variable feature, initially manifesting as executive dysfunction and progressing to global impairment in all cognitive domains and complete care dependency.<sup>2</sup> Migraine with aura affects up to two thirds of patients.<sup>3</sup> In CADASIL, mutant NOTCH3 proteins aggregate in the tunica media of small arteries,<sup>4-6</sup> directly or indirectly compromising cerebrovascular reactivity.<sup>7,8</sup> On MRI, white matter hyperintensities can be observed in pre-manifest patients from the third decade, while lacunes, microbleeds and brain atrophy usually appear later in the disease course.<sup>1,9,10</sup>

Lacunes and brain parenchymal fraction (BPF) have been shown to be predictors of disease progression in CADASIL patients.<sup>11-17</sup> However, a good fluid biomarker would have advantages above the more cumbersome neuroimaging markers and could ideally also be used as a marker for therapeutic response in future clinical trials. Various potential fluid biomarkers have been investigated for CADASIL,<sup>18,19</sup> but most do not seem to be feasible. Recently, serum Neurofilament light-chain levels were shown to correlate with disease severity in CADASIL.<sup>20</sup>

Neurofilament light-chain protein (NfL) levels in serum have made a recent surge in the field of biomarkers for brain disease.<sup>21-27</sup> NfL is a component of the neurofilament complex, which has a scaffolding role in neuronal axons, and is released into the cerebrospinal fluid (CSF) and blood upon neuronal damage,<sup>21</sup> in some studies remaining elevated in blood for several months.<sup>22,23</sup> NfL levels have been shown to correlate with disease severity and progression in Huntington's disease,<sup>24</sup> Frontotemporal Dementia<sup>25,26</sup> and Amyotrophic Lateral Sclerosis.<sup>27</sup> In Multiple Sclerosis, NfL levels in blood have even been shown to be responsive to treatment, showing its potential as a therapeutic response marker.<sup>28,29</sup> In sporadic SVD and CADASIL, serum NfL levels were shown to be associated cross-sectionally with neuroimaging markers, processing speed and disability, but the associations between serum NfL and disease progression and survival were not investigated.<sup>20,22</sup>

Here, we explored whether serum NfL, measured using the ultra-sensitive single molecule array, may be a feasible fluid biomarker for monitoring CADASIL disease severity, predicting disease progression and predicting long-term survival. We used a well characterized cohort of CADASIL patients and controls, which has been uniquely followed-up for 17 years.

## METHODS

### Cohort

At baseline, in 2000, 41 patients and 22 controls, from a total of 15 CADASIL families of which 10 families had  $\geq 2$  participants, were enrolled in the study. Thirty-two patients had a *NOTCH3* mutation in exon 4 and nine patients had a mutation in exon 8, 11, 19 or 20. A full medical history, MRI, serum withdrawal, neuropsychological testing and genetic *NOTCH3* testing was performed, as described earlier.<sup>30</sup> The average age at baseline was 46 years in patients and 39 years in healthy relatives (Table 5.1). Seven years later this same cohort was invited to participate in a follow-up study. Thirty patients consented to participate. Eleven participants were lost-to-follow-up due to death (6 patients) or severe disease (5 patients). Five patients did not consent to MRI in the follow-up study.<sup>15</sup> Seventeen years after baseline, survival data from all participants of the baseline study was obtained from the Dutch population registry. These studies were approved by the medical ethics committee of the Leiden University Medical Center (P80/98) and each participant gave informed consent.

### Neuroimaging and neuropsychological testing

MRI was performed on a 1.5 T MR system at baseline<sup>9</sup> and at 7 year follow-up.<sup>15,16</sup> Lacune count, microbleed count, parenchymal volume, intracranial volume and white matter hyperintensity volume were previously quantified.<sup>15,16,31</sup> Parenchymal volume was normalized to intracranial volume to acquire the brain parenchymal fraction (BPF), as a measure for brain atrophy. White matter hyperintensity volume was normalized to parenchymal volume (WMH<sub>v</sub>). The neuropsychological test battery included the Cambridge Cognitive Examination (CAMCOG), Mini-Mental State Examination (MMSE), the Groningen Intelligence Test (GIT), and the Trail Making Test part A (TMT-A) and part B (TMT-B).<sup>32–35</sup> Disability was assessed using the modified Rankin scale (mRS).

### Serum NfL measurement

At baseline, blood was withdrawn via standard vena puncture and centrifuged at 2750g for 20 minutes at room temperature. The supernatant was aliquoted and stored at -80°C freezer until analysis. Serum NfL levels were quantified using an in-house developed Simoa assay, as previously described.<sup>36</sup> The assay was validated prior to use according to standardized international protocols.<sup>37</sup> The lower level of quantification (LLOQ) was 0.77 pg/mL (10 times the standard deviation of 16 negative samples). Three of the 41 patients (age 22, 30, 39 years) and one of the 22 controls (age 24 years) had a serum NfL below the LLOQ and were excluded from the study. A sensitivity analysis, including these individuals and using half of the LLOQ as the measurement for these individuals, showed similar results.

## Statistics

Non-normally distributed data was transformed to obtain plausible normal distributions for further analyses: serum NfL was natural log (ln) transformed and to facilitate interpretation also  $\log_2$  transformed for Cox-regression; lacune count, WMH<sub>V</sub> and CAMCOG were square root transformed; TMT-A was  $\log_{10}$  transformed; and microbleed count was  $\log_{10}(1+x)$  transformed. To determine the association between NfL levels and brain MRI lesion load and clinical outcomes at baseline, generalized estimated equation multivariable regression models (GEE), using an independent correlation structure and robust variance estimators, were used to enable correction for correlation within families, since 10 families had  $\geq 2$  participants in the study. Sex and age were included in all linear regression GEE analyses. To determine the association between age and NfL in both patients and controls, the GEE model also included mutation status, and the age-mutation status interaction. To determine how NfL compared with MRI markers in predicting disease severity, forward and backward regular linear regression was performed with NfL, lacune count, brain atrophy, WMH<sub>V</sub> and microbleed count as potential predictors. Potential predictors were added only if they significantly contributed to the model.

To determine whether NfL levels were associated with 7-year changes in MRI lesion load and clinical deterioration, GEE models were used with either NfL and sex; or NfL, sex and baseline measurement of the tested outcome. For clarity, the correlations in the figures are presented using Pearson ( $r$ ) or Spearman ( $s$ ) correlation coefficients, together with p-values obtained from GEE regression models. Hazard ratios for the relation of baseline NfL with survival at 17-year follow-up were calculated using a multivariate GEE-based Cox regression analysis, including age and the covariate of interest. Area under the curve (AUC) and confidence intervals were calculated and compared using DeLong tests in R package pROC. We did not formally prove equivalence in the prognostic value of NfL versus the neuroimaging markers, as formal equivalence testing would be under-powered in the current data set. GEE-based logistic regression analyses were performed with an independent correlation structure and were corrected for sex. All other statistical analyses were performed in IBM SPSS Statistics version 23.0.0.2. All statistical tests were two-sided and the threshold for statistical significance was 0.05.

**Table 5.1: Cohort characteristics at baseline and follow-up**

	Cross-sectional study at baseline		7-year follow-up study in patients	
	Controls	Patients	Baseline	Follow-up
	Mean (SD), median (range) or n (%)		Mean (SD), median (range) or n (%)	
N	22	41	30	30
Age, y	39.8 (12.5)	45.8 (10.4)	44.0 (9.8)	51.1 (9.8)
Female	12 (55%)	22 (54%)	17 (57%)	17 (57%)
Prior stroke/TIA	0 (0%)	23 (56%)	16 (53%)	-
Time since last stroke	-	3.3 (0.1–17.7)	3.5 (0.1–14.2)	-
Hypertension	6 (27%)	3 (7%)	2 (7%)	-
Diabetes Mellitus	0 (0%)	3 (7%)	3 (10%)	-
Hyperlipidaemia	4 (18%)	15 (37%)	10 (33%)	-
Current or past smoking	14 (64%)	26 (63%)	19 (63%)	-
Serum NFL (pg/mL)	1.66 (0.77–9.7)	6.31 (1.22–107.7)	5.21 (1.22–31.6)	-
<b>MRI data available (n)<sup>a</sup></b>	<b>21</b>	<b>40</b>	<b>25</b>	<b>25</b>
Lacunae on MRI				
0 lacunes	21 (100%)	8 (20%)	6 (24%)	5 (20%)
1-10 lacunes		15 (38%)	14 (56%)	12 (48%)
>10 lacunes		17 (42%)	5 (20%)	8 (32%)
Brain atrophy (BPF)		82.198 (2.977)	82.648 (2.919)	81.836 (3.065)
WMH <sub>v</sub>	0.003 (0–0.075)	7.297 (0.009–19.209)	4.303 (0.009–13.939)	7.865 (0.005–19.806)
Microbleeds				
0 microbleeds	21 (100%)	29 (73%)	22 (88%)	18 (72%)
1-10 microbleeds		9 (22%)	2 (8%)	5 (20%)
>10 microbleeds		2 (5.0%)	1 (4%)	2 (8%)
<b>Clinical score available (n)<sup>a</sup></b>	<b>22</b>	<b>41</b>	<b>30</b>	<b>30</b>
mRS				
score 0	22 (100%)	13 (32%)	12 (40%)	9 (30%) <sup>b</sup>
score 1-2		17 (42%)	15 (50%)	10 (33%) <sup>b</sup>
score ≥3		11 (27%)	3 (10%)	10 (33%) <sup>b</sup>
CAMCOG	94.2 (4.9)	88.3 (15.0)	93.5 (5.3)	88.1 (13.7)
MMSE	28.3 (1.5)	26.2 (4.3)	27.7 (1.6)	26.2 (5.0)
GIT	105.8 (11.7)	99.8 (16.9) <sup>b</sup>	103.8 (12.5)	100.6 (18.6)
TMT-A	30 (21–90)	37 (10–180) <sup>c</sup>	36 (10–92) <sup>b</sup>	40 (15–349) <sup>c</sup>
TMT-B	74.5 (38–216)	84 (36–540) <sup>f</sup>	82 (36–254) <sup>b</sup>	75.5 (44–300) <sup>d</sup>

<sup>a</sup> At baseline, one patient and one control did not consent to radiological examination. At follow-up, five patients did not consent to radiological examination.

<sup>b</sup> Missing data for one patient.

<sup>c</sup> Missing data for 3 patients.

<sup>d</sup> Missing data for 4 patients.

<sup>e</sup> Missing data for 5 patients.

<sup>f</sup> Missing data for 7 patients.

## RESULTS

NfL levels were higher in patients (median 6.31 pg/mL, range 1.22–107.7 pg/mL) than in controls (median 1.66 pg/mL, range 0.77 to 9.73 pg/mL) ( $P<0.001$ ). NfL levels positively correlated with age in both patients and controls. However, this age-dependent increase was stronger in patients (7.6% increase per year, CI 4.6–10.7%) than in controls (3.7% increase per year, CI: 2.2%–5.3%) ( $P=0.012$ ). In contrast to controls, patients showed a steeper increase in NfL levels from age 40 onwards, which coincided with the presence of lacunes (Figure 5.1).

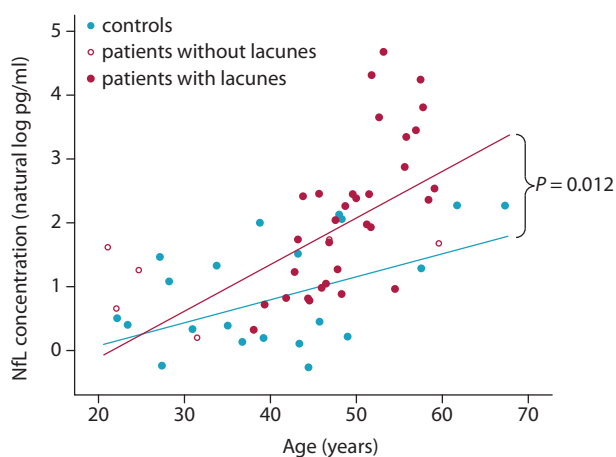


**Figure 5.1: Serum NfL levels show an age-dependent increase in CADASIL patients and controls**

CADASIL patients with lacunes (red dots) show a stronger age-dependent serum NfL increase than patients without lacunes (open circles) and controls (blue dots).

### Correlation of serum NfL with disease severity at baseline

After correcting for age and sex, NfL levels correlated strongly with MRI lacune count ( $s=0.64$ ,  $P=0.002$ ), brain parenchymal fraction ( $r=-0.50$ ,  $P=0.001$ ) and microbleed count ( $s=0.48$ ,  $P=0.044$ ), but not with WMH<sub>V</sub> levels ( $r=0.48$ ,  $P=0.894$ ) (Figure 5.2). Without correcting for age, NfL levels did correlate with WMH<sub>V</sub> ( $r=0.48$ ,  $P<0.001$ ). When including all MRI markers in the model, NfL levels independently correlated with lacune count ( $\beta=0.20$ ,  $P=0.002$ ), brain parenchymal fraction ( $\beta=-0.14$ ,  $P<0.001$ ) and microbleed count ( $\beta=0.56$ ,  $P=0.009$ ). NfL levels did not correlate with time since last clinical stroke (data not shown).

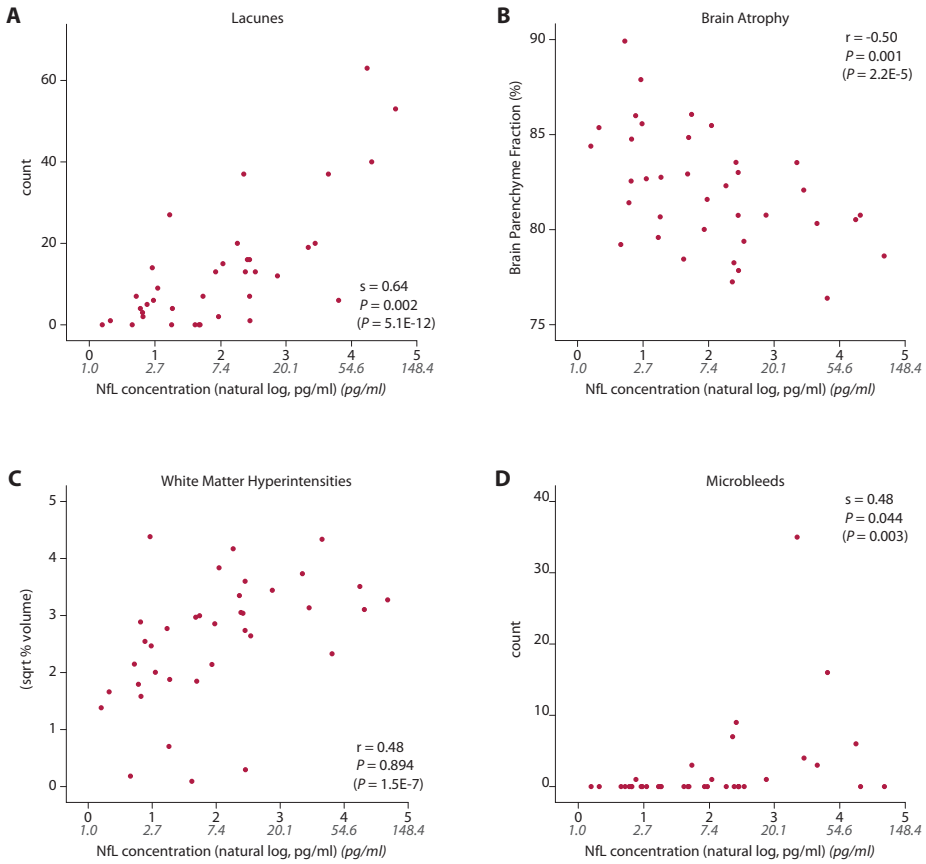


**Figure 5.2: Cross-sectional associations between serum NfL levels and MRI markers**

After correction for age and sex, NfL levels significantly correlate with lacune count (A), brain atrophy (B), and microbleeds (D), but not with white matter hyperintensity volume (C). *P*-values in parentheses represent *P*-value before correction for age and sex. NfL levels were natural log transformed for analyses, non-transformed NfL levels are shown in gray. NfL, Neurofilament light-chain.

Next, the relation of NfL with cognitive outcome measures was assessed. After correcting for sex and age, NfL levels correlated with disability scores of mRS ( $r=0.70$ ,  $P=0.002$ ), and cognitive function determined by CAMCOG ( $s=-0.45$ ,  $P=0.010$ ), MMSE ( $r=-0.61$ ,  $P=0.003$ ), GIT score ( $r=-0.61$ ,  $P<0.001$ ), and TMT-A ( $r=0.70$ ,  $P<0.001$ ), but not with TMT-B ( $s=0.39$ ,  $P=0.115$ ) (Figure 5.3). Serum NfL correlated more strongly with cognitive function (CAMCOG, MMSE and GIT) than any of the MRI markers correlated with cognitive function. NfL was associated less strongly with disability (mRS) and executive function (TMT-A and TMT-B) than lacune count (Table 5.2).

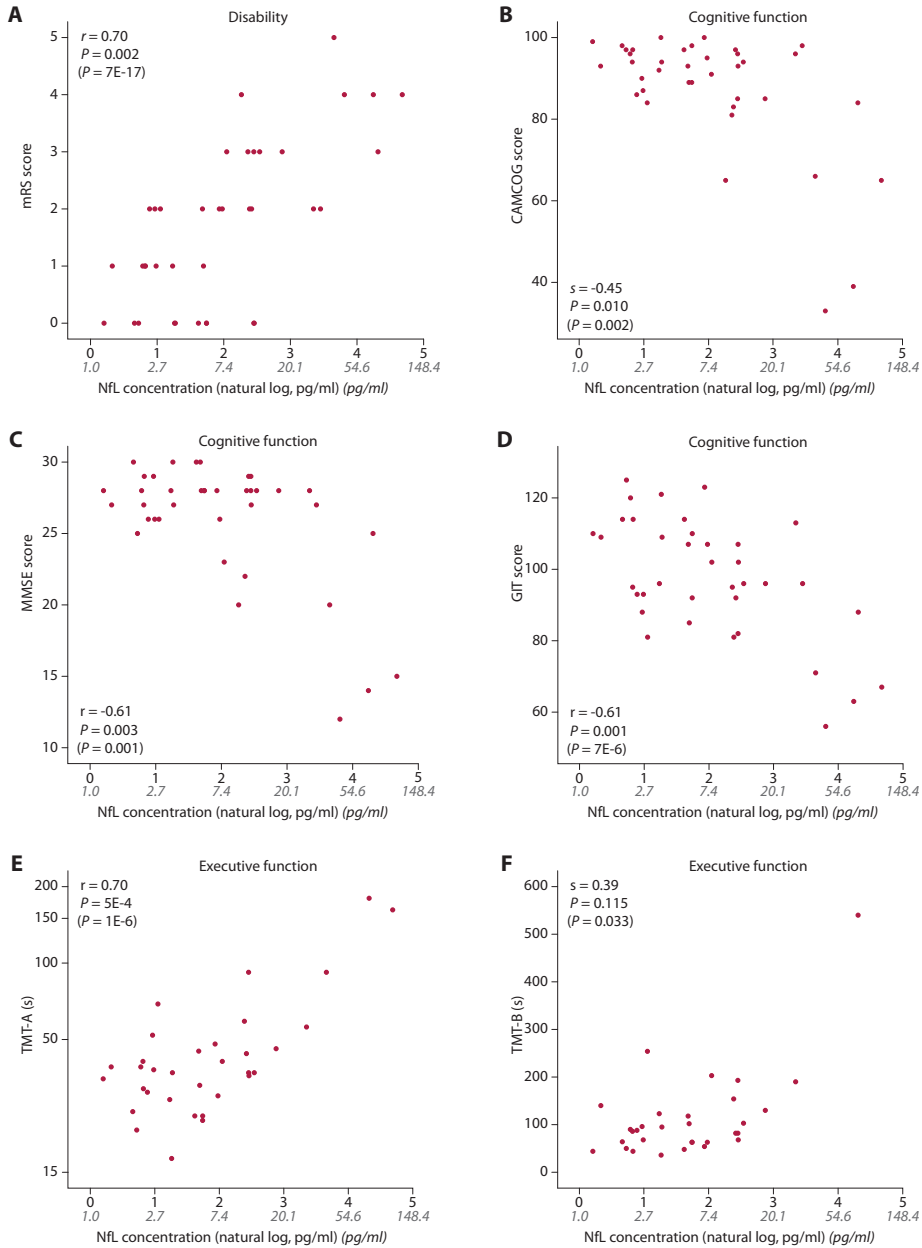


**Figure 5.3: Cross-sectional association between serum NfL levels and disability, cognitive function, and executive function**

NfL levels correlate with disability score mRS (A), cognitive function scores CAMCOG (B), MMSE (C), GIT (D), and executive function score TMT-A (E), but not with TMT-B (F). *P*-values in parentheses represent *P*-value before correction for age and sex. Serum NfL levels were natural log transformed for analyses. Non-transformed NfL levels are shown in gray. NfL, Neurofilament light-chain; mRS, modified Rankin Scale; CAMCOG, Cambridge Cognitive Examination; MMSE, Mini-mental state examination; GIT, Groningen Intelligence Test; TMT-A, Trail Making Test part A; TMT-B, Trail Making Test part B.

**Table 5.2: Independent cross-sectional predictors for disability, cognition and executive function**

	Clinical scores	First predictor			Second predictor		
		Covariate	Std. $\beta$	P-value	Covariate	Std. $\beta$	P-value
Cognition	CAMCOG (sqrt)	NfL	-0.593	<0.001*			
Cognition	MMSE	NfL	-0.609	<0.001*			
Cognition	GIT	NfL	-0.611	<0.001*			
Executive function	TMT-A (log)	Lacunes	0.466	0.008*	NfL	0.382	0.027*
Executive function	TMT-B	Lacunes	0.401	0.002*	NfL	0.362	0.013*
Disability	mRS	Lacunes	0.455	0.006*	NfL	0.381	0.019*

For clinical scores, the covariate with the best correlation is shown in the 'first predictor' column. A second predictor is only shown if it made a significant contribution. Results of forward regression are shown, but were validated with backward regression (not shown). NfL = serum concentration Neurofilament light-chain; mRS = modified Rankin Scale; CAMCOG = Cambridge Cognitive Examination; MMSE = Mini-mental state examination; GIT = Groningen Intelligence Test; TMT-A = Trail Making Test part A; TMT-B = Trail Making Test part B.

### Prediction of seven year disease progression

To determine whether serum NfL levels predict disease progression, we assessed whether baseline serum NfL levels correlated with changes over 7 years in MRI lesion load, disability and cognition. Baseline NfL levels correlated with increased disability (mRS;  $\beta=0.34$ ,  $P<0.001$ ), decline in cognitive function (CAMCOG;  $\beta=-4.94$ ,  $P=0.032$ ), and decline in executive function (TMT-B time;  $\beta=24.55$ ,  $P=0.035$ ) (Table 5.3A). After correction for baseline values of the clinical measures, the correlation between NfL and disability (mRS;  $\beta=0.28$ ,  $P=0.044$ ) and executive dysfunction (TMT-B;  $\beta=29.03$ ,  $P=0.025$ ) remained significant, suggesting that NfL levels measured at any stage of the disease are associated with future disability.

NfL was not associated with an increase in lesion load of any of the MRI measures at follow-up. However, in patients with disability at baseline (mRS>0), baseline NfL levels were associated with an increase in lacune count ( $\beta=0.371$ ,  $P<0.001$ ), as well as with increased disability (mRS;  $\beta=0.33$ ,  $P<0.001$ ), decline in cognitive function (CAMCOG;  $\beta=-5.71$ ,  $P=0.018$ ; MMSE;  $-2.37$ ,  $P=0.037$ ) and decline in executive function (TMT-B time;  $\beta=33.5$ ,  $P=0.030$ ) (Table 5.3B). In patients who had no disability at baseline (mRS=0), serum NfL did not associate with disease progression.

### Prediction of 17-year survival

After correction for age, serum NfL levels significantly predicted 17-year survival (HR 2.3 per 1 unit natural log pg/ml NfL increase, CI: 1.3–4.2,  $P=0.006$ ; corresponding to HR 1.8 per 2-fold increase in absolute NfL levels, CI: 1.2–2.7,  $P=0.006$ ). In patients with the highest

**Table 5.3: Correlation between baseline serum NfL levels and 7-year changes in neuroimaging markers and clinical scores in all patients (A) and in patients with disability at baseline (mRS>0) (B)**

	Model 1, corrected for sex		Model 2, corrected for sex and baseline values of tested covariate			
	NfL		Baseline		NfL	
	$\beta$	<i>P</i>	$\beta$	<i>P</i>	$\beta$	<i>P</i>
<b>(A) All patients</b>						
MRI markers						
$\Delta$ Lacune count (sqrt)	0.325	0.178	0.128	0.001*	-0.149	0.341
$\Delta$ BPF	-0.059	0.879	-0.180	0.249	-0.323	0.504
$\Delta$ WMH <sub>v</sub> (sqrt)	0.074	0.593	0.487	<0.001*	-0.165	0.291
$\Delta$ MB count (log)	0.350	0.643	5.871	0.071	-0.874	0.476
Clinical scores						
$\Delta$ mRS score	0.338	<0.001*	0.072	0.551	0.281	0.044*
$\Delta$ CAMCOG score (sqrt)	-4.944	0.032*	0.782	0.040*	-4.297	0.061
$\Delta$ MMSE score	-2.109	0.051	-0.132	0.595	-2.100	0.053
$\Delta$ GIT score	-1.714	0.462	0.157	0.538	-1.073	0.727
$\Delta$ TMT-A	20.028	0.087	132.81	0.276	9.152	0.306
$\Delta$ TMT-B	24.551	0.035*	-0.175	0.421	29.025	0.025*
<b>(B) Patients with disability at baseline (mRS&gt;0)</b>						
MRI markers						
$\Delta$ Lacune count (sqrt)	0.371	0.007*	0.112	0.003*	-0.187	0.187
$\Delta$ BPF	-0.005	0.989	0.087	0.458	0.106	0.681
$\Delta$ WMH <sub>v</sub> (sqrt)	0.102	0.576	0.774	<0.001	-0.273	0.115
$\Delta$ MB count (log)	0.586	0.479	6.169	0.140	-1.272	0.471
Clinical scores						
$\Delta$ mRS score	0.330	<0.001*	-0.035	0.864	0.356	0.076
$\Delta$ CAMCOG score (sqrt)	-5.705	0.018*	0.528	0.265	-5.879	0.013*
$\Delta$ MMSE score	-2.374	0.037*	-0.412	0.459	-2.311	0.046*
$\Delta$ GIT score	-2.280	0.397	-0.038	0.847	-2.347	0.422
$\Delta$ TMT-A	24.545	0.154	296.25	0.224	4.957	0.747
$\Delta$ TMT-B	33.488	0.030*	-0.548	0.054	53.286	0.001*

Delta indicates the difference between baseline and 7-year follow-up for the respective MRI marker or clinical score; positive value indicate an increase in the score, while negative values indicate a decrease in the score. Data of all patients who participated at seven year follow-up is shown (A), as well as the subset of patients with disability at baseline (B). In model 1 the prognostic value of baseline NfL for the differences in MRI markers and clinical scores are shown, after correcting for sex. In model 2, the prognostic value of baseline NfL and the baseline score of the tested variable are shown, after correcting for sex. NfL levels were natural log transformed. Behind MRI markers and clinical scores the type of transformation of the variable is indicated, if applicable. NfL = serum concentration Neurofilament light-chain; mRS = modified Rankin Scale; CAMCOG = Cambridge Cognitive Examination; MMSE = Mini-mental state examination; GIT = Groningen Intelligence Test; TMT-A = Trail Making Test A; TMT-B = Trail Making Test B.

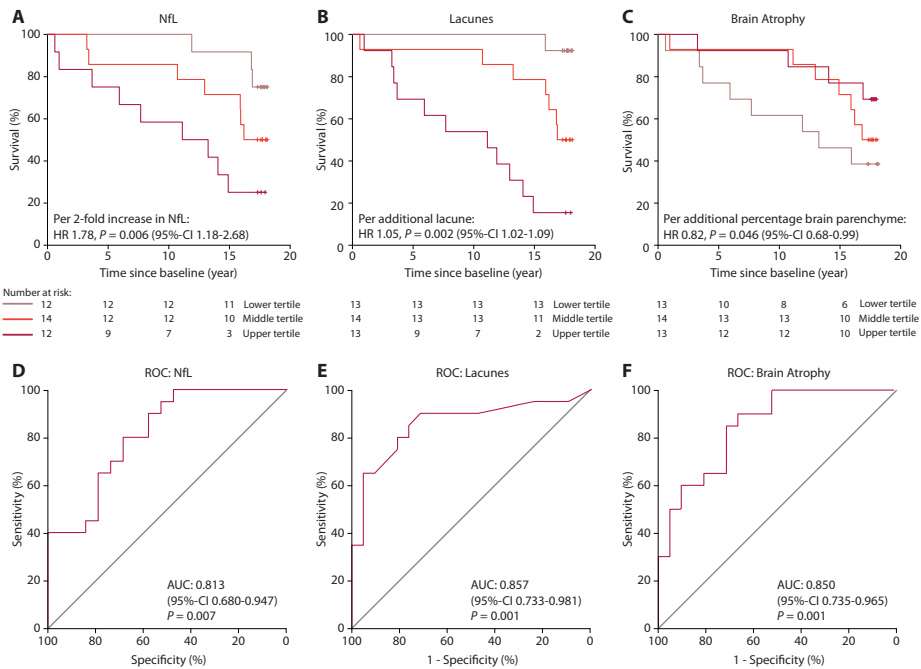


**Figure 5.4: Association between serum NfL levels and 17-year survival**

Kaplan–Meier plots show longitudinal survival divided into tertiles for serum NfL levels (upper tertile >11.2 pg/mL, middle tertile 3.53–11.22 pg/mL, lower tertile <3.53 pg/mL) (A), lacune count (upper tertile >13, middle tertile 4–13, lower tertile ≤3) (B), and brain atrophy (upper tertile > 83.4%, middle tertile 80.7–83.4%, lower tertile <80.7%) (C). Receiver Operating Characteristic curves illustrate the prognostic ability for serum NfL levels (D), lacune count (E), and brain atrophy (F) at baseline to discriminate between live and deceased patients after 17-year follow-up. *P*-values indicate testing with null-hypothesis AUC 0.50 as indicated by the diagonal line. NfL = Neurofilament light-chain; AUC = area under the curve; 95%-CI = 95% confidence interval.

NfL levels at baseline (upper tertile; >11.2 pg/mL), the survival after 17 years was 25%, while survival was 50% and 75% in patients with NfL levels in the middle and lower tertile (<3.55 pg/ml) (log rank *P*=0.012), respectively (Figure 5.4). To determine whether NfL was better in predicting 17-year survival than MRI markers or age, receiver operating characteristic (ROC) analyses were performed. The area under the curve (AUC) was similar for all parameters: 0.813 for serum NfL (CI: 0.680–0.947), 0.857 for lacune count (CI: 0.733–0.981), 0.850 for brain atrophy (CI: 0.735–0.965) and 0.843 for age (CI: 0.726–0.960). In both ROC analyses and logistic regression, the combination of NfL with any MRI marker or with age was not significantly better in predicating 17 year survival than NfL alone.

## DISCUSSION

Here, we validate a recent study showing that serum NfL levels correlate with disease severity in CADASIL. Moreover, we show that serum NfL levels at baseline also predict disease progression as well as 17-year survival in a cohort of well-characterized CADASIL patients.

We found that serum NfL levels correlated with all neuroimaging markers. After correction for age, serum NfL levels at baseline correlated independently with lacune count, brain atrophy and to a lesser extent with microbleed count, but not with WMH. These findings are in line with the recent study by Duering *et al.*, showing serum NfL correlates with all neuroimaging markers in CADASIL.<sup>20</sup>

Although WMH are widely present in patients with SVD, such as CADASIL, and seem to correlate to some extent with NfL in serum or CSF,<sup>20,22,38</sup> other neuroimaging markers, namely brain atrophy and lacunes, correlate more strongly with disease severity.<sup>11-17</sup> In line with this, mean diffusivity from diffusion tensor imaging (DTI) was shown to be most strongly associated with serum NfL levels in CADASIL.<sup>20</sup> Together with our finding that NfL independently correlates with lacunes and brain atrophy, this indicates that serum NfL reflects structural axonal damage, irrespective of the cause, and probably integrates the effect of lacunar infarcts and brain atrophy in a single measure, in a similar way as mean diffusivity does. This may implicate that serum NfL may be a suitable biomarker for manifest CADASIL, but not for the pre-manifest stages of CADASIL *i.e.* when patients only have WMH. However, this needs to be further clarified in larger cohorts of pre-manifest patients.

In agreement with the study by Duering *et al.*, serum NfL levels correlated with disease severity as reflected by disability scores, global cognitive function and executive function. Global cognitive function correlated more strongly with serum NfL levels than with lacune count or BPF, which have been considered to be the best predictors of cognitive function and cognitive decline in CADASIL to date.<sup>11-17</sup> Taken together, the correlation of serum NfL levels with MRI lesion load, cognition and disability, suggests that serum NfL may serve as a feasible fluid biomarker to facilitate assessment of CADASIL disease severity in a single measure at a given time-point.

Moreover, baseline serum NfL predicted seven-year deterioration in disability (mRS), global cognitive function (CAMCOG), and executive function (TMT-B), but did not correlate with seven-year progression in MRI lesion load. Previous studies have shown that brain atrophy and lacunes predict disease progression in CADASIL,<sup>11-17</sup> and both of these strongly

correlate with serum NfL levels. Here, the lack of correlation between NfL and progressive MRI lesions at follow-up is likely explained by the loss to follow up of more severely affected patients. Therefore, patients who were pre-manifest or mildly affected at baseline, were over-represented at seven year follow-up. Indeed, when only including in the analysis those patients who had disability at baseline, serum NfL did correlate with an increase in MRI lesion load (lacune count).

A general weakness of this study is that it was not originally designed for the purpose of a longitudinal study of serum biomarkers, and in this regard the cohort is relatively small.

In several studies, serum NfL has been shown to predict survival in neurodegenerative disease, but not yet in SVD.<sup>25,39,40</sup> Here, we show that NfL also predicts survival in CADASIL, a pure model of SVD. However, as the follow-up period was relatively long and our study lacks longitudinal assessment of serum NfL levels, we were not able to determine whether NfL levels can be used as a disease monitoring biomarker at shorter time intervals or as a potential marker for therapeutic response in future clinical trials. We do find that NfL correlates strongly with lacunes and BPF, which have both been shown to significantly change in a three year timeframe.<sup>14,17</sup> This suggests that serum NfL levels may also show significant changes at shorter intervals in manifest patients with progressive disease.

Like Duering *et al.*, we used the ultra-sensitive single-molecule array (Simoa) for NfL measurements into the pg/mL range at high precision and sensitivity, which outperforms the conventional ELISA and chemiluminescence-based methods.<sup>20,36</sup> Serum NfL levels were lower for both patients and controls in our study. A single-measure serum biomarker such as NfL clearly has many advantages over more complex measures such as MRI markers or neuropsychological testing, which are currently used to assess CADASIL disease severity and predict disease progression.

In conclusion, we validate the recent finding that serum NfL levels correlate cross-sectionally with relevant measures of disease severity in an independent CADASIL sample. Furthermore, we show that serum NfL is predictive of seven year deterioration in cognition and disability, and is associated with 17-year survival. These findings suggest that serum NfL may be useful marker to monitor and predict disease course in this variable disorder, as well as potentially providing a feasible marker for therapeutic intervention in future clinical trials for CADASIL.

## APPENDIX

### Acknowledgments

We acknowledge the support from the Netherlands Brain Foundation (HA2016-02-03). We thank the patients and their family members who participated in this study.

### Contribution

GG, JR and SLO conceived and designed the study. ML and JG performed the MRI studies. IV performed the serum NFL quantification. GG, JR, SB and SLO analysed the data. GG, JR and SLO drafted the manuscript. All authors reviewed the manuscript.

### Disclosures

We report no relevant conflict of interest. GG and JW reports grants from The Netherlands Brain Foundation during the conduct of the study. SLO reports grants from The Netherlands Brain Foundation, during the conduct of the study; grants from VIDI ZonMW, outside the submitted work. In addition, SLO has a patent Means and methods for modulating NOTCH3 protein expression and/or the coding region of NOTCH3 licensed to LUMC. IV reports a grant from Health-Holland via Alzheimer Nederland to support a research collaboration with Crossbeta Biosciences. Non-financial support in the form of research consumables was received from Crossbeta Biosciences for this same project, outside the submitted work. CT reports personal fees from advisory board of Fujirebio and Roche, non-financial support from research consumables from ADxNeurosciences, other from performed contract research or received grants from Janssen prevention center, Boehringer, EIP farma, Roche and Probiodrug, PeopleBio, Charles River, outside the submitted work. AAR reports grants from Netherlands Brain Foundation, during the conduct of the study; grants from EU, grants from ZonMw (Dutch Government), grants from Duchenne Parent Project, grants from Prinses Beatrix Spierfonds, outside the submitted work. In addition, AAR has a patent issued. JG and SB have nothing to disclose.

## REFERENCES

1. Chabriat, Joutel, Dichgans, Tournier-Lasserre, & Bousser. Cadasil. *Lancet. Neurol.* 8, 643–653 (2009).
2. Buffon, Porcher, Hernandez, *et al.* Cognitive profile in CADASIL. *J. Neurol. Neurosurg. Psychiatry* 77, 175–80 (2006).
3. Tan, & Markus. CADASIL: Migraine, encephalopathy, stroke and their inter-relationships. *PLoS One* 11, 1–14 (2016).
4. Joutel, Andreux, Gaulis, *et al.* The ectodomain of the Notch3 receptor accumulates within the cerebrovasculature of CADASIL patients. *J. Clin. Invest.* 105, 597–605 (2000).
5. Opherck, Duering, Peters, *et al.* CADASIL mutations enhance spontaneous multimerization of NOTCH3. *Hum. Mol. Genet.* 18, 2761–2767 (2009).
6. Duering, Karpinska, Rosner, *et al.* Co-aggregate

- formation of CADASIL-mutant NOTCH3: a single-particle analysis. *Hum. Mol. Genet.* 20, 3256–65 (2011).
7. Pfefferkorn, von Stuckrad-Barre, Herzog, *et al.* Reduced cerebrovascular CO(2) reactivity in CADASIL: A transcranial Doppler sonography study. *Stroke* 32, 17–21 (2001).
  8. Singhal, & Markus. Cerebrovascular reactivity and dynamic autoregulation in nondemented patients with CADASIL (cerebral autosomal dominant arteriopathy with subcortical infarcts and leukoencephalopathy). *J. Neurol.* 252, 163–167 (2005).
  9. van den Boom, Lesnik Oberstein, Ferrari, Haan, & van Buchem. Cerebral autosomal dominant arteriopathy with subcortical infarcts and leukoencephalopathy: MR imaging findings at different ages—3rd–6th decades. *Radiology* 229, 683–690 (2003).
  10. Tikka, Baumann, Siitonen, *et al.* CADASIL and CARASIL. *Brain Pathol.* 24, 525–44 (2014).
  11. Liem, Van Der Grond, Haan, *et al.* Lacunar infarcts are the main correlate with cognitive dysfunction in CADASIL. *Stroke* 38, 923–928 (2007).
  12. Viswanathan, Godin, Jouvent, *et al.* Impact of MRI markers in subcortical vascular dementia: a multimodal analysis in CADASIL. *Neurobiol. Aging* 31, 1629–36 (2010).
  13. Chabriat, Hervé, Duering, *et al.* Predictors of clinical worsening in cerebral autosomal dominant arteriopathy with subcortical infarcts and leukoencephalopathy: Prospective cohort study. *Stroke* 47, 4–11 (2016).
  14. Jouvent, Duchesnay, Hadj-Selem, *et al.* Prediction of 3-year clinical course in CADASIL. *Neurology* 87, 1787–1795 (2016).
  15. Liem, Lesnik Oberstein, Haan, *et al.* Cerebral autosomal dominant arteriopathy with subcortical infarcts and leukoencephalopathy: progression of MR abnormalities in prospective 7-year follow-up study. *Radiology* 249, 964–71 (2008).
  16. Liem, Haan, Neut, *et al.* MRI correlates of cognitive decline in CADASIL. *Neurology* 72, 143–148 (2009).
  17. Ling, De Guio, Jouvent, *et al.* Clinical correlates of longitudinal MRI changes in CADASIL. *J. Cereb. Blood Flow Metab.* 39, 1299–1305 (2019).
  18. Formichi, Parnetti, Radi, *et al.* CSF Biomarkers Profile in CADASIL-A Model of Pure Vascular Dementia: Usefulness in Differential Diagnosis in the Dementia Disorder. *Int. J. Alzheimers. Dis.* 2010, (2010).
  19. Pescini, Donnini, Cesari, *et al.* Circulating Biomarkers in Cerebral Autosomal Dominant Arteriopathy with Subcortical Infarcts and Leukoencephalopathy Patients. *J. Stroke Cerebrovasc. Dis.* 1–11 (2016). doi:10.1016/j.jstrokecerebrovasdis.2016.10.027
  20. Duering, Konieczny, Tiedt, *et al.* Serum Neurofilament Light Chain Levels Are Related to Small Vessel Disease Burden. *J. Stroke* 20, 228–238 (2018).
  21. Teunissen, Dijkstra, & Polman. Biological markers in CSF and blood for axonal degeneration in multiple sclerosis. *Lancet Neurol.* 4, 32–41 (2005).
  22. Gattringer, Pinter, Enzinger, *et al.* Serum neurofilament light is sensitive to active cerebral small vessel disease. *Neurology* 89, 2108–2114 (2017).
  23. Thelin, Zeiler, Ercole, *et al.* Serial sampling of serum protein biomarkers for monitoring human traumatic brain injury dynamics: A systematic review. *Front. Neurol.* 8, 1–23 (2017).
  24. Byrne, Rodrigues, Blennow, *et al.* Neurofilament light protein in blood as a potential biomarker of neurodegeneration in Huntington's disease: A retrospective cohort analysis. *Lancet Neurol.* 16, 601–609 (2017).
  25. Meeter, Dopfer, Jiskoot, *et al.* Neurofilament light chain: a biomarker for genetic frontotemporal dementia. *Ann. Clin. Transl. Neurol.* 1–14 (2016). doi:10.1002/acn3.325
  26. Rohrer, Woollacott, Dick, *et al.* Serum neurofilament light chain protein is a measure of disease intensity in frontotemporal dementia. *Neurology* 87, 1329–1336 (2016).
  27. Lu, Macdonald-Wallis, Gray, *et al.* Neurofilament light chain: A prognostic biomarker in amyotrophic lateral sclerosis. *Neurology* 84, 2247–2257 (2015).
  28. Piehl, Kockum, Khademi, *et al.* Plasma neurofilament light chain levels in patients with MS switching from injectable therapies to fingolimod. *Mult. Scler. J.* 135245851771513 (2017). doi:10.1177/1352458517715132
  29. Disanto, Barro, Benkert, *et al.* Serum Neurofilament light: A biomarker of neuronal damage in multiple sclerosis. *Ann. Neurol.* 81, 857–870 (2017).
  30. Lesnik Oberstein, van den Boom, van Buchem, *et al.* Cerebral Microbleeds in CADASIL. *Neurology* 57, 1066–1070 (2001).
  31. van den Boom, Lesnik Oberstein, Spilt, *et al.* Cerebral hemodynamics and white matter hyperintensities in CADASIL. *J. Cereb. Blood Flow Metab.* 23, 599–604 (2003).
  32. Roth, Tym, Mountjoy, *et al.* CAMDEX. A standardised

- instrument for the diagnosis of mental disorder in the elderly with special reference to the early detection of dementia. *Br. J. Psychiatry* 149, 698–709 (1986).
33. Folstein, Folstein, & McHugh. 'Mini-mental state'. A practical method for grading the cognitive state of patients for the clinician. *J. Psychiatr. Res.* 12, 189–198 (1975).
  34. Breteler, van Amerongen, van Swieten, *et al.* Cognitive correlates of ventricular enlargement and cerebral white matter lesions on magnetic resonance imaging. The Rotterdam Study. *Stroke* 25, 1109–15 (1994).
  35. Reitan. The relation of the trail making test to organic brain damage. *J. Consult. Psychol.* 19, 393–4 (1955).
  36. Kuhle, Barro, Andreasson, *et al.* Comparison of three analytical platforms for quantification of the neurofilament light chain in blood samples: ELISA, electrochemiluminescence immunoassay and Simoa. *Clin. Chem. Lab. Med.* 54, 1655–1661 (2016).
  37. Andreasson, Perret-Liaudet, van Waalwijk van Doorn, *et al.* A practical guide to immunoassay method validation. *Front. Neurol.* 6, 1–8 (2015).
  38. Jonsson, Zetterberg, Van Straaten, *et al.* Cerebrospinal fluid biomarkers of white matter lesions - Cross-sectional results from the LADIS study. *Eur. J. Neurol.* 17, 377–382 (2010).
  39. Lu, Macdonald-Wallis, Gray, *et al.* Neurofilament light chain: A prognostic biomarker in amyotrophic lateral sclerosis. *Neurology* 84, 2247–2257 (2015).
  40. Gaiani, Martinelli, Bello, *et al.* Diagnostic and prognostic biomarkers in amyotrophic lateral sclerosis: Neurofilament light chain levels in definite subtypes of disease. *JAMA Neurol.* 74, 525–532 (2017).



# Chapter 6

## Discussion and future perspectives



The aim of this PhD project was to advance CADASIL therapy development. This involved studies aimed at obtaining *in vivo* proof-of-concept for NOTCH3 cysteine correction, as well as generating outcome measures to be used in future (pre-)clinical trials.

There is a high unmet medical need for CADASIL patients given the impact of the disease on the life of patients and their family members, and the lack of a treatment that can cure or delay CADASIL. Although patients may receive symptomatic treatment, this does not avert the development of stroke or vascular dementia. Therapies currently under development for CADASIL are aimed at preventing or halting NOTCH3<sup>ECD</sup> aggregation or mural cell degeneration.<sup>1-4</sup> The optimal time to initiate treatment is probably as early in the disease course as possible, but at least before patients have irreversible brain damage. Young adult patients may already have some NOTCH3<sup>ECD</sup> aggregation and WMH, but they rarely have clinical manifest CADASIL. Pre-symptomatic patients from CADASIL families can be identified via predictive genetic testing. In patients with advanced disease, the therapeutic impact will likely be more limited, as the accumulated brain damage cannot be reversed by therapies that prevent further NOTCH3<sup>ECD</sup> aggregation. However, a potential benefit on disease course cannot be excluded.

### NOTCH3 cysteine correction

NOTCH3 cysteine correction is aimed at restoring the underlying genetic defect in CADASIL, namely restoring the uneven number of cysteine residues in one of the EGFR domains of NOTCH3.<sup>5,6</sup> Priority should be given to the targeting of exon 4, as the majority of severely affected CADASIL patients harbour mutations in this exon.<sup>6</sup> However, cysteine corrective exon skipping can in theory be applied to 18 of the 23 NOTCH3 exons,<sup>1</sup> thus exon skipping strategies targeting exon 4 also serve as a proof-of-concept for skipping of other NOTCH3 exons. Although *in vitro* analysis has shown that cysteine corrected NOTCH3 proteins retain normal signaling capacity, *in vitro* analysis of protein aggregation has been hampered by confounding effects of NOTCH3 overexpression in cell models, resulting in aspecific perinuclear accumulation (data not shown). Other approaches, such as scanning for intensely fluorescent targets (SIFT) in a single particle assay, assesses multimerization of small protein fragments, which may not reflect aggregation properties of the full length skip protein.<sup>7,8</sup> The use of *in vivo* models can circumvent some of the problems encountered in cell models and will, moreover, allow for direct measurement of NOTCH3 protein aggregation in the vessel wall.

To gain more insight into aggregation propensity of NOTCH3 cysteine corrected proteins, we studied a family with naturally occurring cysteine corrective exon skipping, in this case skipping of exon 9 (Chapter 3).<sup>9</sup> Family members with this NOTCH3 variant had only minimal NOTCH3<sup>ECD</sup> aggregation, likely due to some mutant RNA products escaping splicing,

suggesting that cysteine corrected NOTCH3 proteins do not aggregate. The affected family members had a mild CADASIL phenotype, although an (additional) effect of the NOTCH3 mutation position cannot be ruled out.<sup>10</sup> Overall, the knowledge obtained from this unique family encourages the continued development of NOTCH3 cysteine correction as a treatment for CADASIL patients.

Inducing NOTCH3 cysteine correction in the Leiden humanized transgenic *NOTCH3*<sup>Arg182Cys</sup> mouse model would allow for assessing the aggregation propensity of cysteine corrected proteins *in vivo*. The effect of treatment on protein aggregation could be assessed using the NOTCH3 score<sup>11</sup> and the GOM classification system (Chapter 2),<sup>12</sup> both reflecting (the consequences of) NOTCH3<sup>ECD</sup> aggregation in the brain. The first exploratory *NOTCH3* exon skipping experiments were performed in the Leiden mouse model using the *NOTCH3* antisense oligonucleotides (ASOs) developed and tested *in vitro*.<sup>1</sup> Using both systemic and intraventricular administration of ASOs, this showed too low skipping levels in the brain vasculature to allow for reliable assessment of an effect on protein aggregation (data not shown). The low skipping levels are likely due to pharmacodynamics (i.e. insufficient delivery to the vascular smooth muscle cells) and also due to low skipping efficiencies of ASOs not optimized for *in vivo* experiments. For future studies, ASOs should be further developed and optimized in terms of target sequence, ASO chemistry and tissue-homing conjugates, in order to increase skipping efficacy and delivery to vascular smooth muscle cells (VSMCs). As the VSMCs are located within the vessel walls of the brain vasculature, ASO administration could be via the 'blood-side' of the blood-brain barrier (i.e. systemically), or via the 'brain-side' of the blood-brain-barrier (i.e. intracerebroventricularly or intrathecally).<sup>13,14</sup> The advantage of intrathecal administration is that the interval between ASO administration is probably longer compared to systemic administration, because ASOs have a long half-life in the central nervous system.<sup>14,15</sup> However, systemic administration is much less invasive and is easier to perform. Since limited literature is available on cerebral blood vessel wall delivery, the optimization of delivery of the ASOs to the VSMCs will be one of the most crucial challenges to overcome.

As an alternative to NOTCH3 cysteine correction on the mRNA level, NOTCH3 cysteine correction could be achieved by a permanent exon deletion on the DNA level.<sup>16</sup> We have shown this to be feasible *in vitro* using CRISPR/Cas9-based genome editing (Chapter 3).<sup>9</sup> The potential benefit of genome editing is that patients could receive a one-time-treatment and that effects may be permanent. Currently, several *ex vivo* CRISPR/Cas trials are on-going on cells obtained from patients, such as in hematopoietic stem and progenitor cells for hematologic disorders. The CRISPR/Cas-components, i.e. guide RNA and Cas9 or Cas12, can be delivered to the cells *ex vivo* using physical methods (e.g. electroporation), viral vectors (e.g. adeno-associated virus (AAV)-vectors) or biomaterials (e.g. nanoparticles) and then

re-administered to the patient.<sup>17</sup> In case of CADASIL and many other genetic diseases, the affected cells must be gene edited *in vivo*, thus viral vectors or biomaterials must be used as a delivery vehicle.<sup>18</sup> CRISPR/Cas components could, for example, be delivered systemically or intrathecally by AAV-vectors, provided that these vectors have high target specificity and low affinity with non-targeted tissue, which is currently not the case.<sup>17,19</sup> Once in the cell, gene editing efficiency also needs to be high enough, and genomic off-target effects should be negligible, as these genomic changes are also irreversible and might lead to adverse effects.<sup>20</sup>

The effect of permanent NOTCH3 cysteine correction using gene editing could be studied in three dimensional *in vitro* disease models that closely recapitulate human brain vessels. In collaboration with leading experts in the field of organ-on-a-chip models, our group is currently developing a CADASIL-vessel-on-a-chip model using reprogrammed induced pluripotent stem cells (iPSCs) from CADASIL patients. Previous studies by others showed that developing capillary vessels from CADASIL-derived iPSCs is feasible.<sup>21</sup> CADASIL-vessel-on-a-chip models will facilitate the assessment of the morphology and (dys) function of VSMCs, pericytes and endothelial cells in a controlled setting, and even in real time. Potentially, CADASIL-vessel-on-a-chip could also serve as an *in vitro* model to study the effect of ASO-based NOTCH3 exon skipping therapies, as well as to study NOTCH3<sup>ECD</sup> aggregation in the context of the vessel wall.

### CADASIL endpoints and biomarkers in mice

The Leiden transgenic NOTCH3<sup>Arg182Cys</sup> mouse model is highly suitable for testing therapies targeting NOTCH3 RNA and DNA as it contains the full length human NOTCH3 gene, rather than only mouse or rat *Notch3*.<sup>22–24</sup> As mice develop NOTCH3<sup>ECD</sup> granules earlier than GOM deposits,<sup>11</sup> a therapeutic response can probably be observed earlier using the NOTCH3 score than using the GOM classification system. A pre-clinical study testing passive NOTCH3<sup>ECD</sup> immunotherapy showed no effect on NOTCH3<sup>ECD</sup> aggregation or GOM deposition in the transgenic rat genomic *Notch3*<sup>R169C</sup> mouse model, but did show a beneficial effect on cerebral hemodynamics.<sup>2</sup> These results illustrate that functional measures, such as cerebral hemodynamics, have additional value in pre-clinical studies. In contrast to other mouse models, the Leiden mouse model does not show cerebral blood flow deficits or ischemic brain damage (Chapter 2), possibly explained by a different genetic background or fundamentally different measurement techniques.<sup>12,23,25</sup> The Leiden mouse model does not show any signs of vessel wall thickening or mural cell degeneration as is seen in CADASIL patients, probably due to the relatively short life span of mice compared to patients (Chapter 2). Various studies testing hemodynamics have recently been performed in mouse models using a plethora of techniques, including ASL-MRI and laser Doppler flow analysis, often yielding contradictory results.<sup>3,11,12,23–35</sup> For example, cerebrovascular reactivity is

quantified using different measurement techniques between laboratories, as well as using different stimuli to induce increased blood flow, resulting in incomparable results between mouse models.<sup>12,23,25,29</sup>

### **CADASIL endpoints and biomarkers in patients**

Validated outcome measures and biomarkers for CADASIL are a pre-requisite to be able to perform clinical trials. The benefit/risk-analysis performed by the regulator for therapy approval, requires knowledge of the risks (i.e. side-effects of treatment and disease burden if no therapy is given) and the clinical benefit upon treatment, which need to be assessed by an outcome measure that should quantify a therapeutic effect relevant to patients. These outcome measures can be hard clinical endpoints, such as the development of stroke, disability or death. Alternatively, endpoints can be measures for disease progression, for example cognitive performance measured on standardized cognitive scales (e.g. CAMCOG). Showing clinical benefit within the timeframe of a clinical trial (i.e. 1-2 years) is challenging for slowly progressive diseases like CADASIL, especially when therapies aim to slow down or halt disease progression. In order to reduce time span and sample size of a clinical trial, surrogate clinical endpoints can be used, as long as they are measures that anticipate future clinical benefit (e.g. brain atrophy or potentially fluid biomarkers).

Cognitive measures and disability could be used as surrogate endpoints, but require too large sample sizes in symptomatic patients.<sup>36,37</sup> In early disease stages such cognitive measures are likely not sensitive enough to be used as surrogate endpoints, even though some studies have reported executive dysfunction before the onset of stroke.<sup>38</sup> Possibly, developing an integrated measure for disease severity, such as the Unified Huntington's Disease Rating Scale used for Huntington's disease,<sup>39</sup> would allow for increased sensitivity to monitor changes in disease severity over short time intervals. Meanwhile, lacune load and brain atrophy on MRI may be feasible markers to detect differences in 1- or 2-year disease progression. Changes in WHM volume can be measured sensitively over time, including in pre-symptomatic patients, but WMH volume is probably not the best surrogate marker, because it does not correlate with clinical disease severity or progression (Chapter 4).<sup>40-42</sup> Diffusion tensor imaging (DTI) sensitively measures brain damage, was previously estimated to require less patients in a clinical trial than other neuroimaging or cognitive measures, and might be the most promising neuroimaging markers for pre-symptomatic patients.<sup>37,43</sup> Possibly, neuroimaging measures of specific brain regions are suitable surrogate markers.<sup>44,45</sup> Complementary to neuroimaging markers, serum NfL levels could be used as blood biomarker for symptomatic patients, as they correlate with (ischemic) neuronal damage, and cognitive impairment in CADASIL (Chapter 5).<sup>46,47</sup> In a long-term follow-up study, however, there were no significant differences in 18-year increase in serum NfL in pre-symptomatic or mildly affected patients compared to controls, indicating that

NfL is mainly a biomarker for symptomatic patients. More research on the temporal profile of serum NfL is needed, in order to determine the relative contribution of acute ischemia and overall disease progression to serum NfL levels in CADASIL patients. This will help determining whether serum NfL could serve as a biomarker responsive to a therapy, as is the case for Multiple Sclerosis.<sup>48,49</sup>

CADASIL vessel wall pathology seems to precede neuronal damage, therefore markers arising due to blood vessel wall damage might be more sensitive to early disease stages than neuroimaging markers. There have been reports of seemingly contradictory results on resting cerebral blood flow (CBF) and cerebrovascular reactivity (CVR) in patients, probably caused by the heterogeneity of techniques and patients samples used.<sup>50–56</sup> Overall, it seems reduced CBF and CVR can only be reliably measured in severely affected patients, using state-of-the-art analyses, such as CVR measurements of selected brain regions and measurements of temporal dynamics of the vascular reactivity.<sup>54–56</sup>

The amount of NOTCH3<sup>ECD</sup> aggregates or classification of GOM deposits visualized in blood vessel walls in skin biopsies could be associated with disease severity or progression, and could serve as a prognostic or monitoring biomarker. However, a limitation of these markers is that NOTCH3<sup>ECD</sup> aggregates and GOM deposits in skin biopsies might not reflect NOTCH3<sup>ECD</sup> aggregation and GOM deposits in the cerebrovasculature, and that these markers would imply obtaining repeated skin biopsies.

The retina and retinal vessels might reflect changes in the brain and brain vessels, as the retina has the same embryonal origin as the brain and is also affected by CADASIL pathology. In humans, the retina can be visualized non-invasively using optical coherence tomography (OCT), thereby providing a high resolution three dimensional image of the retina. Using OCT, the thickness of retinal arteries was found to be increased in CADASIL patients,<sup>57–59</sup> and the thickness of the retinal nerve fibre layer was reported to be reduced.<sup>60,61</sup> Retinal biomarkers are attractive as they are non-invasive and cheaper than neuroimaging biomarkers, but further investigations are needed, as currently available data is based on only a few studies with limited sample sizes.

The potential blood biomarkers Endostatin, HTRA1, IGF-BP1 and TGF- $\beta$  were not associated with disease severity (Chapter 4). Biomarkers in cerebrospinal fluid (CSF) of CADASIL patients has not been studied extensively yet and may be worth further investigation.<sup>62–64</sup> Identification of fluid biomarkers in blood or CSF would likely be most promising using sensitive multiplex immunoassays or mass spectrometry approaches. Quantification of such identified biomarkers, should preferably be performed using sensitive techniques such as ultra-sensitive single molecule assays.

### CADASIL disease severity and progression

Variability in CADASIL disease course has long been recognized, even between patients of the same family, and in monozygotic twins.<sup>65,66</sup> This variability was also observed in the 18-year follow-up study we performed, which also showed that some patients can remain remarkably stable over the course of almost two decades (Chapter 4). Disease modifier known so far are classical vascular risk factors, such as smoking and high blood pressure,<sup>65,67,68</sup> and the *NOTCH3*<sup>95</sup> mutation position.<sup>10</sup> However, these modifiers do not explain all of the disease variability. Additional disease modifiers must be present and could be either genetic or environmental,<sup>67,69,70</sup> including variants in proteins known to be associated with the molecular disease pathology, such as HTRA1, LTBP-1, TIMP3 or proteins of the ADAM17/HB-EGF/(ErbB1/ErbB4) pathway.<sup>71–73</sup>

### Future perspectives

Within 25 years after the discovery of *NOTCH3* as the causative gene for CADASIL, the CADASIL research field has significantly progressed and has acquired much knowledge on disease pathomechanisms and disease course. Several CADASIL mouse models have been developed, many pre-clinical and clinical measures for disease severity have been described, and the proof-of-concept of several therapeutic approaches has been reported. Now, the time is ripe for the CADASIL research field to advance pre-clinical therapy development and aim for clinical trial readiness. This involves obtaining pre-clinical data showing therapy efficacy and safety, as well as developing validated (surrogate) endpoints for future clinical trials. In order to validate surrogate endpoints, a short-term natural history study must be performed to select the best outcome measures.

## KEY MESSAGES FROM THIS THESIS

- Granular osmiophilic material (GOM) deposits evolve over time with respect to size, morphology and number, which can be classified in a five-stage GOM deposit classification system (Chapter 2).
- The Leiden humanized transgenic *NOTCH3*<sup>Arg182Cys</sup> mouse model recapitulates early signs of CADASIL disease pathology (i.e. *NOTCH3*<sup>ECD</sup> aggregation and GOM deposition), but not other signs of disease pathology observed in CADASIL patients (i.e. blood vessel wall thickening, brain parenchyma pathology and cognitive dysfunction) (Chapter 2).
- Natural occurring *NOTCH3* exon skipping is associated with reduced *NOTCH3* protein aggregation in CADASIL patients, suggesting that cysteine corrected *NOTCH3* proteins do not aggregate (Chapter 3).
- Long-term disease progression is highly variable in CADASIL patients, and a subset of patients remains remarkably stable over the course of 18 years (Chapter 4).
- Cerebral blood flow and cerebrovascular reactivity (measured by gradient-echo phase-contrast MRI) and blood levels of the proteins HTRA1, Endostatin, IGF-BP1 and TGF- $\beta$  (measured by ELISA) are not suitable as biomarkers for CADASIL (Chapter 4).
- Serum Neurofilament Light-chain (NfL) is a blood biomarker for CADASIL in symptomatic patients, reflecting lacune load and brain atrophy, and correlates with disease severity, disease progression and survival (Chapter 5).

## REFERENCES

- Rutten, Dauwerse, Peters, *et al.* Therapeutic NOTCH3 cysteine correction in CADASIL using exon skipping: In vitro proof of concept. *Brain* 139, 1123–1135 (2016).
- Ghezali, Capone, Baron-Menguy, *et al.* Notch3 ECD immunotherapy improves cerebrovascular responses in CADASIL mice. *Ann. Neurol.* 84, 246–259 (2018).
- Liu, Gonzalez-Toledo, Fagan, *et al.* Stem cell factor and granulocyte colony-stimulating factor exhibit therapeutic effects in a mouse model of CADASIL. *Neurobiol. Dis.* 73, 189–203 (2015).
- Machuca-Parra, Bigger-Allen, Sanchez, *et al.* Therapeutic antibody targeting of Notch3 signaling prevents mural cell loss in CADASIL. *J. Exp. Med.* 214, 2271–2282 (2017).
- Joutel, Corpechot, Ducros, *et al.* Notch3 mutations in CADASIL, a hereditary adult-onset condition causing stroke and dementia. *Nature* 383, 707–710 (1996).
- Rutten, Haan, Terwindt, *et al.* Interpretation of NOTCH3 mutations in the diagnosis of CADASIL. *Expert Rev. Mol. Diagn.* 14, 593–603 (2014).
- Opherk, Duering, Peters, *et al.* CADASIL mutations enhance spontaneous multimerization of NOTCH3. *Hum. Mol. Genet.* 18, 2761–2767 (2009).
- Duering, Karpinska, Rosner, *et al.* Co-aggregate formation of CADASIL-mutant NOTCH3: a single-particle analysis. *Hum. Mol. Genet.* 20, 3256–65 (2011).
- Gravesteyn, Dauwerse, Overzier, *et al.* Naturally occurring NOTCH3 exon skipping attenuates NOTCH3 protein aggregation and disease severity in CADASIL patients. *Hum. Mol. Genet.* (2020). doi:10.1093/hmg/ddz285
- Rutten, Van Eijsden, Duering, *et al.* The effect of NOTCH3 pathogenic variant position on CADASIL disease severity: NOTCH3 EGFr 1–6 pathogenic variant are associated with a more severe phenotype and lower survival compared with EGFr 7–34 pathogenic variant. *Genet. Med.* 21, 676–682 (2019).
- Rutten, Klever, Hegeman, *et al.* The NOTCH3 score: a pre-clinical CADASIL biomarker in a novel human genomic NOTCH3 transgenic mouse model with early progressive vascular NOTCH3 accumulation. *Acta Neuropathol. Commun.* 3, 89 (2015).
- Gravesteyn, Munting, Overzier, *et al.* Progression and Classification of Granular Osmiophilic Material (GOM) Deposits in Functionally Characterized Human NOTCH3 Transgenic Mice. *Transl. Stroke Res.* (2019). doi:10.1007/s12975-019-00742-7
- Evers, Toonen, Roon-mom, & van Roon-Mom. Antisense oligonucleotides in therapy for neurodegenerative disorders. *Adv. Drug Deliv. Rev.* 87, 90–103 (2015).
- Crooke, Witztum, Bennett, & Baker. RNA-Targeted Therapeutics. *Cell Metab.* 27, 714–739 (2018).
- Rigo, Chun, Norris, *et al.* Pharmacology of a central nervous system delivered 2'-O-methoxyethyl-modified survival of motor neuron splicing oligonucleotide in mice and nonhuman primates. *J. Pharmacol. Exp. Ther.* 350, 46–55 (2014).
- Nelson, Hakim, Ousterout, *et al.* In vivo genome editing improves muscle function in a mouse model of Duchenne muscular dystrophy. *Science* (80-. ). 351, 403–407 (2016).
- Li, Niu, Ji, & Dong. Strategies for the CRISPR-Based Therapeutics. *Trends Pharmacol. Sci.* 41, 55–65 (2019).
- Maguire, Ramirez, Merkel, Sena-Esteves, & Breakefield. Gene Therapy for the Nervous System: Challenges and New Strategies. *Neurotherapeutics* 11, 817–839 (2014).
- Lau, & Suh. In vivo genome editing in animals using AAV-CRISPR system: applications to translational research of human disease. *Frontiers Research* 6, 2153 (2017).
- Chen. Minimizing off-target effects in CRISPR-Cas9 genome editing. *Cell Biol. Toxicol.* 35, 399–401 (2019).
- Kelleher, Dickinson, Cain, *et al.* Patient-Specific iPSC Model of a Genetic Vascular Dementia Syndrome Reveals Failure of Mural Cells to Stabilize Capillary Structures. *Stem Cell Reports* 13, 817–831 (2019).
- Lundkvist, Zhu, Hansson, *et al.* Mice carrying a R142C Notch 3 knock-in mutation do not develop a CADASIL-like phenotype. *Genesis* 41, 13–22 (2005).
- Joutel, Monet-Leprêtre, Gosele, *et al.* Cerebrovascular dysfunction and microcirculation rarefaction precede white matter lesions in a mouse genetic model of cerebral ischemic small vessel disease. *J. Clin. Invest.* 120, 433–445 (2010).
- Wallays, Nuyens, Silasi-Mansat, *et al.* Notch3 Arg170Cys knock-in mice display pathologic and clinical features of the neurovascular disorder cerebral autosomal dominant arteriopathy with subcortical infarcts and leukoencephalopathy. *Arterioscler. Thromb. Vasc. Biol.* 31, 2881–2888 (2011).
- Lacombe, Oligo, Domenga, Tournier-Lasserre,

- & Joutel. Impaired Cerebral Vasoreactivity in a Transgenic Mouse Model of Cerebral Autosomal Dominant Arteriopathy With Subcortical Infarcts and Leukoencephalopathy Arteriopathy. *Stroke* 36, 1053–1058 (2005).
26. Ehret, Vogler, Pojar, *et al.* Mouse model of CADASIL reveals novel insights into Notch3 function in adult hippocampal neurogenesis. *Neurobiol. Dis.* 75, 131–141 (2015).
  27. Ghosh, Balbi, Hellal, *et al.* Pericytes are involved in the pathogenesis of cerebral autosomal dominant arteriopathy with subcortical infarcts and leukoencephalopathy. *Ann. Neurol.* 78, 887–900 (2015).
  28. Ping, Qiu, Gonzalez-Toledo, Liu, & Zhao. Stem Cell Factor in Combination with Granulocyte Colony-Stimulating Factor reduces Cerebral Capillary Thrombosis in a Mouse Model of CADASIL. *Cell Transplant.* 27, 637–647 (2018).
  29. Dubroca, Lacombe, Domenga, *et al.* Impaired vascular mechanotransduction in a transgenic mouse model of CADASIL arteriopathy. *Stroke* 36, 113–117 (2005).
  30. Cognat, Cleophax, Domenga-Denier, & Joutel. Early white matter changes in CADASIL: evidence of segmental intramyelinic oedema in a pre-clinical mouse model. *Acta Neuropathol. Commun.* 2, 1–16 (2014).
  31. Primo, Graham, Bigger-Allen, *et al.* Blood biomarkers in a mouse model of CADASIL. *Brain Res.* 1644, 118–126 (2016).
  32. Ruchoux, Domenga, Brulin, *et al.* Transgenic Mice Expressing Mutant Notch3 Develop Vascular Alterations Characteristic of Cerebral Autosomal Dominant Arteriopathy with Subcortical Infarcts and Leukoencephalopathy. *Am. J. Pathol.* 162, 329–342 (2003).
  33. Monet, Domenga, Lemaire, *et al.* The archetypal R90C CADASIL-NOTCH3 mutation retains NOTCH3 function in vivo. *Hum. Mol. Genet.* 16, 982–992 (2007).
  34. Monet-Lepretre, Bardot, Lemaire, *et al.* Distinct phenotypic and functional features of CADASIL mutations in the Notch3 ligand binding domain. *Brain* 132, 1601–1612 (2009).
  35. Arboleda-Velasquez, Manent, Lee, *et al.* Hypomorphic Notch 3 alleles link Notch signaling to ischemic cerebral small-vessel disease. *Proc. Natl. Acad. Sci.* 108, E128–E135 (2011).
  36. Peters, Herzog, Opherk, & Dichgans. A two-year clinical follow-up study in 80 CADASIL subjects: Progression patterns and implications for clinical trials. *Stroke* 35, 1603–1608 (2004).
  37. Benjamin, Zeestraten, Lambert, *et al.* Progression of MRI markers in cerebral small vessel disease: Sample size considerations for clinical trials. *J. Cereb. Blood Flow Metab.* 36, 228–240 (2016).
  38. Taillia, Chabriat, Kurtz, *et al.* Cognitive alterations in non-demented CADASIL patients. *Cerebrovasc. Dis.* 8, 97–101 (1998).
  39. Huntington Study Group. Unified Huntington's disease rating scale: Reliability and consistency. *Mov. Disord.* 11, 136–142 (1996).
  40. Liem, Haan, Neut, *et al.* MRI correlates of cognitive decline in CADASIL. *Neurology* 72, 143–148 (2009).
  41. Chabriat, Hervé, Duering, *et al.* Predictors of clinical worsening in cerebral autosomal dominant arteriopathy with subcortical infarcts and leukoencephalopathy: Prospective cohort study. *Stroke* 47, 4–11 (2016).
  42. Jouvent, Duchesnay, Hadj-Seleem, *et al.* Prediction of 3-year clinical course in CADASIL. *Neurology* 87, 1787–1795 (2016).
  43. Holtmannspötter, Peters, Opherk, *et al.* Diffusion magnetic resonance histograms as a surrogate marker and predictor of disease progression in CADASIL a two-year follow-up study. *Stroke* 36, 2559–2565 (2005).
  44. Delorme, De Guio, Reyes, *et al.* Reaction Time Is Negatively Associated with Corpus Callosum Area in the Early Stages of CADASIL. *Am. J. Neuroradiol.* 38, 2094–2099 (2017).
  45. O'Sullivan, Ngo, Viswanathan, *et al.* Hippocampal volume is an independent predictor of cognitive performance in CADASIL. *Neurobiol. Aging* 30, 890–897 (2009).
  46. Gravesteyn, Rutten, Verberk, *et al.* Serum Neurofilament light correlates with CADASIL disease severity and survival. *Ann. Clin. Transl. Neurol.* 6, 46–56 (2019).
  47. Duering, Konieczny, Tiedt, *et al.* Serum Neurofilament Light Chain Levels Are Related to Small Vessel Disease Burden. *J. Stroke* 20, 228–238 (2018).
  48. Piehl, Kockum, Khademi, *et al.* Plasma neurofilament light chain levels in patients with MS switching from injectable therapies to fingolimod. *Mult. Scler. J.* 135245851771513 (2017). doi:10.1177/1352458517715132
  49. Disanto, Barro, Benkert, *et al.* Serum Neurofilament light: A biomarker of neuronal damage in multiple sclerosis. *Ann. Neurol.* 81, 857–870 (2017).

50. Pfefferkorn, von Stuckrad-Barre, Herzog, *et al.* Reduced cerebrovascular CO<sub>2</sub> reactivity in CADASIL: A transcranial Doppler sonography study. *Stroke* 32, 17–21 (2001).
51. van den Boom, Lesnik-Oberstein, Spilt, *et al.* Cerebral hemodynamics and white matter hyperintensities in CADASIL. *J. Cereb. Blood Flow Metab.* 23, 599–604 (2003).
52. Singhal, & Markus. Cerebrovascular reactivity and dynamic autoregulation in nondemented patients with CADASIL (cerebral autosomal dominant arteriopathy with subcortical infarcts and leukoencephalopathy). *J. Neurol.* 252, 163–167 (2005).
53. Cheema, Switzer, McCreary, *et al.* Functional magnetic resonance imaging responses in CADASIL. *J. Neurol. Sci.* 375, 248–254 (2017).
54. Moreton, Cullen, Delles, *et al.* Vasoreactivity in CADASIL: Comparison to structural MRI and neuropsychology. *J. Cereb. Blood Flow Metab.* 38, 1085–1095 (2018).
55. Huneau, Houot, Joutel, *et al.* Altered dynamics of neurovascular coupling in CADASIL. *Ann. Clin. Transl. Neurol.* 5, 788–802 (2018).
56. Yin, Zhou, Yan, & Lou. Effects of cerebral blood flow and white matter integrity on cognition in CADASIL patients. *Front. Psychiatry* 10, 1–6 (2019).
57. Nelis, Kleffner, Burg, *et al.* OCT-Angiography reveals reduced vessel density in the deep retinal plexus of CADASIL patients. *Sci. Rep.* 1–7 (2018). doi:10.1038/s41598-018-26475-5
58. Fang, Yu, Wu, *et al.* Study of enhanced depth imaging optical coherence tomography in cerebral autosomal dominant arteriopathy with subcortical infarcts and leukoencephalopathy. *Chin. Med. J. (Engl)*. 130, 1042–1048 (2017).
59. Alten, Motte, Ewering, *et al.* Multimodal retinal vessel analysis in CADASIL patients. *PLoS One* 9, 1–10 (2014).
60. Parisi, Pierelli, Coppola, *et al.* Reduction of optic nerve fiber layer thickness in CADASIL. *Eur. J. Neurol.* 14, 627–631 (2007).
61. Rufa, Pretegiani, Frezzotti, *et al.* Retinal nerve fiber layer thinning in CADASIL: an optical coherence tomography and MRI study. *Cerebrovasc. Dis.* 31, 77–82 (2011).
62. Dichgans, Wick, & Gasser. Cerebrospinal fluid findings in CADASIL. *Neurology* 53, 233 (1999).
63. Formichi, Parnetti, Radi, *et al.* CSF levels of  $\beta$ -amyloid 1–42, tau and phosphorylated tau protein in CADASIL. *Eur. J. Neurol.* 15, 1252–1255 (2008).
64. Unlü, de Lange, de Silva, Kalaria, & St Clair. Detection of complement factor B in the cerebrospinal fluid of patients with cerebral autosomal dominant arteriopathy with subcortical infarcts and leukoencephalopathy disease using two-dimensional gel electrophoresis and mass spectrometry. *Neurosci. Lett.* 282, 149–52 (2000).
65. Mykkänen, Junna, Amberla, *et al.* Different clinical phenotypes in monozygotic cadasil twins with a novel notch3 mutation. *Stroke* 40, 2215–2218 (2009).
66. Dichgans, Mayer, Uttner, *et al.* The phenotypic spectrum of CADASIL: Clinical findings in 102 cases. *Ann. Neurol.* 44, 731–739 (1998).
67. Singhal, Bevan, Barrick, Rich, & Markus. The influence of genetic and cardiovascular risk factors on the CADASIL phenotype. *Brain* 127, 2031–2038 (2004).
68. Ling, De Guio, Duering, *et al.* Predictors and Clinical Impact of Incident Lacunes in Cerebral Autosomal Dominant Arteriopathy With Subcortical Infarcts and Leukoencephalopathy. *Stroke* 48, 283–289 (2017).
69. Opherk, Peters, Holtmannspötter, *et al.* Heritability of MRI lesion volume in CADASIL: Evidence for genetic modifiers. *Stroke* 37, 2684–2689 (2006).
70. Opherk, Gonik, Duering, *et al.* Genome-wide genotyping demonstrates a polygenic risk score associated with white matter hyperintensity volume in CADASIL. *Stroke* 45, 968–972 (2014).
71. Capone, Dabertrand, Baron-Menguy, *et al.* Mechanistic insights into a TIMP3-sensitive pathway constitutively engaged in the regulation of cerebral hemodynamics. *Elife* 5, 1–26 (2016).
72. Zellner, Scharrer, Arzberger, *et al.* CADASIL brain vessels show a HTRA1 loss-of-function profile. *Acta Neuropathol.* (2018). doi:10.1007/s00401-018-1853-8
73. Kast, Hanecker, Beaufort, *et al.* Sequestration of latent TGF- $\beta$  binding protein 1 into CADASIL-related Notch3-ECD deposits. *Acta Neuropathol. Commun.* 2, 1–12 (2014).





# Appendices

Nederlandse samenvatting

List of abbreviations

List of co-author affiliations

List of publications

Portfolio

Curriculum Vitae

Dankwoord



## NEDERLANDSE SAMENVATTING

### Introductie

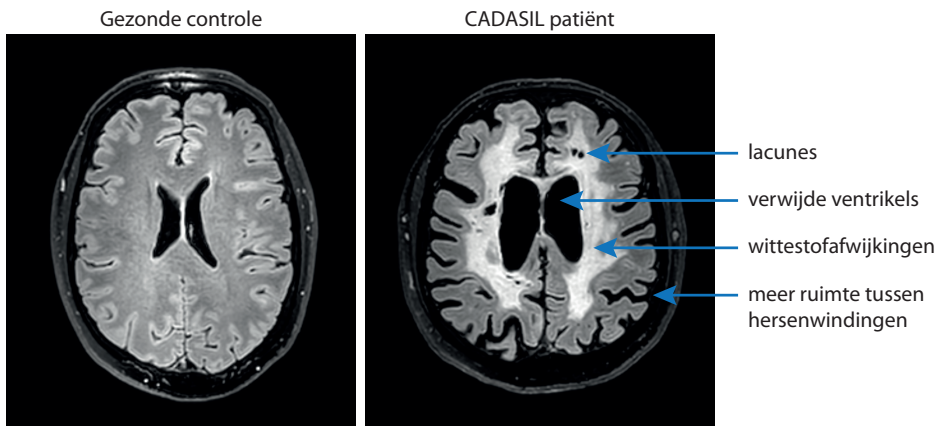
CADASIL is een erfelijke ziekte van de kleine bloedvaten in de hersenen, en gaat gepaard gaat met (meerdere) beroertes, cognitieve achteruitgang en vroegtijdige dementie. Kinderen van patiënten met CADASIL hebben 50% kans om de ziekte-veroorzakende mutatie in het NOTCH3 gen te erven. In Nederland zijn er ongeveer 275 families bekend met CADASIL. Er is geen therapie beschikbaar die het CADASIL ziekteproces kan vertragen of voorkomen.

Het doel van het promotieonderzoek beschreven in deze thesis was om de therapieontwikkeling voor CADASIL te bevorderen, en zo stappen te zetten richting toekomstige klinische studies in patiënten. Dit hoofdstuk bevat een samenvatting van de achtergrond en de resultaten van het onderzoek beschreven in dit proefschrift.

### CADASIL: het klinisch beeld

CADASIL patiënten krijgen hun eerste beroerte (herseneninfarct) vaak tussen het 45<sup>e</sup> en 60<sup>e</sup> levensjaar. Sommige patiënten krijgen hun eerste beroerte echter eerder of later. Het eerste teken van de cognitieve achteruitgang is vaak een verminderde executieve functie (waardoor o.a. planning, redeneren, en het probleemoplossend vermogen achteruit gaan), en dat is soms al aanwezig voor de eerste beroerte. Uiteindelijk ontwikkelen veel CADASIL patiënten dementie. Een deel van de CADASIL patiënten heeft ook migraine en psychiatrische stoornissen, zoals een depressie.

De afwijkingen in het brein als gevolg van het ziekteproces kunnen zichtbaar gemaakt worden met een MRI hersenscan (Figuur 7.1). Op de hersenscan van patiënten zijn al vanaf het 20<sup>e</sup> tot 30<sup>e</sup> levensjaar witte stofafwijkingen te zien, die toenemen met de leeftijd. De herseneninfarcten zijn zichtbaar op de hersenscan als uitsparingen in het breinweefsel, en worden lacunes genoemd. Verdere tekenen op de hersenscan zijn brein atrofie (minder hersenweefsel) en microbloedingen.



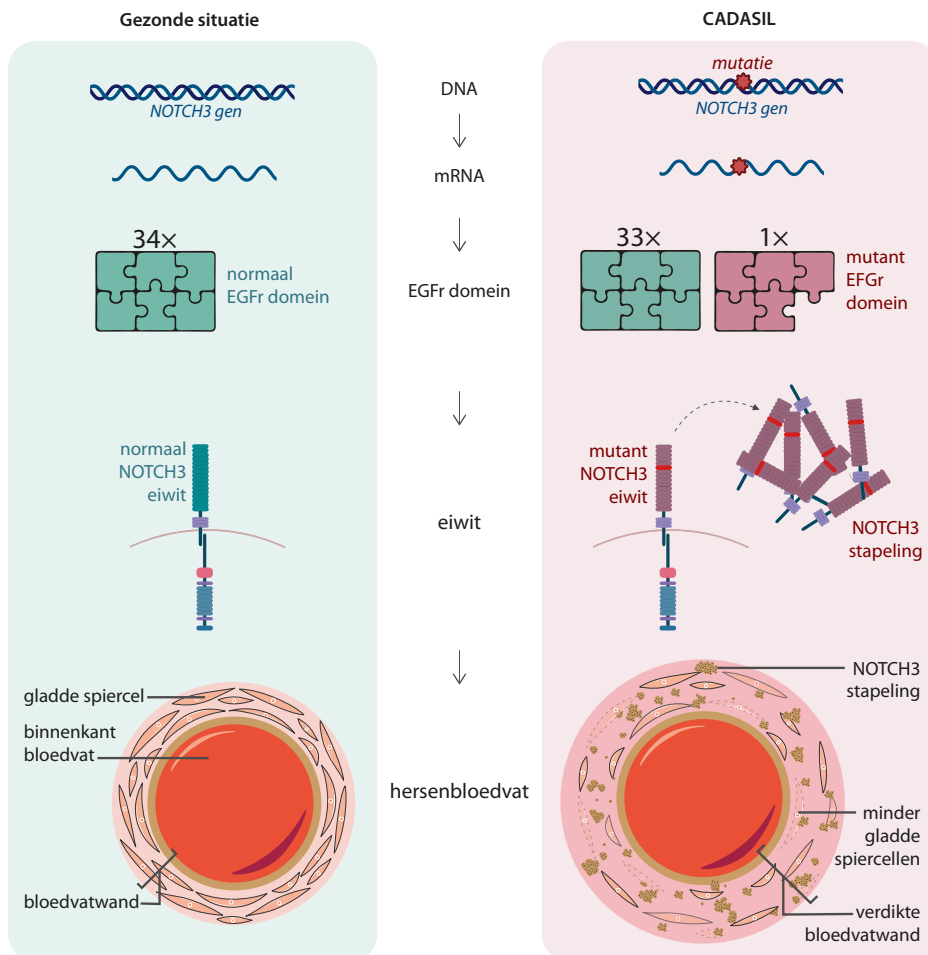
**Figuur 7.1: MRI hersenscan van een gezond persoon en een CADASIL patiënt**

Het brein van een patiënt met CADASIL laat veel witte stofafwijkingen zien. In de afwijkende witte stof zijn ook lacunes te zien: dit zijn gaten in het brein als gevolg van de herseninfarcten. Door de breinschade is er ook sprake van verkleining van het brein, dat te zien is door de verwijding van de ventrikels en de toegenomen ruimte tussen de hersenwindingen.

### CADASIL: een erfelijke ziekte

CADASIL wordt veroorzaakt door een verandering in het DNA (mutatie) van het *NOTCH3* gen. Het *NOTCH3* gen bevat het recept voor het NOTCH3 eiwit, dat wordt gevormd via een kopie genaamd mRNA (Figuur 7.2, links). Het NOTCH3 eiwit is nodig voor de goede aanleg en functie van bloedvaten. Het NOTCH3 eiwit bevat 34 gelijkwaardige EGFr domeinen. Ieder EGFr domein bevat altijd 6 cysteine aminozuren. Die passen als puzzelstukjes in elkaar, en helpen bij de vorming van de juiste structuur van het eiwit.

*NOTCH3* mutaties die bij CADASIL patiënten worden gevonden veranderen altijd het aantal cysteine aminozuren in één van de 34 EGFr domeinen, zodat er niet 6 cysteine aminozuren, maar 5 of 7 cysteine aminozuren aanwezig zijn (Figuur 7.2, rechts). Daardoor is de structuur van één EGFr domein en dus van het NOTCH3 eiwit incorrect, waardoor het mutante NOTCH3 eiwit gaat stapelen. Deze NOTCH3 stapeling vindt plaats in de wanden van de kleine slagaders door het hele lichaam, maar vooral in de hersenvaten. De NOTCH3 stapeling is te zien vlakbij de gladde spiercellen die het NOTCH3 eiwit aanmaken. In de NOTCH3 stapeling worden ook andere eiwitten weggevangen, waardoor die eiwitten hun functie niet meer kunnen uitvoeren. Als gevolg van dit hele proces verdikken de bloedvaatwanden van de kleine hersenslagaders en wordt de doorbloeding naar de hersenen minder. Door onvoldoende bloedtoevoer ontstaat de schade aan het brein die te zien is op de hersenscan. Waarom de NOTCH3 stapeling alleen in het brein tot symptomen leidt is niet bekend.



**Figuur 7.2: Het ziektemechanisme van CADASIL**

Het *NOTCH3* gen (DNA) wordt via een kopie (mRNA) vertaald naar een NOTCH3 eiwit. Het NOTCH3 eiwit heeft normaal gesproken 34 gelijkwaardige EGFr domeinen. Ieder EGFr domein bevat 6 cysteine aminozuren, die als puzzelstukjes in elkaar passen. Bij CADASIL bevat het NOTCH3 gen een mutatie, waardoor een EGFr domein niet zes, maar vijf of zeven cysteine aminozuren heeft. Daardoor gaat NOTCH3 eiwit stapelen. Hierdoor treedt er verdikking van de bloedvatwand op en dit heeft een negatief effect op de functie van de kleine hersenbloedvaten.

### **CADASIL: ziektemodellen**

Ziektemodellen zijn nodig om therapieën voor CADASIL op te testen, voordat dat in patiënten kan. De Leidse onderzoeksgroep heeft een muismodel ontwikkeld met het menselijke *NOTCH3* gen dat een CADASIL mutatie bevat. Vanaf een leeftijd van 6 weken lieten deze muizen *NOTCH3* stapeling in de bloedvaatwanden in het brein zien. Met elektronenmicroscopie laten de muizen vanaf de leeftijd van 6 maanden ook GOM deposities zien, wat een andere uiting is van de *NOTCH3* stapeling.

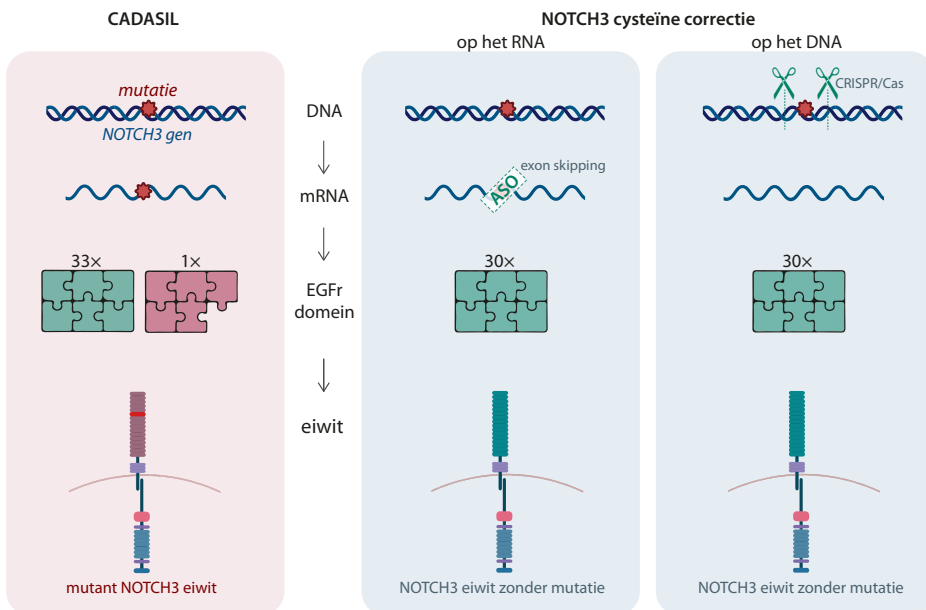
Hoofdstuk 2 bevat een beschrijving van hoe GOM deposities zich ontwikkelen. Naarmate de CADASIL muizen ouder werden hadden zij méér en grotere GOM deposities. In het brein van overleden CADASIL patiënten kwamen GOM deposities nóg veel vaker voor, en waren ze veel groter. Op basis van deze observaties hebben wij vijf GOM stadia bepaald waarin GOM deposities kunnen worden ingedeeld. Deze indeling helpt om de ernst van de GOM deposities te meten, en kan mogelijk gebruikt worden als maat voor de ernst van het CADASIL ziekteproces.

In hoofdstuk 2 wordt ook beschreven dat de hersenbloedvaten van de CADASIL muizen niet verdikt zijn en dat zij normale hoeveelheden gladde spiercellen hebben. Ook vonden wij geen afwijkingen in de witte stof van het brein, de bloedtoevoer naar het brein, en in het geheugen van de CADASIL muizen. De Leidse CADASIL muizen laten dus de vroege fase van de ziekte zien, maar geen andere kenmerken. Deze vroege fase kan worden gemonitord door de hoeveelheid *NOTCH3* stapeling te meten of verschillende stadia van GOM deposities te meten. Andere ziektemodellen, waarbij bijvoorbeeld bloedvaten in het lab worden nagemaakt, kunnen een nuttige aanvulling zijn op de CADASIL muismodellen.

### **Therapie-ontwikkeling: *NOTCH3* cysteïne correctie**

Aangezien de *NOTCH3* stapeling een belangrijke rol speelt in het ziekteproces, ontwikkelen verschillende laboratoria therapieën die *NOTCH3* stapeling tegengaan. Het beste moment om deze therapieën te starten zal waarschijnlijk zijn voordat patiënten onomkeerbare breinschade hebben. De strategie van de Leidse onderzoeksgroep richt zich op het corrigeren van het foutief aantal cysteïne aminozuren per EGFr domein. Deze aanpak heet *NOTCH3* cysteïne correctie (Figuur 7.3).

CADASIL mutaties zijn op RNA niveau 'af te plakken' met een moleculaire pleister (genaamd ASO), zodat er geen mutant *NOTCH3* eiwit ontstaat, maar een *NOTCH3* eiwit zonder mutatie. ASOs worden ook bij andere erfelijke ziekten als moleculaire pleister gebruikt. Door de moleculaire pleisters wordt een deel van het RNA onzichtbaar gemaakt en daardoor overgeslagen als het mRNA wordt gevormd. Vanuit het mRNA wordt het eiwit gemaakt dat de mutatie dan niet meer bevat. Deze techniek wordt 'exon skipping' genoemd.



**Figuur 7.3: NOTCH3 cysteine correctie als mogelijke therapie voor CADASIL**

Bij NOTCH3 cysteine correctie wordt de mutatie uit het RNA of uit het DNA gehaald. Bij exon skipping wordt met een moleculaire pleister (ASO) als het ware over de mutatie heen geplakt op het RNA. Bij CRISPR/Cas wordt met een moleculaire schaar het stukje DNA met de mutatie uit het gen geknipt. In beide gevallen ontstaat een iets korter, maar functioneel NOTCH3 eiwit waar de mutatie niet meer in zit.

Eerdere studies van de Leidse onderzoeksgroep toonden aan dat NOTCH3 exon skipping technisch mogelijk is in kweken van cellen in het lab. Het was niet mogelijk om het effect op NOTCH3 stapeling te bestuderen, omdat NOTCH3 stapeling niet goed na te bootsen is in celkweken.

Hoofdstuk 3 beschrijft een familie met een bijzondere NOTCH3 mutatie die enerzijds een 'gewone' CADASIL mutatie lijkt te zijn; maar anderzijds ook uit zichzelf werkt als een moleculaire pleister. Deze bijzondere mutatie 'behandelt' zichzelf dus op een zelfde manier als NOTCH3 cysteine correctie dat doet. De familie met deze mutatie is uitgebreid onderzocht om de effecten van cysteine correctie op de NOTCH3 stapeling in mensen te bepalen. Familieleden met deze mutatie hadden geen GOM deposities en zeer weinig NOTCH3 stapeling in vergelijking tot andere CADASIL patiënten. Wel hadden zij iets meer NOTCH3 stapeling dan gezonde personen. Dit kan worden verklaard doordat de mutatie waarschijnlijk niet als perfecte moleculaire pleister werkt, waardoor er nog een kleine beetje mutant NOTCH3 eiwit wordt gevormd dat wel gaat stapelen. De familieleden hadden een relatief mild CADASIL ziektebeeld.

Op basis van deze resultaten concluderen we in hoofdstuk 3 dat NOTCH3 cysteïne correctie leidt tot een vermindering van de NOTCH3 stapeling, en mogelijk ook tot een milder ziektebeloop met een latere beginleeftijd van de klachten. Deze bevindingen zijn bemoedigend voor een verdere ontwikkeling van NOTCH3 cysteïne correctie als therapeutische strategie voor CADASIL.

Voor de verdere ontwikkeling van de NOTCH3 cysteïne correctie therapie, zijn binnen dit promotietraject ASOs toegediend aan CADASIL muizen om te testen of NOTCH3 exon skipping werkt in muizen, en om te testen of dit de NOTCH3 stapeling afremt. Er was wel sprake van exon skipping, maar dit was zo weinig dat het effect op de NOTCH3 stapeling niet te meten was. Een verklaring hiervoor kan zijn dat de ASOs niet goed genoeg zijn, of dat zij onvoldoende worden afgeleverd in de wanden van de hersenbloedvaten. Beter ASOs kunnen worden ontwikkeld door biotechnologie bedrijven, die grote hoeveelheden ASOs tegelijk kunnen testen om te kijken welke ASO de het beste werkt én op de goede plek in het lichaam wordt afgeleverd.

Een alternatief voor NOTCH3 cysteïne correctie op het RNA (met exon skipping) is om de correctie op het DNA uit te voeren met een moleculaire schaar (CRISPR/Cas). In hoofdstuk 3 wordt beschreven dat dit in het lab technisch mogelijk is in celkweken. CRISPR/Cas is een relatief nieuwe methode en wordt ook bij andere erfelijke ziektes als mogelijke therapie getest. Het voordeel van NOTCH3 cysteïne correctie met CRISPR/Cas is dat het exon met de mutatie permanent uit het DNA wordt geknipt. Er zijn echter nog vele nadelen: de bezorging van CRISPR/Cas9 naar de gladde spiercellen in de bloedvatwanden zal een enorme uitdaging zijn. Daarnaast kan deze methode blijvende, niet-bedoelde veranderingen veroorzaken op het DNA, dat mogelijk veel bijwerkingen kan geven.

### Variatie in het CADASIL ziektebeloop

Voor toekomstige therapeutische klinische studies in patiënten moet het ziektebeloop duidelijk zijn en ook welke variatie in ziektebeloop er is tussen patiënten. In eerdere wetenschappelijke studies werden CADASIL patiënten onderzocht met een tussenpoos van 2, 3 of 7 jaar. In hoofdstuk 4 wordt een studie beschreven waarin CADASIL patiënten na 18 jaar opnieuw werden onderzocht. Het merendeel van de patiënten ging achteruit gedurende deze periode, maar een klein deel (ongeveer een vijfde) van de patiënten bleef opvallend stabiel. Een paar patiënten bleven vrij van beroerte tot (boven) het 60<sup>e</sup> levensjaar. Tevens bleek uit onze studie dat het hebben van (veel) lacunes een voorspeller is voor snellere achteruitgang. Welke andere factoren het ziektebeloop bepalen is slechts deels bekend. Patiënten met een mutatie in EGF<sub>R</sub> domein 1 tot en met 6 hebben gemiddeld genomen een ernstiger ziektebeloop. Ook roken en hoge bloeddruk geven een ernstiger beloop. De ontdekking van andere erfelijke en niet-erfelijke factoren kunnen wellicht helpen in het voorspellen van het ziektebeloop.

### Ziekte-ernst meten

Als een therapie kan worden getest in CADASIL patiënten, moet ook gemeten kunnen worden of de therapie werkzaam is. Hiervoor zijn 'uitleesmaten' nodig. Gebeurtenissen zoals een beroerte en het ontstaan van een handicap of dementie kan hiervoor gebruikt worden. Ook cognitieve testen zouden gebruikt kunnen worden als uitleesmaat. Het nadeel van deze uitleesmaten is dat studies dan lang moeten duren om een effect van de therapie te kunnen meten, terwijl klinische studies normaliter niet langer dan 1 of 2 jaar duren. Een alternatief is het gebruik van surrogaat uitleesmaten. Surrogaat uitleesmaten (ookwel surrogaat markers of biomarkers) moeten meetbaar zijn, moeten geassocieerd zijn met het ziektebeloop, en moeten in een kort tijdsbestek veranderingen in ziekte-ernst kunnen oppikken.

Metingen op MRI hersenscans kunnen gebruikt worden als surrogaat markers. Het aantal lacunes en de hoeveelheid brein atrofie zijn sterk gerelateerd aan de klinische en cognitieve achteruitgang. De hoeveelheid witte stofafwijkingen is in veel mindere mate gerelateerd aan cognitieve achteruitgang. De bloedtoevoer naar het brein werd in eerdere studies genoemd als mogelijke biomarker, maar de bevindingen beschreven in hoofdstuk 4 onderschrijven dat niet. Een nadeel van gebruik van biomarkers die kunnen worden gemeten met een hersenscan, is dat hersenscans relatief duur en tijdrovend zijn.

Biomarkers in het bloed zouden hiervoor een oplossing kunnen zijn, aangezien bloedprikken relatief gemakkelijk is en vaker gedaan kan worden. In hoofdstuk 5 wordt beschreven dat Neurofilament Light-chain (NfL) in het bloed een goede biomarker is. De hoeveelheid NfL in het bloed is gerelateerd aan de hoeveelheid hersenschade (lacunes en brein atrofie) en aan de cognitieve achteruitgang. Daarnaast hebben patiënten met meer NfL in het bloed een ernstiger ziektebeloop en komen zij sneller te overlijden. NfL zou in de toekomst in klinische studies gebruikt kunnen worden als surrogaat marker, en dan met name bij patiënten die al symptomen hebben.

## Stand van zaken

Er is veel onderzoek dat nog gedaan moet worden voordat NOTCH3 cysteïne correctie getest kan worden bij CADASIL patiënten. NOTCH3 cysteïne correctie, of een therapie die door andere labs wordt ontwikkeld, moet eerst voldoende effectief blijken in CADASIL ziektemodellen. Daarnaast moeten biomarkers ontwikkeld, getest en gevalideerd worden, zodat de ziekte-ernst en het effect van een therapie gemeten kan worden. Tevens blijft verder onderzoek nodig naar ziektemechanismen en beschermende factoren, omdat die ook kunnen bijdragen aan de ontwikkeling van andere mogelijke therapieën. Deze onderzoeken zijn gaande: zeker vier labs wereldwijd richten zich op de ontwikkeling van een therapie voor CADASIL. Ook worden grote groepen CADASIL patiënten momenteel vervolgd, inclusief patiënten met een relatief mild beeld, om nieuwe biomarkers te identificeren en het beloop van de ziekte te kunnen voorspellen.

Hoewel er nog veel onderzoek gedaan moet worden, is in afgelopen 25 jaar de aandacht voor en het onderzoek naar CADASIL enorm toegenomen. Er is veel progressie geboekt sinds de ontdekking van *NOTCH3* mutaties als oorzaak voor CADASIL: er is meer duidelijk over het ziekteproces, er zijn meerdere ziektemodellen ontwikkeld, en er zijn verschillende uitleesmaten voor de ziekte-ernst beschreven. Hoewel wetenschappelijk onderzoek in kleine stappen voortschrijdt, levert iedere stap een belangrijke bijdrage. Het onderzoek beschreven in dit proefschrift draagt bij aan het grote doel: het voorbereiden van een therapie voor CADASIL patiënten.

## LIST OF ABBREVIATIONS

ADAM17	a disintegrin and metalloproteinase domain containing protein 17
ASL	arterial spin labeling
ASO	antisense oligonucleotides
AUC	area under the curve
BOLD	blood-oxygen-level dependent
BPF	brain parenchymal fraction
CADASIL	cerebral autosomal dominant arteriopathy with subcortical infarcts and leukoencephalopathy
CAMCOG	Cambridge cognitive examination
Cas	CRISPR-associated genes
CBF	cerebral blood flow
CI	confidence interval
CRISPR	clustered regularly interspaced short palindromic repeats
CSF	cerebrospinal fluid
CVR	cerebrovascular reactivity
DAT-scan	dopamine transporter scintigraphy
DTI	diffusion tensor imaging
EGFr	epidermal growth factor-like repeat domains
ELISA	enzyme-linked immunosorbent assay
FLAIR	fluid-attenuated inversion recovery
GEE	generalized estimated equation
GIT	Groningen intelligence test
GOM	granular osmiophilic material
HB-EGF	heparin-binding epidermal-growth-factor-like growth factor
HR	hazard ratio
HTRA1	high-temperature requirement protein A1
IGF-BP1	insulin like growth factor binding protein 1
LBD	ligand binding domain
LLOQ	lower level of quantification
LTBP-1	latent TGF $\beta$ -binding protein 1
MDRS	Mattis dementia rating scale
MMSE	mini-mental state examination
mRS	modified Rankin scale
NfL	neurofilament light-chain protein
NOTCH3 <sup>CYS</sup>	cysteine altering missense mutation in NOTCH3
NOTCH3 <sup>ECD</sup>	extracellular domain/ectodomain of NOTCH3 protein
NOTCH3 <sup>ICD</sup>	intracellular domain of NOTCH3 protein

NRR	negative regulatory region
PC-MRA	gradient-echo phase-contrast MRI technique
PCR	polymerase chain reaction
RBPJ	recombining binding protein suppressor of hairless
ROC	receiver operating characteristic
RT-PCR	reverse transcription polymerase chain reaction
SD	standard deviation
SMA	smooth muscle actin
SVD	small vessel disease
SWI	susceptibility weighted imaging
TGF- $\beta$	transforming growth factor $\beta$
TIMP3	tissue inhibitor of metalloproteinases 3
TMT	trail making test
VSMC	vascular smooth muscle cell
WAIS	Wechsler adult intelligence scale
WMH	white matter hyperintensity
WMH <sub>v</sub>	white matter hyperintensity volume
WMS	Wechsler memory scale

## LIST OF CO-AUTHOR AFFILIATIONS

**Annemieke Aartsma-Rus, PhD**

Department of Human Genetics, Leiden University Medical Center (LUMC), Leiden, The Netherlands.

**Joseph F. Arboleda-Velasquez, MD, PhD**

Schepens Eye Research Institute of Mass Eye and Ear; Department of Ophthalmology, Harvard Medical School, Boston, MA, USA.

**Frank Baas, MD, PhD**

Department of Clinical Genetics, Leiden University Medical Center, Leiden, The Netherlands.

**Stefan Böhringer, PhD**

Department of Biomedical Data Sciences, Leiden University Medical Center, Leiden, The Netherlands.

**Gwendolyn Brouwer, MSc**

Department of Human Genetics, Leiden University Medical Center, Leiden, The Netherlands.

**Johannes G. Dauwerse**

Department of Human Genetics, Leiden University Medical Center, Leiden, The Netherlands.

**Marc Derieppe, PhD**

Department of Radiology, Leiden University Medical Center, Leiden, The Netherlands; Department of Pediatric Neuro-Oncology, Prinses Máxima Center for Pediatric Oncology, Utrecht, The Netherlands.

**Sjoerd G. van Duinen, MD, PhD**

Department of Pathology, Leiden University Medical Center, Leiden, The Netherlands.

**Bastian J. van Eijsden, MD**

Department of Clinical Genetics, Leiden University Medical Center, Leiden, The Netherlands.

**Jeroen van der Grond, PhD**

Department of Radiology, Leiden University Medical Center, Leiden, The Netherlands.

**Remco J. Hack, MD, MSc**

Department of Clinical Genetics, Leiden University Medical Center, Leiden, The Netherlands.

**Ingrid Hegeman**

Department of Pathology, Leiden University Medical Center, Leiden, The Netherlands.

**Carolina R. Jost, PhD**

Department of Cell and Chemical Biology, Leiden University Medical Center, Leiden, The Netherlands.

**Abraham J. Koster, PhD**

Department of Cell and Chemical Biology, Leiden University Medical Center, Leiden, The Netherlands.

**Mark C. Kruit, MD, PhD**

Department of Radiology, Leiden University Medical Center, Leiden, The Netherlands.

**Saskia A.J. Lesnik Oberstein, MD, PhD**

Department of Clinical Genetics, Leiden University Medical Center, Leiden, The Netherlands.

**Michael K. Liem, MD, PhD**

Department of Radiology, Leiden University Medical Center, Leiden, The Netherlands;  
Department of Radiology, Lange Land Ziekenhuis, Zoetermeer, The Netherlands.

**Arn M.J.M. van den Maagdenberg, PhD**

Department of Human Genetics, Leiden University Medical Center, Leiden, The Netherlands;  
Department of Neurology, Leiden University Medical Center, Leiden, The Netherlands.

**Onno C. Meijer, PhD**

Department of Internal Medicine, Leiden University Medical Center, Leiden, The Netherlands.

**Huub A.M. Middelkoop, PhD**

Department of Neurology, Leiden University Medical Center, Leiden, The Netherlands;  
Institute of Psychology, Health, Medical and Neuropsychology Unit, Leiden University, Leiden, The Netherlands.

**Aat A. Mulder**

Department of Cell and Chemical Biology, Leiden University Medical Center, Leiden, The Netherlands.

**Leon P. Munting, MSc**

Department of Radiology, Leiden University Medical Center, Leiden, The Netherlands.

**Anna M. van Opstal, PhD**

Department of Radiology, Leiden University Medical Center, Leiden, The Netherlands.

**Maurice Overzier**

Department of Human Genetics, Leiden University Medical Center, Leiden, The Netherlands.

**Mar D.M. Rodriguez Gironde, PhD**

Department of Biomedical Data Sciences, Leiden University Medical Center, Leiden, The Netherlands.

**Julie W. Rutten, MD, PhD**

Department of Clinical Genetics, Leiden University Medical Center, Leiden, The Netherlands;  
Department of Human Genetics, Leiden University Medical Center, Leiden, The Netherlands.

**Gisela M. Terwindt, MD, PhD**

Department of Neurology, Leiden University Medical Center, Leiden, The Netherlands.

**Charlotte E. Teunissen, PhD**

Department of Clinical Chemistry, Amsterdam UMC, Amsterdam, The Netherlands.

**Inge M.W. Verberk, MSc**

Department of Clinical Chemistry, Amsterdam UMC, Amsterdam, The Netherlands.

**Louise van der Weerd, PhD**

Department of Radiology, Leiden University Medical Center, Leiden, The Netherlands;  
Department of Human Genetics, Leiden University Medical Center, Leiden, The Netherlands.

## LIST OF PUBLICATIONS

Gravesteijn C, Hack RJ, Van Opstal AM, Van Eijnsden BJ, Overzier M, Arboleda-Velasquez JF, Middelkoop HAM, Rodriguez Girondo MDM, Teunissen CE, Aartsma-Rus A, Van de Grond J, Rutten JW, Lesnik Oberstein SAJ. *Long-term disease progression, prediction and survival in CADASIL: an 18-year follow-up study*. Submitted.

Rutten JW, Hack RJ, Duering M, Gravesteijn C, Dauwese JG, Overzier M, Van der Akker EB, Slagboom E, Holstege H, Nho K, Saykin A, Dichgans M, Malik R, Lesnik Oberstein SAJ. *Broad phenotype of cysteine altering NOTCH3 variants in UK Biobank: CADASIL to non-penetrance*. *Neurology* 2020. doi: 10.1212/WNL.000000000010525.

Gravesteijn C, Dauwese JG, Overzier M, Brouwer G, Hegeman I, Mulder AA, Baas F, Kruit MC, Terwindt GM, van Duinen SG, Jost CR, Aartsma-Rus A, Lesnik Oberstein SAJ, Rutten JW. *Naturally occurring NOTCH3 exon skipping attenuates NOTCH3 protein aggregation and disease severity in CADASIL patients*. *Human Molecular Genetics* 2020; 29(11):1853-1863. doi: 10.1093/hmg/ddz285.

Gravesteijn C, Munting LP, Overzier M, Mulder AA, Hegeman I, Derieppe M, Koster AJ, van Duinen SG, Meijer OC, Aartsma-Rus A, van der Weerd L, Jost CR, van den Maagdenberg AMJM, Rutten JW, Lesnik Oberstein SAJ. *Progression and Classification of Granular Osmiophilic Material (GOM) Deposits in Functionally Characterized Human NOTCH3 Transgenic Mice*. *Translational Stroke Research* 2020; 11(3):517-527. doi: 10.1007/s12975-019-00742-7.

Gravesteijn C, Rutten JW, Verberk IMW, Böhringer S, Liem MK, van der Grond J, Aartsma-Rus A, Teunissen CE, Lesnik Oberstein SAJ. *Serum Neurofilament light correlates with CADASIL disease severity and survival*. *Annals of Clinical and Translational Neurology* 2018;6(1):46-56. doi: 10.1002/acn3.678.

Gravesteijn C, Donker Kaat L, Kruit MC, Terwindt GM, Lesnik Oberstein SAJ. *Cerebrale hereditaire angiopathieën (CHA)*. *Nervus* 2017;1:20-28. (not peer-reviewed)

Rutten JW, Dauwese HG, Gravesteijn C, van Belzen MJ, van der Grond J, Polke JM, Bernal-Quiros M, Lesnik Oberstein SA. *Archetypal NOTCH3 mutations frequent in public exome: implications for CADASIL*. *Annals of Clinical and Translational Neurology* 2016;3(11):844-853. doi: 10.1002/acn3.344.

de Groot S, Vreeswijk MP, Welters MJ, Gravesteijn C, Boei JJ, Jochems A, Houtsma D, Putter H, van der Hoeven JJ, Nortier JW, Pijl H, Kroep JR. *The effects of short-term fasting on tolerance to (neo) adjuvant chemotherapy in HER2-negative breast cancer patients: a randomized pilot study*. *BMC Cancer* 2015; 15:652. doi: 10.1186/s12885-015-1663-5.

## PORTFOLIO

### Education and Courses

Prime time for precision diagnostics driven by unmet clinical needs	2019
Analysis of Repeated Measurements	2019
Academic Writing	2018
Regression Analysis	2018
Basiscursus Regelgeving en Organisatie voor Klinisch onderzoekers (eBROK)	2017
Photoshop and Illustrator CS6 for PhD-students and other researchers	2016
Laboratory Animal Course (FELASA)	2016
Basic Methods and Reasoning in Biostatistics	2016
PhD Introductory Meeting	2016

### Internship abroad

Two-month internship at Arboleda-Velasquez's lab, Schepens Research Institute, Harvard Medical School, Boston, USA.	2018
---	------

### Conferences, symposia and meetings

#### Oral presentations

<i>NOTCH3 exon skipping as a rational therapeutic approach for CADASIL: lessons from a family with naturally occurring exon 9 skipping.</i> 25th Workshop of the International Stroke Genetics Consortium. Queens' college, University of Cambridge, Cambridge, United Kingdom.	2019
<i>Testing blood biomarkers in cerebral small vessel disease CADASIL.</i> Leiden Network for Personalized Therapeutics Conference, Leiden University Medical Center, The Netherlands. Invited speaker.	2018
<i>From gene to patient: NOTCH3 cysteine correction therapy development for CADASIL.</i> Donders Discussions. Donders Institute for Brain, Cognition and Behaviour, Radboud University, The Netherlands. Invited speaker.	2018
<i>Testing blood biomarkers in CADASIL: Serum NfL correlates with disease severity.</i> MGC Symposium, Theater ins blau, Leiden, The Netherlands. Invited speaker.	2018

---

### Oral presentations (continued)

---

Testing blood biomarkers in CADASIL. MGC workshop, Texel, The Netherlands.	2018
Testing blood-based biomarkers in CADASIL: NOTCH3ECD, IGF-BP1, TGF- $\beta$ , HTRA1 and Endostatin. D'Amore lab meeting, Schepens Research Institute, Harvard Medical School, Boston, USA.	2018
Neurofilament Light Chain is a promising biomarker for CADASIL. Science & Education day Clinical Genetics, Oegstgeest, The Netherlands.	2017
The NOTCH3 score biomarker: from mouse to man? Landelijk Overleg Genetica, Utrecht.	2016

### Poster presentations

---

Naturally occurring NOTCH3 exon skipping attenuates CADASIL in patients. Nederlandse Vereniging voor Humane Genetica & Belgian Society for Human Genetics Symposium, Veldhoven, The Netherlands.	2019
In vivo testing of NOTCH3 exon skipping in a humanized CADASIL mouse model. LUMC Medical Research Profile Translational Neuroscience (LCTN) Annual Symposium, LUMC, Leiden, The Netherlands.	2017
In vivo testing of NOTCH3 exon skipping in a humanized CADASIL mouse model. MGC workshop, Leuven, Belgium. Poster prize for best poster/poster pitch.	2017
In vivo testing of NOTCH3 exon skipping in a humanized CADASIL mouse model. RNA & Oligonucleotide Therapeutics, Cold Spring Harbour meeting, Cold Spring Harbor, NY, USA.	2017

---

### Teaching activities

---

#### Teaching

Daily supervision Master's thesis project (3 months).	2019
Daily supervision Master's internship (6 months).	2017 - 2018
Daily supervision foreign PhD student (2 months).	2017
Daily supervision Bachelor's internship (5 months).	2016 - 2017

#### Related activities

Member in Board of Examiners of Medicine (LUMC).	2017 - present
--	----------------

---

---

**Prizes and personal grants**


---

Best oral presentation at Donders Discussions, Nijmegen, The Netherlands.	2018
Best oral presentation at MGC workshop, Texel, The Netherlands.	2018
Personal grant from Alzheimer Foundation-The Netherlands for international exchange at Schepens Research Institute, Harvard Medical School, Boston, USA.	2018
Personal grant from Leiden University Fund for international exchange at Schepens Research Institute, Harvard Medical School, Boston, USA.	2018
Best poster/pitch prize at MGC workshop, Leuven, Belgium.	2017

---

**Societal outreach**


---

Oral presentations at Platform CADASIL patient day, Leiden, The Netherlands.	2016 - 2019
Oral presentation at Middle Donor Event, Netherlands Brain Foundation, Utrecht, The Netherlands.	2018
Organization Running for CADASIL, Leiden, The Netherlands.	2016 - 2018
Participation LUMC Science Day.	2017

---

## CURRICULUM VITAE

Gido Gravesteijn werd geboren op 19 juli 1989 in Zaanstad en groeide op in Uitgeest. Hij behaalde in 2007 zijn VWO diploma aan het Bonhoeffer college te Castricum.

In 2007 startte Gido met de bacheloropleiding Biomedische Wetenschappen aan de Universiteit Leiden en het Leids Universitair Medisch Centrum (LUMC). Vanaf 2009 combineerde hij dit met de bachelor Geneeskunde. Na het behalen van de bachelor diploma's Geneeskunde (cum laude) en Biomedische Wetenschappen (cum laude), vervolgde Gido zijn opleiding in Leiden. In 2015 behaalde hij de Master Geneeskunde (cum laude) en de Master Biomedische Wetenschappen (summa cum laude).

In het kader van zijn opleiding deed Gido drie onderzoekstages, waarbij hij ervaring opdeed met zowel preklinisch als klinisch onderzoek. Voor zijn bachelorstage ontving hij de Prof. dr. E.L. Noachprijs 2010. Tijdens zijn eerste masterstage richtte hij zich op exon skipping in celkweken als mogelijke therapie voor twee vormen van spinocerebellaire ataxie, onder supervisie van dr. M.M. Evers en dr. W.M.C. van Roon-Mom (Humane Genetica, LUMC). Voor deze stage ontving hij de LUMC student Research Award 2013 en een beurs van het Jo Keur Fonds. Tijdens zijn tweede masterstage deed hij onderzoek naar het effect van kortdurend vasten op DNA schade en op de bijwerkingen van chemotherapie bij patiënten, onder supervisie van Prof. dr. H. Pijl (Endocrinologie, LUMC), dr. J. Kroep (Medische Oncologie, LUMC), en dr. M.P.G. Vreeswijk (Tumorgenetica, LUMC). In het kader van de Geneeskunde opleiding volgde hij de semi-artsstage bij de afdeling Klinische Genetica van het LUMC. Tijdens zijn opleiding volgde Gido tweemaal onderwijs aan het Karolinska Institutet in Stockholm. Tevens gaf hij les bij Stichting Studiebegeleiding Leiden, waar hij examencursussen biologie verzorgde en nieuwe docenten opleidde.

In 2015 is Gido gestart met een promotieonderzoek in de CADASIL onderzoeksgroep van het LUMC, onder supervisie van dr. S.A.J. Lesnik Oberstein, dr. J.W. Rutten en prof. dr. A. Aartsma-Rus. Binnen dit translationele promotietraject deed hij preklinisch en klinisch onderzoek, waarvan de resultaten zijn beschreven in dit proefschrift, alsmede gepresenteerd op verschillende (inter)nationale bijeenkomsten. Voor deze presentaties heeft hij verschillende prijzen ontvangen. Als onderdeel van het promotieonderzoek deed Gido twee maanden onderzoek aan het Schepens Eye Research Institute, Harvard Medical School, Boston, USA, onder supervisie van dr. J.F. Arboleda-Velasquez, waarvoor hij beurzen ontving van het Leids Universitair Fonds en Alzheimer Nederland. Gido heeft zich tijdens zijn promotietraject ingezet voor CADASIL patiënten en lotgenoten via Stichting Platform CADASIL en Running For CADASIL. Sinds 2017 neemt Gido zitting in de examencommissie van de Leidse Geneeskunde opleiding. Na afronding van zijn proefschrift vervolgde Gido het onderzoek naar CADASIL als postdoc onderzoeker in dezelfde onderzoeksgroep.

## DANKWOORD

Dit proefschrift is het product van vele samenwerkingen. Ik wil iedereen bedanken die heeft bijgedragen aan dit proefschrift: met jullie hulp werd dit promotietraject leuker, beter en haalbaarder.

Saskia en Julie, jullie hulp bij dit proefschrift is van onschatbare waarde, en ik ben dankbaar voor jullie laagdrempelige en persoonlijke supervisie, evenals de gezellige sfeer. Bedankt dat jullie vijf jaar geleden het vertrouwen hadden dat ik kon bijdragen aan het project. Saskia, jouw enthousiasme voor het CADASIL onderzoek is ontelbaar en dat motiveert enorm. Ik heb veel bewondering voor hoe jij het CADASIL onderzoek hebt laten opbloeien tot een onderzoekslijn. Julie, jouw enthousiasme voor onderzoek is even zo groot en jouw talent voor multitasking is een voorbeeld voor mij. Annemieke, jouw enthousiaste en gestructureerde kijk op wetenschap is een voorbeeld voor iedere PhD student. Bedankt voor jouw exon skip expertise en je promoterschap.

Maurice, jij hebt op allerlei manieren bijgedragen aan dit proefschrift: van coauteur tot supporter, van collega tot reisgenoot. Het is een plezier om met je te werken dankzij jouw humor en expertise, veel dank daarvoor! Hans, jouw kloner- en moleculair biologische werk zijn van zo'n hoog niveau dat het magie lijkt, en heeft flink bijgedragen aan dit proefschrift. Dank voor al je hulp, tips en trics! Remco en Marc, leuk dat jullie het team zijn komen versterken en het is een plezier samen te werken met jullie.

Coauteurs, ik ben jullie allen zeer dankbaar, omdat zonder jullie hulp, inzicht en expertise de papers nooit deze vorm hadden kunnen krijgen. Carolina en Aat, jullie introduceerden mij in de wondere wereld van de elektronenmicroscopie, bedankt voor de fijne samenwerking. Ingrid, jij hebt ontelbare kleuring gedaan; bedankt voor al het werk en je grote flexibiliteit hierin. Leon, bedankt voor je hulp bij de MRI analyses.

Joe, thanks for the inspiring supervision during my internship at your lab and our discussions on CADASIL. Danesh and Santiago, many thanks for showing me around in the lab and the Red Hat. Thanks to Kat, Max and Merve, it was a pleasure being your daily supervisor, and I wish you all the best in your careers. Bas, veel dank voor het monnikenwerk dat nodig was voor de huidbioptanalyse.

Kantoorgenoten, Maurice, Ivo, Mark I, Mark II, Tom, Boyd en Nisha, bedankt voor jullie humor, hulp, suggesties, wetenschappelijke discussies, en gezellig uitjes buiten werktijd. Graag bedank ik ook de afdeling Humane genetica voor het beschikbaar stellen van een

werkplek, en in het bijzonder de DMD-groep voor het opnemen van mij als volwaardig groepslid. Bedankt collega's van de vierde voor jullie collegialiteit en gezelligheid.

Daarnaast een grote blijk van waardering richting de Hersenstichting en haar donateurs, die dit promotieonderzoek financieel mogelijk hebben gemaakt. Evenzo richting Stichting Platform CADASIL en het initiatief For CADASIL, die zich beiden enorm inzetten voor het CADASIL onderzoek.

Het leven naast het promotietraject was een stuk leuker dankzij fantastische vrienden en familie, ik koester de momenten met jullie! Bas, Robin, Leon en Patrick, onze vriendschap voor het leven is een rijkdom, zeker met Zosha en Dongdong erbij. Sarah, Vera en Patrick, dankzij jullie weet ik dat geen berg te hoog is en er *always a game* is. Ype, Marnix, Pien, Lotte, Leonieke, Thomas, Ineke, Alex, en Ahmed; gezellige etentjes, pauzewandelingen en koffies zijn heerlijke ontspanmomenten die ik niet had willen missen. Dubbeltrajectvrienden, Lianne, Kimberly, Sanne, Jaap, Lennard en Erik, met hetzelfde startpunt en verschillende passies dat een recept is voor interessante gesprekken, dank daarvoor! VV'ers, dankzij jullie blijf ik bijleren over de meest exotische onderwerpen. Stockholm friends, tack för det jättebra fikas. Erik, ik koester onze vriendschap, gezellige etentjes en wetenschappelijke discussies. Dank voor jouw scherpe blik en steun gedurende onze gehele opleiding en daarbuiten, daar heb ik veel aan gehad.

Familie en schoonfamilie, jullie liefde en steun heeft mij enorm gemotiveerd afgelopen periode, veel dank daarvoor! Lieve Nick, samen laten wij zien dat alles mogelijk is, van de luchtvaart tot de wetenschap. Veel dank voor je steun. Lieve Fred en Thea, jullie hebben mij altijd gestimuleerd het beste uit mijzelf te halen. Ik ben jullie enorm dankbaar voor jullie vertrouwen, trots en onvoorwaardelijke steun, wat de basis is van al mijn prestaties, inclusief dit proefschrift.

Lieve lieve Karen, ik ben enorm blij met jou in mijn leven, en ik ben je dankbaar voor jouw onvoorwaardelijke steun en liefde.

